ChemSusChem
Review
doi.org/10.1002/cssc.202201955
Chemistry Europe
European Chemical Societies Publishing
www.chemsuschem.org

# The Colloidal Properties of Nanocellulose

Tobias Benselfelt,*[a, b, c] Nico Kummer,[d, e] Malin Nordenström,[a, b] Andreas B. Fall,[f] Gustav Nyström,[d, e] and Lars Wågberg[a, b]

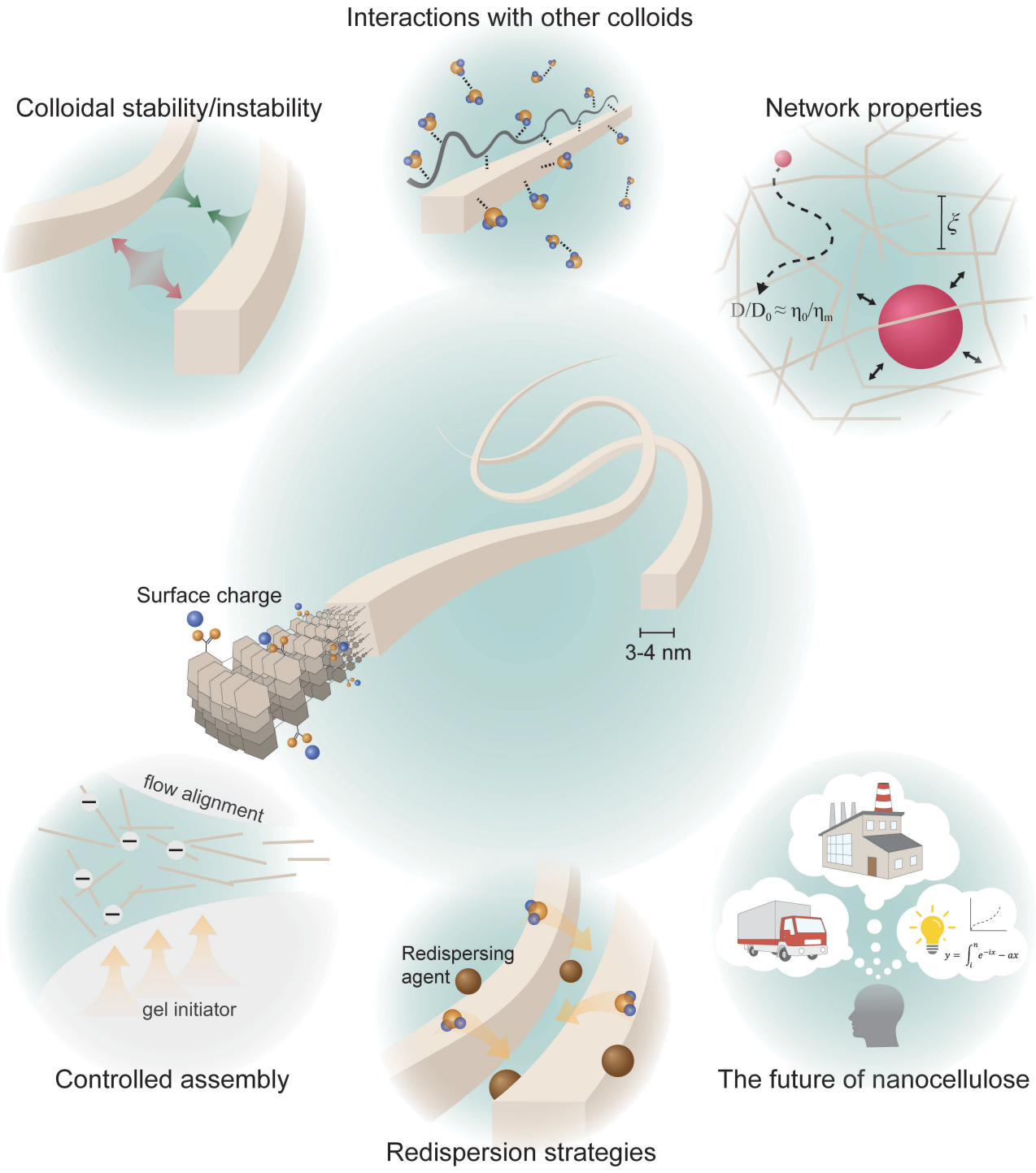



© 2023 The Authors. ChemSusChem published by Wiley-VCH GmbH

Nanocelluloses are anisotropic nanoparticles of semicrystalline assemblies of glucan polymers. They have great potential as renewable building blocks in the materials platform of a more sustainable society. As a result, the research on nanocellulose has grown exponentially over the last decades. To fully utilize the properties of nanocelluloses, a fundamental understanding of their colloidal behavior is necessary. As elongated particles with dimensions in a critical nanosize range, their colloidal properties are complex, with several behaviors not covered by classical theories. In this comprehensive Review, we describe the most prominent colloidal behaviors of nanocellulose by combining experimental data and theoretical descriptions. We discuss the preparation and characterization of nanocellulose dispersions, how they form networks at low concentrations, how classical theories cannot describe their behavior, and how they interact with other colloids. We then show examples of how scientists can use this fundamental knowledge to control the assembly of nanocellulose into new materials with exceptional properties. We hope aspiring and established researchers will use this Review as a guide.

## 1. Introduction

With the development of different types of nanocellulose, the research on cellulose-based materials has experienced a minor revolution. There are numerous publications every year with exciting material developments and inspiring applications. Many scientists believe that nanocellulose has a great future as a renewable material that can limit our dependence on oil-based products. In this golden age of nanocellulose, where we chase the next revolutionary application, it is easy to forget the fundamentals. The fundamentals are essential not only for the advancement of science but also when designing new materials. Understanding the fundamental properties of nanocellulose and their interactions makes it easier to define the problem that needs to be solved and, even better, to think of new processing ways and new experiments that no one has thought of before. To develop this understanding, a summary of our current knowledge concerning the colloidal properties of nanocellulose is essential and will benefit nanocellulose research. We hope that after reading this, scientists will have a broader understanding of nanocellulose that may help them solve some of the challenges they encounter.

This work aims not to summarize all the published studies on the subject but to provide a comprehensive overview of the most prominent behaviors we observe. We base this story on carefully chosen old and new publications describing fundamental theories and developments toward applications. We include the most recent conclusions and theoretical advancements based on established data. The work is based on our experience in this research field and, in our opinion, the most exciting aspects of nanocellulose, which can be understood using fundamental colloidal science. A restriction is that the discussion in this summary is based primarily on wood or cotton-derived nanocellulose. Nanocelluloses produced from other plants or by bacteria, algae, or animals are not explicitly discussed, although the same colloidal principles apply.

### 1.1. Introduction to colloidal chemistry and nanocellulose

In the 1940s, the scientists Derjaguin, Landau, Verwey, and Overbeek, in parallel, developed a theory to describe the interaction between particles in aqueous dispersions, which was later named the DLVO theory after its creators.[1] The theory deals with systems of small particles in which the importance of gravity and inertia decreases and colloidal forces dominate. The balance between these forces, that is, the attraction from van der Waals forces and repulsion induced by overlapping electrical double layers, decides if the system is colloidally stable or unstable. Although the theory is based on ideal solution theory and continuum electrostatics, which can be considered inaccurate assumptions for most nano-colloidal systems, it has survived until today. It has been the fundament of colloidal science due to its simplicity, making it qualitatively and quantitatively easy to understand colloidal behaviors. Since the 1940s, numerous colloidal systems have been understood thanks to the DLVO theory, both in academic research and industrial development. Understanding how to prepare stable particle dispersions or cause aggregation is crucial for many industrial processes and developing new materials.

Nanotechnology has grown popular since the beginning of the 21st century and exposes many shortcomings in our understanding of colloidal chemistry.[2] Cellulose nanoparticles (nanocelluloses) are an example of such challenging systems which demonstrate behaviors that the DLVO theory cannot fully

[a] Dr. T. Benselfelt, Dr. M. Nordenström, Prof. L. Wågberg
Department of Fibre and Polymer Technology
KTH Royal Institute of Technology
10044 Stockholm (Sweden)
E-mail: bense@kth.se
[b] Dr. T. Benselfelt, Dr. M. Nordenström, Prof. L. Wågberg
Wallenberg Wood Science Center
KTH Royal Institute of Technology
10044 Stockholm (Sweden)
[c] Dr. T. Benselfelt
School of Materials Science and Engineering
Nanyang Technological University
639798 Singapore (Singapore)
[d] N. Kummer, Dr. G. Nyström
Laboratory for Cellulose & Wood Materials
Empa – Swiss Federal Laboratories for Materials Science and Technology
Überlandstrasse 129, 8600 Dübendorf (Switzerland)
[e] N. Kummer, Dr. G. Nyström
Department of Health Sciences and Technology
ETH Zürich
8092 Zürich (Switzerland)
[f] Dr. A. B. Fall
RISE Bioeconomy
11428 Stockholm (Sweden)

© 2023 The Authors. ChemSusChem published by Wiley-VCH GmbH. This is an open access article under the terms of the Creative Commons Attribution Non-Commercial License, which permits use, distribution and reproduction in any medium, provided the original work is properly cited and is not used for commercial purposes.



1864564x, 2023, 8, Downloaded from https://chemistry-europe.onlinelibrary.wiley.com/doi/10.1002/cssc.202201955 by Paul Scherrer Institut PSI, Wiley Online Library on [08/05/2023]. See the Terms and Conditions (https://onlinelibrary.wiley.com/terms-and-conditions) on Wiley Online Library for rules of use; OA articles are governed by the applicable Creative Commons License

explain. Here, we thus aim to describe the colloidal properties of nanocelluloses from the perspective of the DLVO theory and beyond. We also elaborate on how to use the transition between stability and instability to control the assembly of new nanostructured materials from nanocellulose.

### 1.2. The DLVO theory

The DLVO theory uses mean-field approximations to limit the computational cost by averaging properties rather than calculating pairwise interactions between molecules. However, as later discussed in Section 5, the continuum models in the DLVO theory are inaccurate in many situations.

In the DLVO theory, the Hamaker and Lifshitz theories describe van der Waals attraction using a Hamaker constant ($A$) to determine the magnitude of force ($F$) in Equation (1), in the case of two flat surfaces where $D$ is the separation distance.[3]

$$F(D) = -\frac{A}{6\pi D^3} \tag{1}$$

The Hamaker constant is based on average electrodynamic properties represented by the dielectric constant ($\varepsilon$) of the bulk materials and the solvent in between.

The electrical double layer describes a charged surface with tightly bound counterions, often called the Stern layer, and the diffuse layer of mobile counterions with a concentration that decays exponentially with distance away from the charged surface. Theoretically, the Poisson–Boltzmann equation describes this ionic distribution using associated approximations such as the Gouy–Chapman and Debye–Hückel theories.[4] The repulsion arises when two or more double layers overlap, leading to an increased salt concentration in the region between the particles relative to the surrounding solution. Since the surface potential of the particles confines these ions, the only way to dilute this entropically unfavorable ion concentration is for water to enter between the particles to push them apart. Colloidal chemists often use the word electrostatic repulsion to describe double layer repulsion. Unfortunately, this is somewhat misleading since the force originates from entropy and, in the DLVO theory, is characterized by ideal osmotic pressure. Section 5 deals with the impact of nonideal osmotic pressure.

The repulsive force between two charged, flat surfaces is in the analytical version of the DLVO theory represented by Equation (2),

$$F(D) = \frac{\kappa^2}{2\pi} Z \exp(-\kappa D) \tag{2}$$

in which $Z$ is the interaction parameter shown in Equation (3),

$$Z = 64\pi\varepsilon_0\varepsilon_r \left(\frac{k_B T}{e}\right)^2 \tanh^2\left(\frac{ze\psi_0}{4k_B T}\right) \tag{3}$$

where $\kappa^{-1}$ is the Debye length describing the correlation distance between two charges and depends on the ionic

Tobias Benselfelt received his Ph.D. in fiber and polymer science from KTH Royal Institute of Technology (Stockholm, Sweden) in 2019. He continued as a postdoctoral researcher within the digital cellulose center at KTH and is currently a Wallenberg postdoctoral fellow at Nanyang Technological University in Singapore. His research aims to develop theories for nanocellulose hydrogel networks and use these networks as a framework for soft conductors, tunable membranes, and actuators. He utilizes fundamental colloidal interactions between nanocellulose and other components to assemble new interactive materials.

Gustav Nyström received his Ph.D. in engineering physics from Uppsala University, Sweden, in 2012. Following postdoctoral work at KTH Royal Institute of Technology (Stockholm) and ETH Zurich, Switzerland, where he focused on fundamental studies of nanocellulose and amyloid fibril nanostructure characterization and liquid crystal self-assembly, he is now the Head of the Cellulose & Wood Materials laboratory at Empa (Dübendorf, Switzerland) and a Lecturer at ETH Zurich. His research aims to develop a new generation of active, renewable, and highly functional biomaterials using cellulose and wood as material resources.

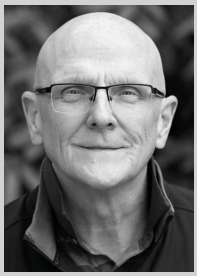

Lars Wågberg has been a professor in fiber technology at KTH Royal Institute of Technology, Stockholm, Sweden, since 2002. The focus of his and his team's efforts has been to quantify the molecular interactions at model surfaces of cellulose, lignin, and hemicellulose, to allow the preparation of new materials from these components using a bottom-up design with, for example, layer-by-layer self-assembly. During the last 15 years, his and the Fibre Technology team's efforts have been on characterizing cellulose nanofibrils to incorporate these materials in new, interactive materials where the properties of this renewable and biodegradable nanomaterial are utilized in the most efficient way by using different self-assembly methodologies.


© 2023 The Authors. ChemSusChem published by Wiley-VCH GmbH

1864564x, 2023, 8, Downloaded from https://chemistry-europe.onlinelibrary.wiley.com/doi/10.1002/cssc.202201955 by Paul Scherrer Institut PSI, Wiley Online Library on [08/05/2023]. See the Terms and Conditions (https://onlinelibrary.wiley.com/terms-and-conditions) on Wiley Online Library for rules of use; OA articles are governed by the applicable Creative Commons License

strength of the solvent, $k_B$ is the Boltzmann constant, $e$ is the elementary charge, and $z$ is the valency of the electrolyte. The surface potential ($\psi_0$) depends primarily on the charge density of the particle, which means that a highly charged particle is more stable than a particle with a low charge since the double layer repulsion is more likely to dominate over van der Waals attraction. The approximate form of the disjoining osmotic pressure ($\Pi$)[5] between two flat surfaces with low surface potentials in Equation (4), shows the relationship between repulsion and surface potential.

$$\Pi(D) = 2\varepsilon_0\varepsilon_r\kappa^2\psi_0^2 \exp(-\kappa D) \quad (4)$$

Neutralizing the surface charge (reduced $\psi_0$) or increasing the ionic strength of the solvent (reduced $\kappa^{-1}$) reduces the magnitude and range of repulsive double layer interactions and can lead to the association of the colloids due to van der Waals attraction. As later discussed in Section 7, nanocelluloses can be assembled into hierarchical materials by controlling these forces.

### 1.3. Nanocellulose

Nanocelluloses is a trivial terminology for isolated semicrystalline cellulose nanoparticles, each being a parallel assembly of β-1,4-glucan polymers. In 1949, Rånby described the isolation of nanocellulose for the first time using acid hydrolysis to disintegrate cellulose fibers.[6] He observed somewhat colloidally stable dispersions of particles, now known as cellulose nanocrystals (CNCs). The next milestone in the development of nanocellulose came 34 years later, in 1983, when Turbak et al. disintegrated cellulose fibers using mechanical force, leading to an opaque viscous paste called microfibrillated cellulose (MFC).[7] These microfibrils are aggregates of nanofibrils, the fundamental building block of trees and plants. Isolation of nanofibrils requires high amounts of energy, and even when successfully isolated, they will spontaneously and rapidly associate back into an aggregated state due to their limited colloidal stability.

The key to preparing completely isolated and dispersed cellulose nanofibrils (CNFs) is found in the DLVO theory by the understanding that double layers lead to repulsion between particles. The formation of double layers requires a surface potential generated by adding charged groups to the surface of the particles, which is precisely what Wågberg and Lindström, with co-workers, demonstrated in 1987 using carboxymethylation.[8] However, it was not until the beginning of the 21st century before the research interest in CNFs rapidly increased, sparked by the adaption of TEMPO-mediated oxidation by Saito et al. in 2006[9a] and further developments by Wågberg et al. in 2008.[9b] After these initial papers, the number of publications has increased exponentially, especially during the latest decades, and several methods of adding surface charge have been developed (see Section 2). In the present work, the colloidal properties of nanocellulose are primarily presented from the perspective of CNFs since their colloidal stability is more challenging than for CNCs. Still, we also mention special situations for CNCs.

## 2. Nanocellulose Manufacturing by Chemical Modification and Disintegration of Cellulose Fibers

Colloidal stability is a requirement for dispersing nanoparticles, which is crucial for accessing the advantageous nano-scale properties utilized in the assembly of new materials and devices. The most straightforward and effective stabilization strategy is to add charged groups to the nanoparticles generating a repulsive osmotic pressure due to the overlapping double layers of adjacent particles according to the classical DLVO theory (Section 1.2).[5,10] Nanocelluloses are liberated from the fiber wall (top-down) rather than being synthesized in a dispersed state (bottom-up), and the introduction of charged groups in wood fibers has the essential benefit of inducing swelling of the fiber wall, which facilitates the disintegration into nano-sized particles (Figure 1).

There are two main methods of preparing nanocelluloses: i) acid hydrolysis to manufacture low aspect ratio CNCs or ii) mechanical disintegration to manufacture high aspect ratio CNFs. While the terms CNFs and CNCs are frequently used in the literature, there is no globally established definition of the difference. One of the most followed definitions is from the Canadian Standards Association (CSA Group), where CNFs are described as: "a cellulosic object composed of at least one primary fibril (dimensions typically 3–15 nm in cross-section), containing crystalline and amorphous regions, with aspect ratio usually greater than 50, which may exhibit longitudinal splits, entanglement between cellulose nanofibrils or network-like structure," whereas CNCs are described as: "singular member of the family of cellulosic nanomaterials, having a high degree of crystallinity, a high degree of short-range order, and consisting of $>99$% pure cellulose." One of the primary distinctions is thus that CNCs are stiff and shorter rods, while CNFs are longer and more flexible, with kinks and splits that lead to entanglement. Another distinction that is true in many cases, but not all, is that CNCs can form nematic phases (Section 5.5), whereas CNFs form arrested states (Section 4) before they reach the concentration needed for nematic phases. In conference presentations,

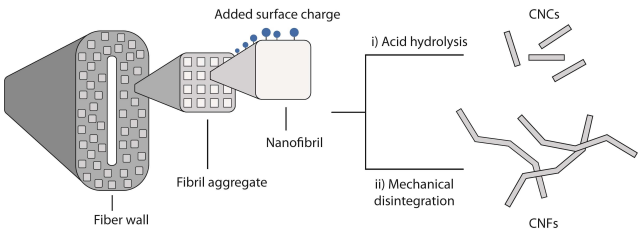


**Figure 1.** Schematic drawing of the hierarchical structure of the fiber wall and how its disintegration produces nanocellulose.


© 2023 The Authors. ChemSusChem published by Wiley-VCH GmbH

1864564x, 2023, 8, Downloaded from https://chemistry-europe.onlinelibrary.wiley.com/doi/10.1002/cssc.202201955 by Paul Scherrer Institut PSI, Wiley Online Library on [08/05/2023]. See the Terms and Conditions (https://onlinelibrary.wiley.com/terms-and-conditions) on Wiley Online Library for rules of use; OA articles are governed by the applicable Creative Commons License

the difference has been visualized by comparing CNCs to rice and CNFs to spaghetti or noodles.

### 2.1. Different ways of adding surface charge

There are different ways of adding surface charge, for example, anionic or cationic groups with different chemistries that also affect the properties of the nanoparticles. Manufacturing of CNCs does not per se require the introduction of charged groups. Still, the frequently used sulfuric acid hydrolysis introduces sulfate half-esters on the surface of the CNCs (Figure 2a), which is a basis for their colloidal stability.[11]

It is more challenging to produce CNFs than CNCs since they require chemical modification and more energy to disperse. The high aspect ratio of CNFs also leads to a higher degree of entanglement and, thus, colloidal, shipping, and storing challenges. These challenges for CNFs are, for example, reflected in that CNCs are commercially sold as dry powders, while CNFs are sold as gels or dispersions at a smaller scale.

Frequently used isolation procedures for CNFs are homogenization or pulp grinding followed by sonication. These are energy-demanding processes, but introducing charged groups in the fiber wall reduces the energy consumption from 30 000 kWh t$^{-1}$ down to less than 1000 kWh t$^{-1}$ and increases the nano-yield.[12] The higher the surface charge density, the easier the disintegration, with the trade-off being a reduced degree of polymerization at higher degrees of modification and hence shorter fibrils.[13] Thus, for CNFs, the introduction of charged groups is crucial to make the manufacturing process cost-effective and achieve colloidal stability since the high aspect ratio of CNFs makes them more susceptible to aggregation and flocculation than CNCs. For the same reasons, post-functionalization of CNFs in dispersion is more challenging than for CNCs, and modifications can, if possible, be performed on the pulp before disintegration.[14] The importance of aspect ratio on the colloidal behavior of nanocellulose is discussed in further detail in Section 4.

Most of the current research on nanocellulose is based on sulfated CNCs or carboxylated CNFs. Sulfated CNCs (Figure 2a) were introduced by Marchessault et al. in 1959[15] and later studied by Gray and co-workers in detail.[16] Carboxylated CNFs (Figure 2b and c) were introduced by Saito and Isogai with co-workers in 2006–2007 using TEMPO (2,2,6,6-tetramethylpiperidine-1-oxyl radical)-mediated oxidation (TO-CNFs),[9a,17] or by Wågberg and Lindström with co-workers in 1987 using carboxymethylation (CM-CNFs).[8,9b] Both techniques provide individual fibrils with average diameters of 2–5 nm and lengths spanning a few hundred nanometers up to a few microns (Figure 3).

A sufficient charge density is necessary to liberate the nanofibrils from the fiber wall[19] and achieve colloidal dispersions of high yield.[20] At low TEMPO oxidation degrees, only the external surfaces of the fibril aggregates are charged. The initially inaccessible surfaces between the fibrils will become available once fibril aggregates swell during the progression of the oxidation process. At a charge density of 1.3 mmol g$^{-1}$, assuming square dimensions of the fibrils with a size of 4 nm,[19] all available surface hydroxyls will be oxidized. This number is in good agreement with data from Fall et al.,[20] who found that at a charge of 0.38 mmol g$^{-1}$, only 47% of the original fiber material was colloidally stable, probably reflecting that the material contained an inhomogeneous mixture of more and less charged fibrils. At a charge density of around 0.6 mmol g$^{-1}$, almost the entire fiber material could be converted to a colloidally stable CNF dispersion even though some inhomogeneity exists on the nano level.

In addition to TO-CNFs and CM-CNFs, CNFs have been produced by several other methods. One of the first alternatives to reduce the energy consumption of the fibrillation process

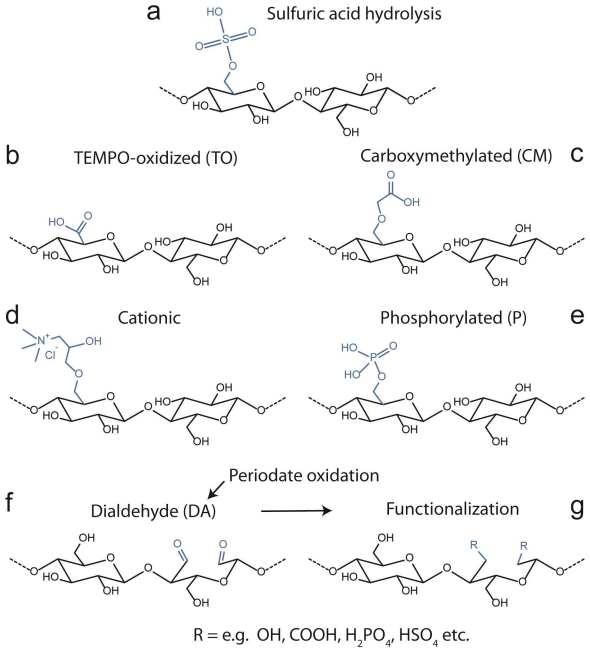


**Figure 2.** Overview of chemical structures achieved by different chemical modifications of cellulose to add charged groups to the surfaces of the cellulose fibrils.

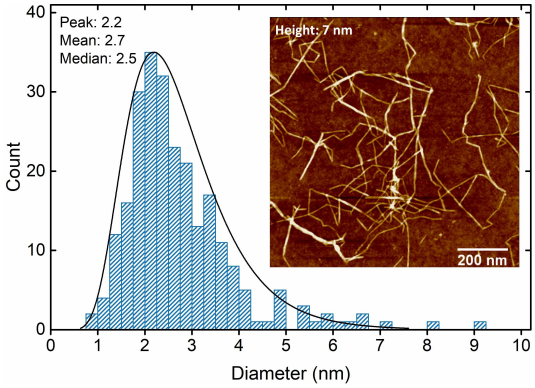


**Figure 3.** Diameter distribution from AFM images (inset) of typical CM-CNFs with a charge density of 0.6 mmol g$^{-1}$. Reproduced from Ref. [18] with permission from the Royal Society of Chemistry.


© 2023 The Authors. ChemSusChem published by Wiley-VCH GmbH

1864564x, 2023, 8, Downloaded from https://chemistry-europe.onlinelibrary.wiley.com/doi/10.1002/cssc.202201955 by Paul Scherrer Institut PSI, Wiley Online Library on [08/05/2023]. See the Terms and Conditions (https://onlinelibrary.wiley.com/terms-and-conditions) on Wiley Online Library for rules of use; OA articles are governed by the applicable Creative Commons License

was enzymatic CNFs produced by treating the pulp with endoglucanases to loosen the fiber wall before mechanical disintegration, either indirectly by fungi shown by Janardhnan and Sain in 2006[21] or directly by pure enzymes developed by Berglund and co-workers in 2007.[22] However, enzymatic fibrils contain only the inherent charge of residual hemicelluloses, which in most cases is not enough to achieve a complete liberation and satisfactory colloidal stability. Consequently, these fibrils are bound in larger aggregates with average sizes of roughly 15–75 nm with limited colloidal stability.

Gray and co-workers were the first to produce cationic CNCs in 2008 by reacting pulp with *N*-(2,3 epoxypropyl)trimethylammonium chloride (Figure 2d).[23] Wågberg and co-workers were the first to produce cationic CNFs in 2010 using the same approach as that used for CNCs,[24] and Pei et al. further developed this method.[25]

Phosphorylated CNFs (Figure 2e) are an even more recent development, based on earlier established chemistry,[26] achieved by either enzymatic modification by Kokol and co-workers in 2014[27] or chemical modification by Wågberg and co-workers in 2015.[28]

Periodate oxidation of cellulose has been used to derivatize cellulose since at least the early 20$^{th}$ century. It is a broad toolbox that differs from the other modification procedures in the sense that the cellulose is first oxidized into dialdehyde cellulose by cleaving the bond between C2 and C3 (Figure 2f) and then further modified to add a wide variety of chemical functionalities such as carboxylates,[29] sulfonates,[30] phosphates,[31] and many more (Figure 2g).[32] The ring opening leads to a different structure than other modification techniques that mainly act on C6 and sometimes C2 and C3 without disrupting the cyclic sugar unit.

Holo-cellulose fibrils are one of the most recent advances by Berglund and co-workers starting in 2015.[33] In this pulping process, which is optimized for the production of CNFs, a mild peracetic acid delignification adds charge and preserves most of the native hemicelluloses that also carry charged groups.[34] Furthermore, the hemicellulose forms a lubricating layer that prevents cellulose-cellulose contact even under acidic conditions where the surface charge is neutralized and traditional CNFs form gels or aggregates (see Section 3.5). This method preserves the molecular weight of the cellulose and hence the length of the fibrils, which is favorable for stress transfer in materials.[35]

The above-mentioned techniques of adding charge or other functionalities have advantages and disadvantages in industrial applicability, colloidal stability, nanocellulose dimensions, and end-use. The specific chemical nature of the charged groups also influences how the particles interact with each other or other colloids and chemicals, further discussed in Sections 5 and 6. Another critical but often overlooked parameter is the source of cellulose which affects, for example, the crystal dimensions or surface properties via, for example, residual lignin and hemicelluloses.[36] It is, therefore, preferable to base models for colloidal stability and interactions of nanocelluloses on high-purity nanocellulose derived from cotton or dissolving grade pulps with diminishing amounts of residual lignin and hemicelluloses.[9b]

Most cellulose sources are heterogeneous, so the modifications will occur heterogeneously and sequentially as the fiber wall opens up during modification. The inevitable result is that some fibrils have more charge than others, and the measured surface charge density should be considered an average value with wide deviations on both sides. Thus, a relatively high degree of modification is needed to have enough charged groups for the fibrils with less charge, which is reflected in the measured nanomaterial yields (Section 3.1).

## 3. Introduction to the Colloidal Properties of Nanocellulose

The preparation of nanocellulose from wood using different chemical or chemo-mechanical processes (Section 2) has brought the cellulose-rich fiber-producing industry into nanoscience, including both possibilities and challenges.

The possibilities are bottom-up engineering using nanocelluloses and their excellent mechanical properties, ease of chemical functionalization, resistance to harsh chemical environments, and high aspect ratio. The fact that nanocelluloses are renewable and biodegradable also suits today's sound demands for circular chemistry for new materials. Today, the literature is filled with scientific papers and patents showing how nanocelluloses can be used to prepare new devices and platforms for interactive materials.[37]

The challenges are related to their anisotropic nano dimensions, resulting in the formation of volume-spanning arrested states (Section 4) with a high viscosity already at concentrations below 1 wt%.[38] These arrested states, especially of CNFs, are hard to dewater, and their transportation over larger distances becomes very expensive. Hence, there is a huge demand for knowledge about the colloidal properties of nanocellulose dispersions, their self-organization ability (Section 5.5), and how to increase their concentration without reaching unreasonable viscosities or jeopardizing the colloidal stability of the dispersions (Section 8).

### 3.1. Nanocellulose dispersions

Following the liberation of the nanocellulose from the raw material, CNCs are already in a dispersed state, whereas CNFs are usually in the form of a gel, even at low concentrations.[20,39] From a colloidal point of view, this gel is somewhat ill-defined since little is known about the different structural levels within it, and the state of the individual nanofibrils in these gels is unknown. It is, therefore, necessary to isolate the nanoparticles to study their colloidal behavior.

The isolation of nanocelluloses from gels has been addressed by several investigators.[20,40] To have a solid foundation, it has been suggested to start by determining the fraction of the colloidally stable material that allows continued


© 2023 The Authors. ChemSusChem published by Wiley-VCH GmbH

1864564x, 2023, 8, Downloaded from https://chemistry-europe.onlinelibrary.wiley.com/doi/10.1002/cssc.202201955 by Paul Scherrer Institut PSI, Wiley Online Library on [08/05/2023]. See the Terms and Conditions (https://onlinelibrary.wiley.com/terms-and-conditions) on Wiley Online Library for rules of use; OA articles are governed by the applicable Creative Commons License

characterization and evaluation. This determination is achieved by diluting the gel and subjecting the inhomogeneous dispersion to high-intensity mixing and/or ultrasonication, followed by centrifugation to collect the colloidally stable phase in the supernatant and discard the aggregated phase in the pellet (Figure 4). The treatment enables the determination of the gravimetric nano fraction yield. It should be noted that it is nearly impossible to claim that a stable nanocellulose dispersion has been achieved without centrifugation since it contains a mixture of nanocellulose and larger aggregates. Qualitative quality assurance is to inspect the dispersion visually; if it is cloudy, it contains larger aggregates that should be disintegrated by more sonication or removed by centrifugation. An excellent nanocellulose dispersion should look like water, even in a gelled state.

Stability and yield also depend on the concentration at which the fibrils are dispersed. There may not be enough space to separate all fibrils at higher concentrations, and under such conditions, centrifugation is not possible due to the interconnectivity of their network (see Section 4). Dispersions with considerable viscosity should thus be further diluted before characterization.

Once dispersed, the added surface charge (Section 2) prevents nanocelluloses from reaggregating due to double layer repulsion, according to the DLVO theory. However, for CNFs with very high aspect ratios, the charge is insufficient to prevent the fibrils from associating long before the classical colloidal theory predicts. This behavior is related to the specific properties of the CNFs, but it is indeed a commonly detected phenomenon for nanoparticles for which the assumptions of the DLVO theory are largely inaccurate. Apart from the nano dimensions, their surface charge is frequently so high that the CNFs will, also in this respect, be outside the limits of the validity of the classical DLVO theory.[41] The threshold depends on the properties of the surface and the counterions but occurs roughly at charge densities of 0.1–0.2 $C\,m^{-2}$. For nanocellulose, this is an approximate charge density of 0.4–0.6 $mmol\,g^{-1}$. It is evident that a more advanced description of the colloidal interactions in CNF systems is needed, and a new approach is outlined in more detail under Section 5.

Despite the shortcomings of the DLVO theory, it has been used in several attempts to describe the behavior of nanocelluloses. It was found that the influence of simple salts on the stability of the dispersions could be reasonably well described regardless of the significant simplifications.[20,42] The double layer repulsion was, as an example, calculated using the determined zeta-potentials, except in Fall et al.,[20] where the surface potential was calculated by matching potentiometric titration data with a theoretical model. For the model to fit the titration, $Na^+$ ions were simulated to be strongly associated with the carboxyl groups through a specific binding constant.[43] This model could nicely predict the experimentally determined aggregation of differently charged CNFs at increasing NaCl concentrations. These results also showed that the surface potentials were 2–3 times larger than the zeta potentials, demonstrating that using zeta potentials instead of surface potentials is a severe simplification.

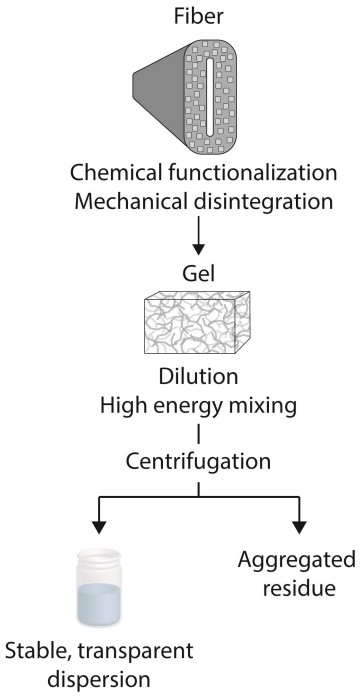


**Figure 4.** Schematic description of the preparation of a stable colloidal dispersion of nanocellulose.

### 3.2. Characterization of nanocellulose dispersions

Once nanocelluloses have been liberated and isolated, their properties can be characterized. The charge of the nanocellulose can easily be accessed by conductometric titration or polyelectrolyte titration using standard methods.[20] Following this, the dimensions can be determined by TEM (transmission electron microscopy),[9b] SEM (scanning electron microscopy)[38b] or AFM (atomic force microscopy),[44] or by combinations of SEM or AFM, and DLS (dynamic light scattering).[45] These measurements can give, among others, width, length, shape, segment lengths, and kinks; to have representative values requires the measurements of a large enough sample of the dispersion. There is, as an example, an open-access software for evaluating fundamental properties of fibrillar materials provided that high-resolution AFM, TEM, or SEM images of the nanocellulose are available.[46] Such software is an ample opportunity for the future characterization of nanocelluloses which requires collecting high-quality data and sophisticated data analysis.

DLS measurements must be carefully performed and evaluated, considering that the technique can only detect the movements of nanocelluloses in a solvent, most frequently water, which is naturally dependent on different factors, such as CNF concentration, pH, salt concentration, and temperature. However, the technique is beneficial for collecting "fingerprints" of different types of nanocelluloses and combining them with width thickness (*d*) measurements from AFM to determine the


© 2023 The Authors. ChemSusChem published by Wiley-VCH GmbH

1864564x, 2023, 8, Downloaded from https://chemistry-europe.onlinelibrary.wiley.com/doi/10.1002/cssc.202201955 by Paul Scherrer Institut PSI, Wiley Online Library on [08/05/2023]. See the Terms and Conditions (https://onlinelibrary.wiley.com/terms-and-conditions) on Wiley Online Library for rules of use; OA articles are governed by the applicable Creative Commons License

hydrodynamic length of the nanocellulose ($L$) and the aspect ratio ($L\,d^{-1}$) of nanocelluloses using Equation (5),

$$D = \frac{k_B T}{3\pi\eta L}\left(\ln L - \ln d + c_0 + \frac{c_1 d}{L} + \frac{c_2 d^2}{L^2}\right) \quad (5)$$

where $D$ is the diffusion coefficient, $\eta$ is the viscosity of the solvent, and $c_0$, $c_1$, and $c_2$ are constants.[47] The aspect ratio is crucial to describe the behavior of nanocelluloses in more condensed states, such as colloidal gels and glasses described in Section 4.[38a,45] The strength of DLS is the statistical probing of the whole "ensemble" of particles, but this also comes with the weakness that larger particles have more influence in scattering techniques, so the dimensions are often overestimated. AFM or TEM and image analysis are more accurate but more tedious options to determine the aspect ratio.

Control and evaluation of the colloidal stability of the nanocellulose materials are vital in most applications to fully utilize the inherent properties of the nanocellulose and to tailor the properties of films, aerogels, or gels through a bottom-up engineering approach. However, the characterization of nanocelluloses is a complicated task due to the high aspect ratio of the materials, which in some situations disqualifies many of the standard procedures used for evaluating the colloid stability of colloidal dispersions of spherical particles, such as turbidimetric measurements, dynamic light scattering, or stopped-flow measurements. This challenge means that the colloid properties and the change in colloidal stability of the highly anisotropic nanocelluloses must be evaluated with great care using special methods. Figure 5 shows a summary of suitable methods.

### 3.3. Dissolution at a high enough surface charge

At moderate degrees of modification, the charge is mainly located on surfaces of fibril aggregates, but, as mentioned, when that charge density reaches 1.3 mmol g$^{-1}$, almost all surface hydroxyl groups of the cellulose are substituted. Since about 50% of the cellulose chains are located at the surface, 1.3 mmol g$^{-1}$ corresponds to an effective charge density of 2.6 mmol g$^{-1}$. This effective charge density can be compared to the solubility limit of charged cellulose, such as carboxymethyl cellulose (CMC), which is soluble at a degree substitution of 0.5 to 1.2, corresponding to a charge density of 2.5–5 mmol g$^{-1}$.

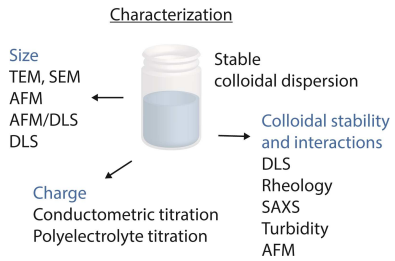


**Figure 5.** Suggested methods for characterizing the colloidal properties of nanocelluloses and evaluating colloidal stability and fibril interactions.

This comparison shows that for highly charged nanocelluloses, the degree of substitution of cellulose chains located at surfaces is in the range where they become soluble. Free soluble chains have indeed been observed by AFM[44] or lost during the regeneration of dissolved highly charged pulps.[48] The resulting mix of intact nanocelluloses and free or partially released charged cellulose chains will affect the colloidal properties and the properties of assembled materials. Fractionating such mixtures is challenging and has not yet been demonstrated. The recommendation for preparing highly charged nanocelluloses that remain intact is to stop at a charge density closer to 1 mmol g$^{-1}$, and not aim for 1.5 mmol g$^{-1}$ as reported in many publications.

### 3.4. Steric stabilization

Adding surface charge is not the only stabilizing mechanism. The second most widely used technique is often referred to as steric stabilization.[49] Steric stabilization involves grafting polymer chains to the nanoparticle's surface, typically polyethylene glycol (PEG), but the modification of the surface of CNCs has also been shown to lead to a loose sterically stabilizing layer.[50] When sterically stabilized nanoparticles come in close contact, the stabilizing polymer chains compress into an entropically unfavorable state since their local concentration increases, similar to the increasing salt concentration in charge stabilization. Likewise, steric stabilization leads to an increased osmotic pressure between the nanoparticles that act to push them apart.

PEG stabilization of nanocellulose has attracted considerable attention and was thoroughly discussed by Kaldéus et al.[51] A general challenge is that the low lateral dimension and large surface area of the nanocelluloses mean that the stabilizing polymer constitutes most of the final material, even at a modest surface coverage. The advantage of sterically stabilized nanocelluloses is that they are theoretically less sensitive to salt,[51] pH, and other solvents.[50,52] Surface modification is often required to provide good compatibility for dispersing nanocelluloses in organic solvents and polymer matrices.[53] Regarding PEG, Fujisawa et al.[52] showed that a physically grafted PEG enabled CNF dispersion in organic solvents and an efficient route for the reinforcement of composites.

### 3.5. Colloidal instability

Colloidal stability is required to utilize nanocellulose to assemble homogeneous or organized materials. In contrast, colloidal instability is a challenging obstacle when working with nanocellulose but can be a valuable tool when controlling the assembly of nanocellulose into materials, which is discussed in Section 7.

For charge-stabilized nanocelluloses, the colloidal stability is very sensitive to the salt concentration or changes in pH value. Salt reduces the repulsion, while reduced pH results in the protonation of titrating groups and reduction of the surface


© 2023 The Authors. ChemSusChem published by Wiley-VCH GmbH

1864564x, 2023, 8, Downloaded from https://chemistry-europe.onlinelibrary.wiley.com/doi/10.1002/cssc.202201955 by Paul Scherrer Institut PSI, Wiley Online Library on [08/05/2023]. See the Terms and Conditions (https://onlinelibrary.wiley.com/terms-and-conditions) on Wiley Online Library for rules of use; OA articles are governed by the applicable Creative Commons License

charge or surface potential. At an added monovalent salt concentration of 10 mM NaCl, the Debye length is only 3 nm, a separation distance at which van der Waals interactions are significant.[10] Around this salt concentration, nanocellulose dispersions often become thick and gelly. The gelling depends not only on the properties and concentration of the nanocellulose but also on the type of added salt, further discussed in Section 5.

The influence of changes in pH depends primarily on the $pK_a$ of the charged groups. Carboxylic acid-functionalized nanocellulose are sensitive to pH below 4, whereas sulfated nanocellulose can handle much lower pH value. The advantage of quaternized nanocellulose dispersion is that they are essentially not influenced by pH value. It is, however, essential to note that a change in pH value equals a change in salt concentration, following $c_s = 10^{-pH}$ so that a pH of 2 or 12 corresponds to 10 mM salt.

Changing the solvent of nanocellulose dispersions considerably impacts colloidal stability, although a maintained dispersion can still be achieved by careful solvent exchange.[54] Depending on the polarity of the solvent, it can also lead to a solvophobic phase separation with a strong attraction between the nanocellulose particles. Scientists who have tried to change the solvent of nanocellulose gels know that they become stiffer in low-polarity solvents. Careful step-wise solvent exchange has been used to preserve the open structure of nanocellulose networks or modified fibers.[55]

Besides the pure solvophobic effects, the solvent also affects the surface charge. The dissociation of a charged group and its counterion is only favorable if the polarity of the solvent is high enough to compensate for the lost enthalpy when the salt dissolves to favor entropy. In solvents with lower polarity, the counterion thus remains condensed on the charged group, known as Mannings condensation, which can also occur in water.[43] The onset of counterion condensation is related to the Bjerrum length ($\lambda_B$) according to Equation (6).

$$\lambda_B = \frac{e^2}{4\pi\varepsilon_0\varepsilon_r k_B T} \quad (6)$$

Where $e$ is the elementary charge, $\varepsilon_r$ is the relative dielectric constant of the medium and $\varepsilon_0$ the vacuum permittivity. $\lambda_B$ is the separation at which the electrostatic interaction between two elementary charges is similar in magnitude to the thermal energy ($k_BT$). Having two immobile charged groups at a closer distance is thus unfavorable, and the counterion will condense on one of them to minimize the free energy. Thus $\lambda_B$ is the shortest possible distance between two charges on the nanocellulose before condensation occurs and relate to the maximum effective charge density. However, the theoretical average distance between charges on the nanocellulose surface in water approaches 1 nm at charge densities above 1 mmol $g^{-1}$. Still, considerable condensation was needed to explain the colloidal behavior of nanocellulose, which might relate to the heterogeneous coverage of charged groups.[20]

This effect is more pronounced in other solvents since a reduced dielectric constant of the solvent ($\varepsilon_r$) results in an increased Bjerrum length according to Equation (6) and, thus, a lower maximum effective charge density of the nanocellulose. The remaining double layer repulsion is also reduced according to Equation (3).

A final complication is aging of nanocellulose dispersions. If the colloidal stability is insufficient, longer-term aging may lead to the association of fibrils. Following probability, some fibrils will collide over time and fall into a primary minimum of van der Waals attraction, slowly creating a network. This behavior is common for colloidal systems since most are in a semi-stable state.

## 4. Volume-Spanning Arrested States: Colloidal Glasses and Gels

Due to their high aspect ratio, nanocelluloses form networks where fibrils affect other fibrils over large distances via a series of connections. One can picture it as a nanoscale game of jackstraws or Jenga, with the difficult task of removing sticks or blocks without disturbing the load-bearing network. The interlocking of fibrils in nanocellulose dispersions results in volume-spanning arrested states at very low solids content, and these states depend on the aspect ratio of the fibrils. The formation of arrested states is thus more prevalent for high aspect ratio CNFs than for lower aspect ratio CNCs.

The volume-spanning arrested states allow easy preparation of useful gels but are also challenging when processing nanocelluloses into materials. For example, nanocelluloses at high concentrations are too viscous to be processed homogeneously. These states also prevent efficient transportation of nanocellulose samples since they have to be manufactured as gels containing 90–99% water. This section contains a theoretical description of nanocellulose networks and the challenges and opportunities related to their properties. For further reading, we refer to a recent review by Stokes and co-workers, also discussing the rheological properties in different concentration regimes.[56]

### 4.1. Overlap concentration and volume-spanning arrested states

The concept of overlap concentration was developed for polymer solutions to describe dilute, semi-dilute, or concentrated regimes for which different theoretical models apply.[57] The overlap concentration is when the total volume of unperturbed polymer coils is the same as the volume of the solution, which is often determined by rheological measurements or estimated by scattering techniques. Above this critical concentration, polymer coils overlap and affect each other.

This concept can also be applied to rod-shaped nanoparticle dispersions, such as nanocelluloses. In this case, the rod dimensions are described by the aspect ratio: $a = L\,d^{-1}$ in which $L$ and $d$ are the length and diameter of the rod, respectively. The crowding factor ($N_{3D}$), which is commonly used in the pulp


© 2023 The Authors. ChemSusChem published by Wiley-VCH GmbH

18645564x, 2023, 8, Downloaded from https://chemistry-europe.onlinelibrary.wiley.com/doi/10.1002/cssc.202201955 by Paul Scherrer Institut PSI, Wiley Online Library on [08/05/2023]. See the Terms and Conditions (https://onlinelibrary.wiley.com/terms-and-conditions) on Wiley Online Library for rules of use; OA articles are governed by the applicable Creative Commons License

and paper industry to characterize flocculation, can be adapted to describe the number of rods occupying a spherical volume with a diameter equal to the length of the rods according to Equation (7).[58]

$$N_{3D} = \frac{2}{3}\phi a^2 \tag{7}$$

Where $\phi$ is the volumetric concentration, also called volume fraction or solidity. A similar geometric model based on the number of rods ($n$) and the box they occupy ($nL^3$) is frequently used.[56] The crowing factor model applies to networks of nanoparticles that repel each other via, for example, overlapping double layers.

In the case $N_{3D}=1$, that is, $\phi = 1.5\,a^{-2}$, spheres formed by the rotational volume of individual nanocellulose particles start to overlap, and the volumetric overlap concentrations occur (3D overlap). Typical CNFs with a length of 600 nm and width of 3 nm are estimated to have an overlap concentration of 56 mg $L^{-1}$ or 0.0056 wt%, assuming a cellulose density of 1500 kg $m^{-3}$.[38b] The low overlap concentration shows that it is rarely reasonable to think of CNFs as freely rotating rods defined by the dilute regime. For typical CNCs with a length of 200 nm and diameter of 7 nm, the overlap concentration is 2.8 g $L^{-1}$ or 0.28 wt%, which shows the significant difference between these nanocelluloses.[38a]

At concentrations above the volumetric overlap concentration, in the semi-dilute regime, there is an increasing probability of interactions and restrictions with increasing concentration. However, in a simplified perspective, the rods are mainly prevented from rotating in three dimensions and are still allowed to translate or rotate parallel to each other. The network is thus liquid. However, the gradually increased restrictions manifest in a significantly increased viscosity with increasing concentration and, at some point, a transition from a Newtonian to a viscoelastic behavior. This transition occurs at a crowding factor of roughly 16, representing a concentration of 0.05–0.06 wt% for fibrils with a length of 600 nm and a diameter of 2–3 nm (Figure 6).[38b] Based on the percolation theory of fibers, $N_{3D}=16$ has been determined to be the gel crowding factor, whereas $N_{3D}=1$ is the collision threshold.[59] In percolation theory, $N_{3D}=60$ represents the rigidity threshold of a mechanical network that requires at least 3 contacts per fibril.

At even higher concentrations, the elasticity of the network increases until a volume-spanning arrested state (VAS) is reached with restricted movement and relaxation times so long that the network has the properties of a solid. The VAS threshold is the transition to the concentrated regime that depends mainly on the aspect ratio of the nanoparticle. Nordenström et al. showed that the relationship between the volumetric concentration at the VAS threshold and the aspect ratio of nanocelluloses (Figure 7) is described by Equation (8).[38a]

$$\phi_{VAS} = \frac{3}{2}a^{-1} \tag{8}$$

By inserting Equation (8) in Equation (7), it can be shown that the VAS threshold occurs approximatively when the crowding factor is equal to the aspect ratio of the particle ($N_{3D} \sim a$). A qualitative geometrical meaning is the overlap of cylinders formed by rotating CNFs, which can be called the 2D overlap concentration. A typical CNF dispersion has a VAS threshold at a concentration of 1 wt% or at $N_{3D}=a=200$. In the case of CNCs, the VAS threshold is at roughly 8 wt% or at $N_{3D}=a=30$.

In the same way as the 3D crowding factor, we derived a 2D crowding factor based on cylinders with a diameter equal to the length of the nanocellulose particle and the height as the effective thickness. By assuming a circular cross-section of the particles, same as in Equation (7), the 2D crowding factor is given by Equation (9),

$$N_{2D} = \phi a \tag{9}$$

which is the same expression as the previously used dimensionless concentration $c=\phi a$ suitable for comparing nanocelluloses with vastly different aspect ratios within a single phase diagram.[56] At $N_{2D}=1$ the 2D overlap occurs, that is, at $\phi = a^{-1}$.

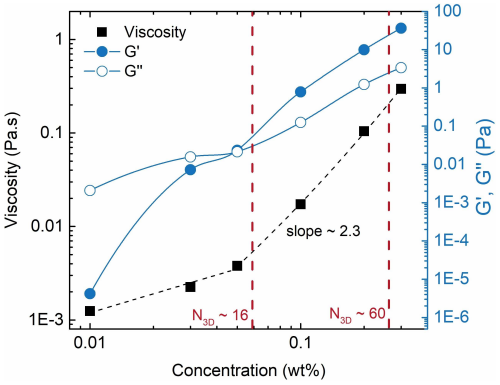


**Figure 6.** Rheological properties of TO-CNF networks with a charge density of 0.38 mmol $g^{-1}$ and their transitions from percolation theory. The data were kindly provided by Geng et al.[38b]

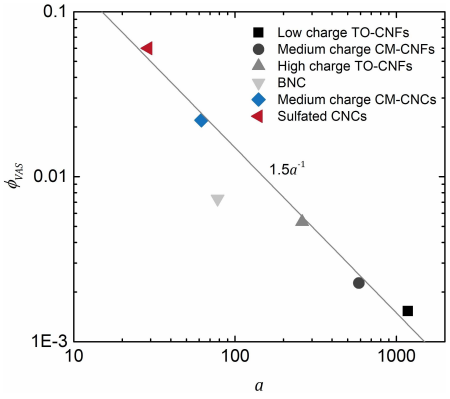


**Figure 7.** Relationship between the VAS threshold and aspect ratio of different nanocelluloses. BNC is short for bacterial nanocellulose. The data were kindly provided by Nordenström et al.[38a]


© 2023 The Authors. ChemSusChem published by Wiley-VCH GmbH

1864564x, 2023, 8, Downloaded from https://chemistry-europe.onlinelibrary.wiley.com/doi/10.1002/cssc.202201955 by Paul Scherrer Institut PSI, Wiley Online Library on [08/05/2023]. See the Terms and Conditions (https://onlinelibrary.wiley.com/terms-and-conditions) on Wiley Online Library for rules of use; OA articles are governed by the applicable Creative Commons License

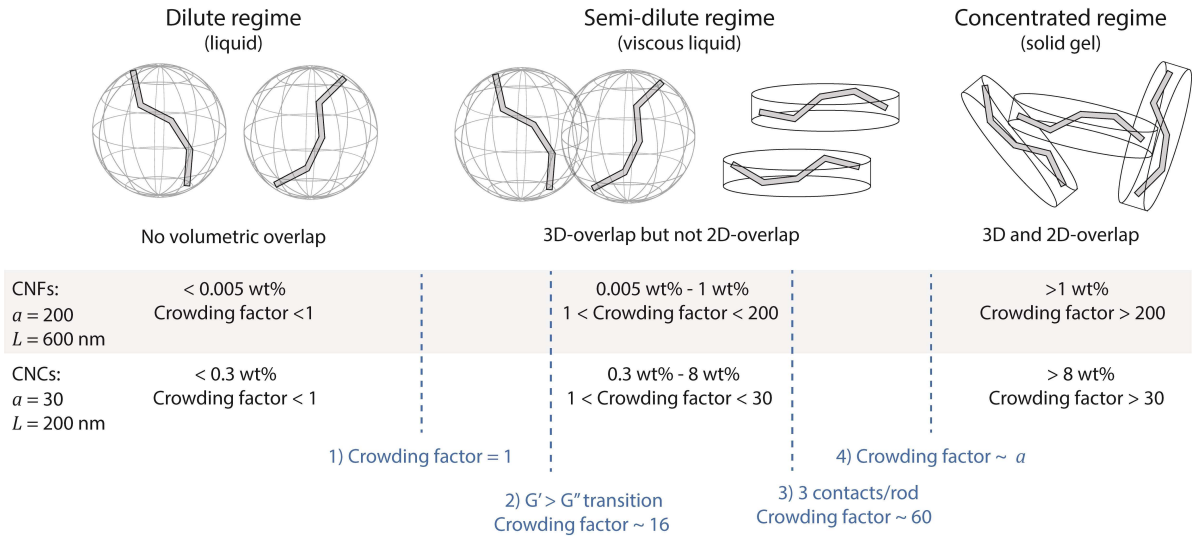


**Figure 8.** Schematic representations and typical values of the different concentration regimes for nanocelluloses. Dashed lines mark the transitions 1–4 discussed in the text.

The difference between this and the experimental relationship in Equation (8) is a factor of 1.5, which can be considered a shape factor representing kinks in the fibrils or other physical properties that make the cylinder's effective thickness slightly larger.

Table 1 shows how the 2D crowding factor model compares to the transition from the semi-dilute to the concentrated regime using the VAS threshold measurements. Calculations on the effective thickness estimated by the Debye length based on the double layer extension under the salt concentration at the VAS threshold are included. The 2D crowding factor model gives concentrations in the same order of magnitude, that is, 0.75 and 5.2 wt% for CNFs and CNC, respectively, compared to 1 and 7.7 wt% in the experimental VAS model.[38a] To reach the same concentration, the effective thickness or height of the cylinder containing a particle has to be 4 and 11 nm, respectively, about a factor 1.5 larger, as mentioned above. By adding the double layer extension to the solid particle thickness in both directions, the estimated effective thickness is 9 and 11 nm, respectively. The model thus fits better for CNCs, maybe because CNFs are not stiff rods because the kinks provide some flexibility and the effective aspect ratio is smaller. Nevertheless, despite its simplicity and assumptions, the crowding factor model is surprisingly accurate in describing the concentration regimes of nanocellulose dispersions.

**Table 1.** Comparison of the 2D crowding factor model and the experimental VAS threshold model to describe the transition from the semi-dilute to the concentrated regime.[38a]

| Property | CNFs | CNCs |
|---|---|---|
| $L$ [nm] | 600 | 200 |
| $d$ [nm] | 3 | 7 |
| $a$ | 200 | 30 |
| charge density [mmol g$^{-1}$] | 1 | 0.35 |
| VAS threshold [wt%][a] | 1 | 7.7 |
| $N_{2D} = 1$ [wt%] | 0.75 | 5.2 |
| fitted $d_{eff}$ [nm][b] | 4 | 11 |
| $c_{salt}$ [mM][c] | 10 | 27 |
| Debye length [nm] | 3 | 2 |
| estimated $d_{eff}$ [nm][d] | 9 | 11 |

[a] From the experimental model. [b] Thickness of particle required for the 2D crowding factor model to agree with the experimental VAS threshold: $\phi = 3/2\,a^{-1}$. [c] Calculated from the concentration of counterions at the VAS threshold, i.e., charge density times weight of nanocellulose. [d] Estimated by adding the Debye length on each side of the particle: $d_{eff} = d + 2\,\kappa^{-1}$.

In conclusion, nanocellulose dispersions undergo four transitions when the concentration is gradually increased (Figure 8):

1) The overlap concentration: dilute to semi-dilute transition (3D overlap)
2) The transition between a Newtonian and a viscoelastic behavior in the semi-dilute regime
3) The rigidity threshold of 3 contacts/rod
4) The VAS threshold (3D + 2D overlap): transition to the concentrated regime

The aspect ratio of the nanoparticle determines the concentration at which these transitions occur and the range of the semi-dilute regime (Figure 8). For high aspect ratio CNFs, the 3D-overlap occurs at very low concentrations, and the semi-dilute regime is wide. For low aspect ratio CNCs, 3D and 2D overlap are closer but at a significantly higher concentration. The 3D and 2D overlap for a spherical particle is the same thing. The aspect ratio of nanocelluloses depends mainly on the source of the cellulose and the preparation process. For instance, a higher degree of modification, that is, higher charge density results in more hydrolysis and shorter CNFs.[13,38,60]


© 2023 The Authors. ChemSusChem published by Wiley-VCH GmbH

1864564x, 2023, 8, Downloaded from https://chemistry-europe.onlinelibrary.wiley.com/doi/10.1002/cssc.202201955 by Paul Scherrer Institut PSI, Wiley Online Library on [08/05/2023]. See the Terms and Conditions (https://onlinelibrary.wiley.com/terms-and-conditions) on Wiley Online Library for rules of use; OA articles are governed by the applicable Creative Commons License

### 4.2. Colloidal glasses and gels

It is essential to note that the crowding factor models describe a repulsive network. If there is an attraction between particles, aggregation and gelation would be observed in the dilute and semi-dilute regimes. For example, in Figure 7, the VAS threshold of the bacterial nanocellulose (BNC) is lower than expected based on the aspect ratio, probably because BNC has a low charge density of only 0.06 mmol $g^{-1}$ compared to at least 0.3 mmol $g^{-1}$ for all the other nanocellulose samples in the study.[38a] A lower charge means the double layer repulsion is weak, and attraction between particles is expected to initiate an arrested state already in the semi-dilute regime. These two types of VASs are separated according to the interactions that govern their formation; colloidal gels form due to attractive interactions, while colloidal glasses result from mainly repulsive interactions.[61]

In a colloidal glass, the particles are constrained by volume per particle limitations, also known as caging. Because of the repulsive interparticle interactions, a colloidal glass can be diluted back to the semi-dilute regime,[62] or its properties can be changed by changes in pH, ionic strength,[61] temperature,[63] or mechanical force.[63] Conversely, a colloidal gel is a percolated network that forms due to attraction between particles and is caused by aggregation and gelation. The gelation can be reversible or irreversible but is not as dynamic as a colloidal glass.[61]

Although the VAS of CNFs is often called a gel (even we do it due to the intuitive feeling associated with a gel), to be accurate, it should be called a colloidal glass in cases where an increased concentration of repulsive nanocelluloses forms the VAS.[38a] However, the glass or gel formation depends on the charge density and environment where the nanocellulose is dispersed. For example, treating charged nanocelluloses with acid to neutralize the surface charge and removing the double layer repulsion is a well-known method of forming gel networks even at concentrations below the VAS threshold.[64] In this case, the overlap concentration ($N_{3D}=1$) or the gel crowding factor ($N_{3D}=16$) is the theoretical limit of where a self-supporting gel network can be formed. Adding multivalent ions is another way of inducing attraction between charged nanocelluloses to initiate gel formation (Section 5).[65] A schematic phase diagram for the formation of glasses and gels from nanocellulose is shown in Figure 9a, and Section 7 elaborates on how gel-initiation mechanisms are used in the design of hydrogels and strong filaments.

The VAS-threshold of nanocelluloses can be compared to those of other rod-shaped particles using the phase diagrams of Solomon and Spicer with boundaries from percolation theory.[66] The boundary for dilute to semi-dilute is, in this case, $24a^{-2}$ which is the gel crowding factor of $N_{3D}=16$. The glass region is between a lower percolation bound of $0.7a^{-1}$ and a maximum packing of stiff rods $5.4a^{-1}$. The data by Nordenström et al. end up in the lower third of this region (Figure 9b), whereas other CNC examples fall just below. Discrepancies are probably related to the method used to determine the aspect ratio or the influence of the effective aspect ratio due to double

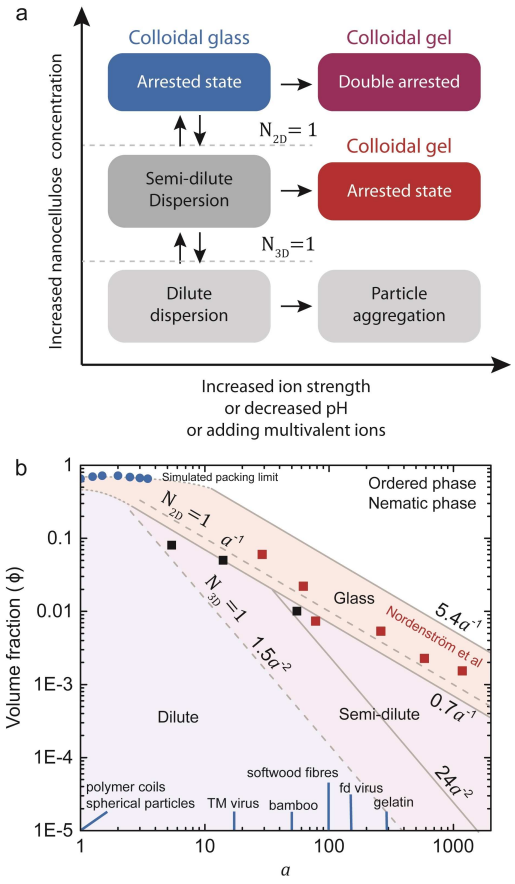


**Figure 9.** a) Schematic phase diagram of how colloidal glasses and gels are formed from nanocellulose. b) regime diagram of rod-shaped particles inspired by Solomon and Spicer.[66] Data points represent measured transitions to a glass. Red squares are wood-derived CNFs (carboxylated) and CNCs (sulfated or carboxylated) from Nordenström et al.[38a] Black squares are wood-derived CNCs (sulfated).[67]

layers. Random networks cannot fit in the available volume at volume fractions above the upper bound of $5.4a^{-1}$, and only ordered phases are possible at these concentrations. One ordered phase common for rods, such as CNCs, is the nematic phase discussed in Section 5.5.

### 4.3. Characterizing arrested state transitions and their properties

DLS has been a valuable tool to characterize the change from a liquid colloidal dispersion to an arrested state.[64] An example of this is shown in Figure 10, where the intensity correlation function curves are shown for different times (1 min between each curve) after adding HCl to a free-flowing dispersion of 1 g $L^{-1}$ of CNFs. Three minutes after HCl addition, there is a development of two correlation plateaus where the second plateau starts at around $10^4$ μs indicating a structure with a much slower relaxation time, that is, the gel state. In this state, the fibrils are locked together in contact points due to attractive van der Waals interactions preventing the fibrils from sliding


© 2023 The Authors. ChemSusChem published by Wiley-VCH GmbH

1864564x, 2023, 8, Downloaded from https://chemistry-europe.onlinelibrary.wiley.com/doi/10.1002/cssc.202201955 by Paul Scherrer Institut PSI, Wiley Online Library on [08/05/2023]. See the Terms and Conditions (https://onlinelibrary.wiley.com/terms-and-conditions) on Wiley Online Library for rules of use; OA articles are governed by the applicable Creative Commons License

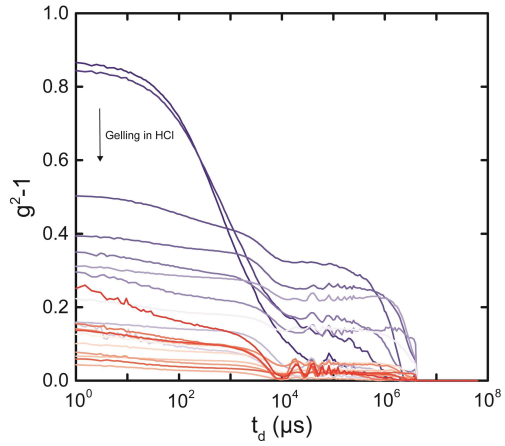


**Figure 10.** Intensity Correlation Functions for a CNF dispersion with a concentration of 1 g $L^{-1}$. The top curve is the reference curve collected 1 min after adding a drop of 0.1 M HCl and then each subsequent curve represents measurements after one additional minute (dark blue to dark red). The data were kindly provided by Fall et al.[64]

along each other's surfaces. This association can be explained by the balance between double layer repulsion and van der Waals attraction in the DLVO theory.

There is no macroscopic aggregation of the fibrils into larger flocs inside these gels since the fibrils do not have the freedom to relax due to the volumetric overlap. At a concentration of 1.4 g $L^{-1}$, it was estimated that the average distance between two contact points in such a gel was 170–220 nm showing that very few contact points per fibril are needed to achieve elastic properties of the gels.[64] These in situ formed gels were further evaluated with careful rheological measurements using strain-relaxation measurements. It was shown that bending of the fibrils dominated at small deformations, whereas sliding started to occur at larger deformations. A new equilibrium could be reached after stress release, indicating a reorientation of the fibrils without a macroscopic failure of the gel.[64] The reorientation was shown along the loading axis using polarized optical microscopy. The recovery of network properties is known as the unique stick-slip-stick behavior of nanofibrils.[68]

Rheological evaluation of nanocellulose is a powerful tool but must be performed with great care when evaluating gel properties. The gel initiation should be performed inside the rheometer setup to avoid moving and damaging the gels after locking. Care should also be taken to avoid slippage between the gel and the rheometer surfaces, especially when evaluating gels with higher elastic moduli.

### 4.4. The mesh size of nanocellulose networks

Liquid or arrested nanocellulose networks have a characteristic mesh size ($\xi$) depending on the dimensions, stiffness, and concentration of the particles. The mesh size determines diffusion inside nanocellulose networks, which can be utilized to separate or stabilize other colloidal or macroscopic particles, further discussed in Section 7.9. Simple geometrical calculations can estimate the mesh size,[66] but measuring the mesh size is more challenging. In this review, mesh size refers to both the static mesh size in a locked network and the effective mesh size of a dynamic network.

One indirect approach for estimating the mesh size of nanocellulose networks was demonstrated by Arcari et al.[69] by combining rheology and theoretical considerations. The underlying assumption guiding this experiment was that at semi-dilute conditions, where a mesh size can be defined, the physical properties of the nanocellulose network are only dependent on the concentration and not on the size of the nanocellulose particles.[70] By studying the elastic shear moduli of the nanocellulose networks for samples at two different concentrations (0.06–0.07 wt% and 0.4 wt%), gelled by HCl addition and by changing the aspect ratio, it was found that the modulus of the gel at the higher concentration remained constant independent of the size or aspect ratio of the particles as expected in the semi-dilute regime. For the lower concentration, a change from an aspect ratio-dependent network modulus to a plateau of constant aspect ratio-independent network stiffness was observed (Figure 11). This sudden change in behavior was interpreted as an aspect ratio-driven transition from dilute to semi-dilute conditions, and the transition point was used to estimate the mesh size using Equation (10), valid for stiff fibrils ($L_p \gg L$),[71]

$$\xi = \sqrt{\frac{2L_m^3}{3L_p}} \tag{10}$$

where $L_p$ is the persistence length, $L$ the contour length and $L_m$ the concentration-dependent entanglement length. Taking $L_m = L$ at the transition point where the shear modulus ($G'$) shows a kink in Figure 11 and inserting the contour length for this sample ($L_m = 292$ nm) and the persistence length of TO-CNF ($L_p = 2.5$ μm[44]), a mesh size of 81 nm was estimated.

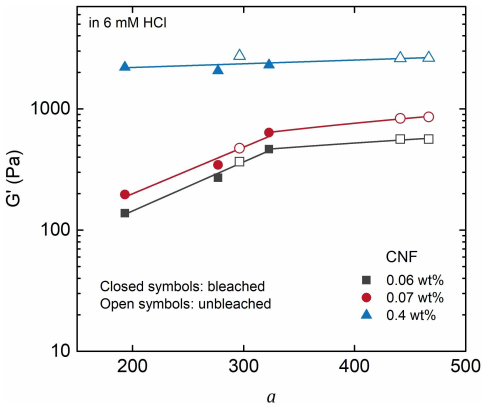


**Figure 11.** The elastic shear modulus ($G'$) for gels formed from CNFs of different aspect ratios obtained from rheology at $\omega = 1$ rad $s^{-1}$, $\gamma = 0.5$%, and 20 °C for different concentrations after adding 6 mM HCl. The colors indicate different concentrations, and the squares and circles represent CNFs from bleached and unbleached pulps. The data were kindly provided by Arcari et al.[69]


© 2023 The Authors. ChemSusChem published by Wiley-VCH GmbH

18645564x, 2023, 8, Downloaded from https://chemistry-europe.onlinelibrary.wiley.com/doi/10.1002/cssc.202201955 by Paul Scherrer Institut PSI, Wiley Online Library on [08/05/2023]. See the Terms and Conditions (https://onlinelibrary.wiley.com/terms-and-conditions) on Wiley Online Library for rules of use; OA articles are governed by the applicable Creative Commons License

A direct way to measure mesh sizes was demonstrated by Nordenström et al.[72] using the diffusion of spherical tracer particles and fluorescent correlation spectroscopy. The Langevin–Rondelez approach[73] was used to distinguish between particles with a diameter ($d$) that were in the mesh mode ($d/\xi <$ 1) and diffused according to the macroscopic viscosity of the network or particles that were more influenced by direct contact with the network ($d/\xi > 1$).

The experiments showed that below 0.2 wt% ($N_{3D} = 89$), but still above the rigidity threshold of 3 contacts per fibril, the network was highly dynamic and had little effect on the diffusion of the tracer particles. Above 0.2 wt%, particles with a size of 20–40 nm diffused in a static network as predicted by the Stokes–Einstein equation and the Langevin–Rondelez model, whereas particles with sizes of 100–500 nm were trapped in the network (Figure 12a), reasonably agreeing with the estimated mesh size of 81 nm from the previously discussed rheological approach.[69]

A relative diffusion proportional to roughly $c^{-2}$, where $c$ is concentration, was observed following the macroscopic viscosity of nanocellulose dispersions. These experimental findings were compared to a coarse-grained molecular dynamics simulation which showed excellent agreement (Figure 12b).[72]

The mesh size is inversely proportional to the shear modulus of fibril networks; for semi-flexible actin fibrils, a smaller mesh size gives stiffer networks, according to Equation (11),[74]

$$G' \approx \frac{\kappa^2}{k_B T}\ \xi^{-5} \tag{11}$$

where $\kappa$ represents the bending stiffness of the fibril and relates to $L_p$. The same expression for polymer (molecular) networks is Equation (12),[74a]

$$G' \approx k_B T\ \xi^{-3} \tag{12}$$

showing that the stiffness of fibrillar gels scales with the mesh-size to the power of $-5$ while polymer gels to the power of $-3$, directly demonstrating the higher stiffness of fibrillar networks at low concentrations. Inserting $\xi = 80$ nm based on the above calculation and $L_p = 2.5$ µm in the approximate relation $\kappa \approx L_p k_B T$,[74b] the calculated modulus is 8 kPa which is a bit high but of reasonable magnitude compared to Figure 11. Compared to Figure 6, which shows the moduli of unlocked nanocellulose networks (colloidal glass), Equation (11) better explains gels formed by adding acid (colloidal gel) that are more similar to interconnected actin networks on which the model was based. HCl addition to a nanocellulose network increases the stiffness by about two orders of magnitude.[64] Models for colloidal glasses that consider dynamic fibril–fibril interactions are still needed, and the variety of surface chemistries that can be applied (Section 2) will significantly influence fibril-fibril interactions.

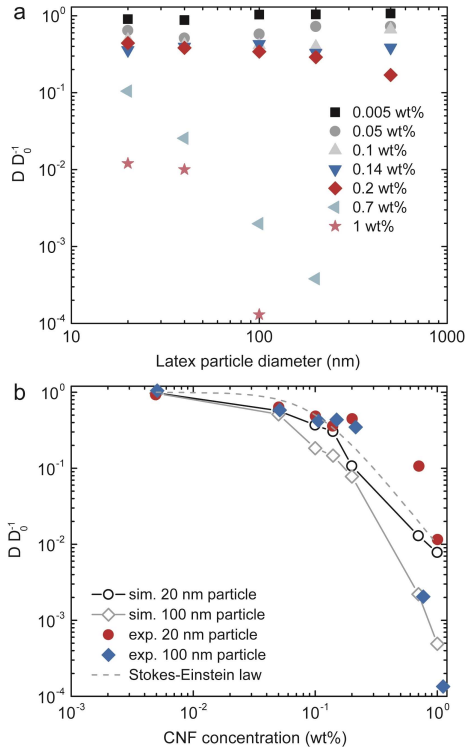


**Figure 12.** a) Relative diffusion of tracer particles of different sizes in TO-CNF networks of different concentrations. b) Comparison of experimental data and coarse-grained molecular dynamic simulations. The data were kindly provided by Nordenström et al.[72]

### 4.5. Shear-thinning

The VAS-formation does not mean the absence of movement of the nanocelluloses constituents. They can still move or diffuse in the network, but the relaxation times are exceptionally long. However, a flowing liquid state can be achieved by assisting the nanocelluloses to overcome the energy barrier of the network by mechanical agitation. Specifically, shear or accelerated flows formed, for example, when a VAS is forced through a narrow channel, resulting in fibril alignment, reducing their three-dimensional restrictions from overlap and allowing them to flow (Figure 13).[75] In rheology terms, this is called shear-thinning and is defined as a liquid whose viscosity decrease under shear strain. The parallel conformation is not energetically favorable since the double layer repulsion is maximized in this configuration. Thus, due to repulsion and rotary diffusion, the network will return to an orthogonal random network when the shearing or acceleration stops.[76] At specific conditions, the parallel configuration remains stable, occurs spontaneously, and is called a nematic phase, discussed in Section 5.5.

Shear-thinning is an intrinsic and valuable property of nanocellulose dispersion. It is crucial during the disintegration of fibers into fibrils via homogenization and the transition from a flowing state in a needle to a locked gel network when the flow stops, which allows 3D printing of nanocelluloses.[77] Nanocelluloses can thus be used to develop bio-inks for the 3D printing of hydrogel scaffolds aimed toward regenerative medicine.[78] The same principle makes nanocelluloses, espe-


© 2023 The Authors. ChemSusChem published by Wiley-VCH GmbH

1864564x, 2023, 8, Downloaded from https://chemistry-europe.onlinelibrary.wiley.com/doi/10.1002/cssc.202201955 by Paul Scherrer Institut PSI, Wiley Online Library on [08/05/2023]. See the Terms and Conditions (https://onlinelibrary.wiley.com/terms-and-conditions) on Wiley Online Library for rules of use; OA articles are governed by the applicable Creative Commons License

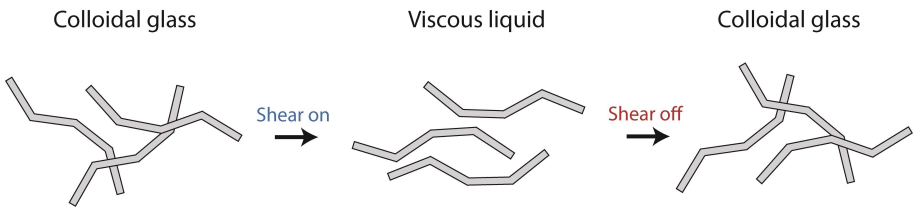


**Figure 13.** Nanomechanical description of shear-thinning of a nanofibril network.

cially CNFs, very efficient thickeners in food processing industries or, for example, in the production of inks for gel-based ballpoint pens.[79]

A phenomenon related to shear thinning is what scientists often observe as the formation of weak physical gels (glasses) after aging nanocellulose dispersions for a few hours or days. The explanation is that when a nanocellulose dispersion is prepared by diluting a more concentrated gel, stirring or mixing provides shear forces that lead to a local alignment of fibrils, which is unavoidable. The fibrils will then strive to return to a random network when the dispersion is left to rest, and this can take some time, given that the network has to reorganize. Slight shaking or stirring will reintroduce alignment and return it to a flowing state. The alignment can be visually observed if the stirred dispersion is placed between crossed polarizers.

### 4.6. Materials processing limitations due to volume-spanning arrested states

The high aspect ratio of CNFs is an opportunity to create low-density solid networks, such as hydrogels and aerogels.[37a,80] However, the VAS is also a challenge that creates problems already during the homogenization of fibers into nanofibrils. For the homogenization to be efficient, the fibers are disintegrated at a concentration of around 2 wt%. Concentrations above this are not feasible because the gel is so thick that even shear-thinning cannot make it flow properly. In contrast, homogenization at concentrations below the VAS threshold increases the time and energy consumption of the disintegration.

An undesirable outcome of the processing at 2 wt% is that there is not enough room to form a homogenous random network in the gel (Figure 14b). The fibrils are thus forced into a parallel orientation during the shearing in the homogenization step, and when the shear stops, the fibrils cannot go back to a random distribution due to network restrictions. Remember that at 2 wt%, the concentration is twice the overlap where 3D and 2D rotations of fibrils are restricted. In most CNF gels with a concentration above 1 wt%, this network heterogeneity can be shown by birefringence under crossed-polarizers (Figure 14a). Domains with a parallel orientation of CNFs are visible by birefringence. These domains do not contribute to the network strength to the same degree and could be called defects in the network. Hydrogels prepared of CNF dispersions that have not been diluted to below the VAS threshold thus have inferior network structure because there is insufficient volume to form a homogeneous network. Increasing the concentration from a

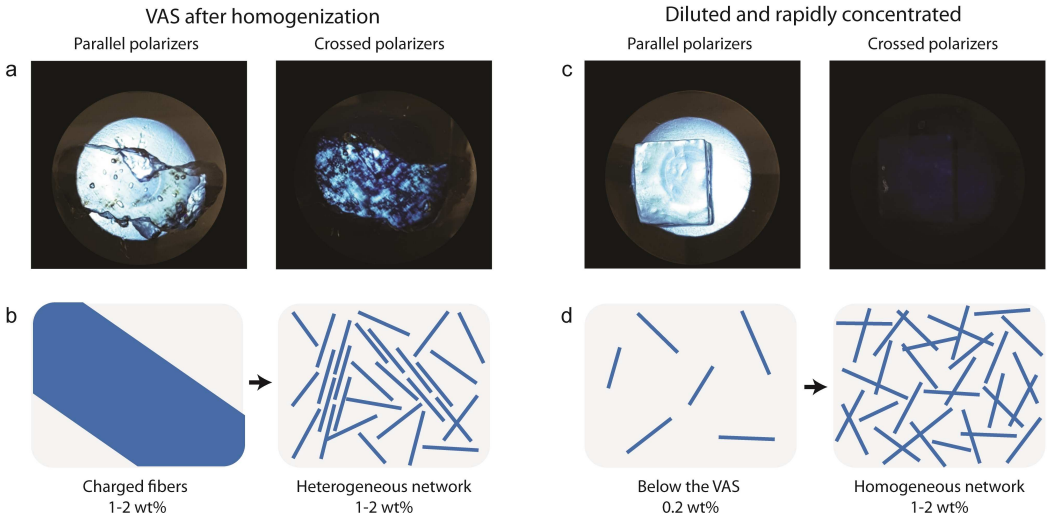


**Figure 14.** Birefringence and schematic representation of a, b) a typical CNF gel formed by homogenization at a concentration above the VAS threshold, and c, d) a CNF gel formed by rapidly increasing the centration, using vacuum filtration, starting at a concentration below the VAS threshold. Partly adapted with permission from Benselfelt et al.[81] Copyright 2019 American Chemical Society.


© 2023 The Authors. ChemSusChem published by Wiley-VCH GmbH

1864564x, 2023, 8, Downloaded from https://chemistry-europe.onlinelibrary.wiley.com/doi/10.1002/cssc.202201955 by Paul Scherrer Institut PSI, Wiley Online Library on [08/05/2023]. See the Terms and Conditions (https://onlinelibrary.wiley.com/terms-and-conditions) on Wiley Online Library for rules of use; OA articles are governed by the applicable Creative Commons License

diluted state results in a random network where most of the fibrils carry the load (Figure 14d), and the outcome is robust and self-supporting hydrogels such as the square piece in Figure 14c.[81] When preparing films by casting or vacuum filtrations, starting below the VAS threshold is vital to prepare homogeneous networks. However, it should be noted that over time even semi-dilute dispersions start to self-organize into nematic phases (Section 5.5), and the above discussion is valid for reasonably rapid processing such as vacuum filtration or quick gelling by acid or metal ions.

## 5. Colloidal Stability Beyond Continuum Electrostatics

The properties of different charged groups on the nanoparticle surface (Section 2) are not considered in the DLVO theory. Based on predictions from this theory, nanocelluloses with different surface groups would behave more or less the same. However, in a more realistic model, the properties of a carboxyl group are significantly different from those of a phosphate group in terms of, for example, size, charge density, hydration, and polarizability. The surface charge is compensated for by counterions with properties that can also differ dramatically. The counterion properties are essential for nanoparticles since the counterion cloud makes up most of the effective particle volume, unlike for microparticles, where the counterion cloud is negligible to the particle size (Figure 15). Hence, the counterion cloud determines much of the properties of the nanoparticle in dispersion and exchanging the counterions impacts the colloidal behavior.[2] Furthermore, nanoparticles with asymmetric shapes have asymmetric surface potentials, influencing their organization and self-assembly. These nano-effects are most prominent for particles in the lower nanometer range and are also crucial for other research areas, such as nanoelectrodes, which are described by the same theories as those used for charged colloids.[82]

In the DLVO theory, the Poisson–Boltzmann equation describes the counterion cloud using average ion concentrations and bulk properties, known as mean-field approximations or continuum electrostatics. In a continuum electrostatic model, the counterion concentration is assumed to be the same at every point in a given plane outside the surface (Figure 16a).

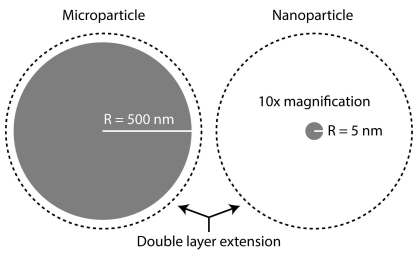


**Figure 15.** Schematic drawing of the double layer extension relative to the particle size. The extension depends on the electrolyte concentration and is described by the Debye length.

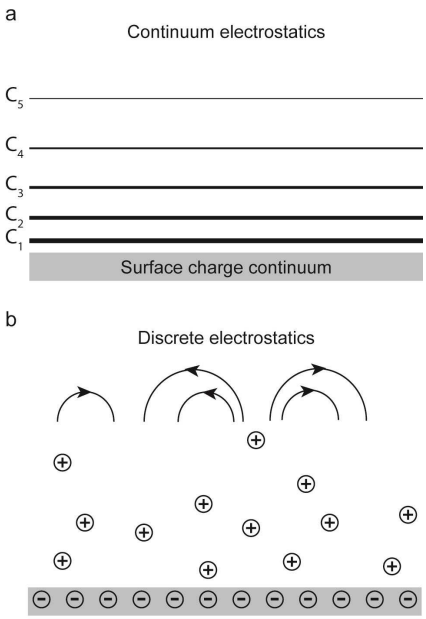


**Figure 16.** Schematic drawing of a continuum (a) and a discrete (b) model of a charged surface and its double layer; $C_1$–$C_5$ in (a) are continuum ion concentrations in different planes outside the surface. The heterogeneous distribution of counterions in (b) leads to a polarization of the counterion cloud, represented by the field lines.

However, in reality, ions are discrete, and the local ion concentration fluctuates over time which is induced by thermal energy ($k_BT$) or influence from nearby electrical fields (Figure 16b).[83] Consequently, the DLVO theory fails for certain colloidal systems, and specific ion properties and the discreteness of ions and charged groups must be considered.

Additional problems of using classical DLVO theories for predicting nano-colloidal stability/instability have recently been summarized.[2,84] Apart from the obvious fact that the particle dimensions are often smaller than the Debye length, the assumptions that hydrated ions have no volume compared to the nanoparticle and the assumptions of bulk dielectric constants at these dimensions become very questionable.

The DLVO theory is still surprisingly accurate for many colloidal systems and is most useful for academic and industrial research and development. However, more realistic theories are needed to better understand complex systems such as nanocelluloses. In this respect, and today, the theories of ion–ion correlation and specific ion effects have been developed to explain situations that continuum models in the DLVO theory cannot describe.

### 5.1. Ion–ion correlation

Oosawa first introduced a theory for the heterogeneity of the counterion cloud in 1971,[83] followed by Bratko et al.[41b] and Kjellander and Marcělja,[85] who developed the more detailed theory of ion–ion correlation in the 1980s. In principle, Ion–ion correlation is similar to the electron-electron correlation (elec-


© 2023 The Authors. ChemSusChem published by Wiley-VCH GmbH

1864564x, 2023, 8, Downloaded from https://chemistry-europe.onlinelibrary.wiley.com/doi/10.1002/cssc.202201955 by Paul Scherrer Institut PSI, Wiley Online Library on [08/05/2023]. See the Terms and Conditions (https://onlinelibrary.wiley.com/terms-and-conditions) on Wiley Online Library for rules of use; OA articles are governed by the applicable Creative Commons License

trodynamic), which is called dispersion or London-dispersion interactions in the van der Waals theory. In the same way as quantum oscillations of electrons in molecules correlate in a way that generates attraction,[86] so do fluctuating ion densities in counterion clouds. At a given time, the ion distribution outside a charged surface is heterogeneous, leading to a polarization of the counterion cloud (Figure 16b). When two charged surfaces of the same sign approach each other, the fluctuation of local ion concentration starts to correlate, resulting in attraction. Ion–ion correlation is omnipresent, but for surfaces with low charge density and monovalent counterions, the effect is small compared to the double layer repulsion. When the charge density of the surface increases and the counterions are multivalent, ion–ion correlation can overpower the double layer repulsion completely so that overall attraction occurs between like-charged particles. The system changes from repulsive to attractive when monovalent counterions are exchanged for divalent ions for colloids with a surface charge higher than 0.1–0.2 $C\,m^{-2}$.[41] Many nanocelluloses fall within this range, and the assumptions of the DLVO theory are completely inaccurate for such systems.

It is experimentally challenging to study the effect of ion–ion correlation since it overlaps with specific-ion effects (Section 5.2). Qualitative experimental insight can be attained when both theories are simultaneously considered, which is discussed in Section 5.3. Another challenge is the potential nonadditivity at the nanoscale mentioned in Section 5.4.

### 5.2. Specific ion effects

Hofmeister first introduced specific ion effects in 1888 in his study of how different salts affected the colloidal behavior of proteins.[87] His observations initiated the development of the famous Hofmeister series of how different salts induce aggregation (salting out) or increase the solubility (salting in) of proteins, but at the time, no detailed explanation of the observations was provided. More than 100 years later, the subject is still a highly discussed and relevant scientific challenge that remains elusive, but the most reliable theories are gathered under specific ion (or ion-specific) effects.

Specific ion effects theories consist mainly, but not exclusively, of four proposed mechanisms (Figure 17). The basis for the first mechanism is the classification of ions based on their chaotropic or kosmotropic nature. Chaotropic ions (order breakers) are less hydrated and disrupt the hydrogen-bonded water network, whereas kosmotropic ions (order makers) are highly hydrated and increase the strength of the hydrogen bonds between water molecules close to the ion. Chaotropic ions accumulate close to chaotropic surfaces to limit their perturbation of water, while kosmotropic ions are excluded from the surface to reside in the bulk water phase (Figure 17a), or vice versa in the case of kosmotropic surfaces.[88] Noteworthy is that surfaces with weak acidic groups, such as TO-CNFs or CM-CNFs, can change from being chaotropic at low pH (associated acids) to kosmotropic at high pH values (dissociated acids) depending on the charge density.[88b,d]

In the second mechanism (Figure 17b), for which Ninham and Nostro[89] were dedicated advocates, the polarizabilities of ions are considered. Polarizable ions bind to surfaces and other ions via dispersion interactions. The adsorption of ions to surfaces depends on the difference in the dielectric response of the colloid and the medium, and a significant difference promotes adsorption. Consequently, polarizable ions frequently migrate to water-air interfaces or adsorb to less hydrophilic surfaces. In surface and colloidal science, it is well known that uncharged surfaces in a salt solution usually attain a slight negative charge by anion adsorption to the interface since the excess electrons of anions make them more polarizable than cations.

There is a strong connection between chaotropic and polarizability, and separating these mechanisms is challenging. A general description of both would be to consider the charge density of the ion. The charge density dictates the restriction of

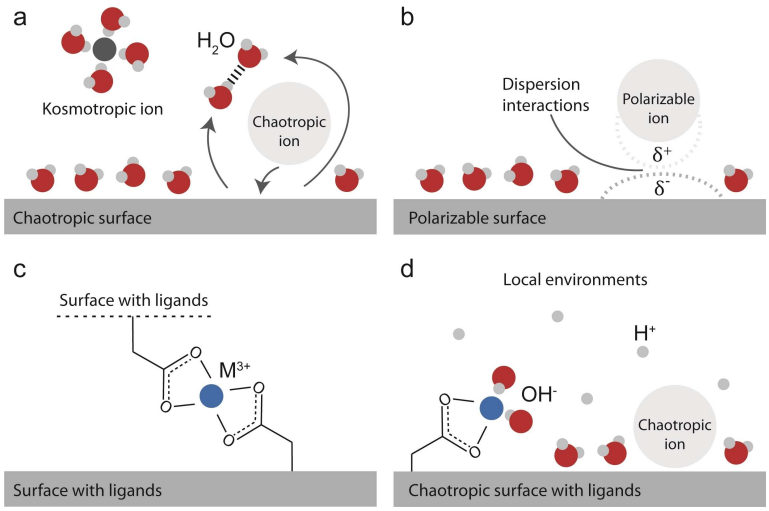


**Figure 17.** Schematic drawing of different specific ion effects. Reproduced from Mittal et al.[91] with permission from Wiley-VCH.


© 2023 The Authors. ChemSusChem published by Wiley-VCH GmbH

18645564x, 2023, 8, Downloaded from https://chemistry-europe.onlinelibrary.wiley.com/doi/10.1002/cssc.202201955 by Paul Scherrer Institut PSI, Wiley Online Library on [08/05/2023]. See the Terms and Conditions (https://onlinelibrary.wiley.com/terms-and-conditions) on Wiley Online Library for rules of use; OA articles are governed by the applicable Creative Commons License

electrons by the nucleus (polarizability) or the strength of the interaction with water (chaotropic or kosmotropic).

Predicting the outcome of hydration and polarizability effects is easier for cations than for anions since the size of a cation is more or less directly related to its properties. Small cations have a high charge density, are highly hydrated and kosmotropic, and the electrons are tightly bound, so they are not polarizable. The most chaotropic and polarizable cations are thus found going down in groups I and II in the periodic table. $K^+$, $Rb^+$, $Cs^+$, $Ca^{2+}$, $Sr^{2+}$, and $Ba^{2+}$ have many filled orbitals, making them large with a low charge density. The most kosmotropic and least polarizable cations ions are thus small, such as $Li^+$, $Mg^{2+}$, and most transition metal ions.

Anions are more complicated since they have excess electrons and are generally more polarizable than cations. Many anions are also organic, and their three-dimensional structure affects their properties, such as forming multipoles or having directional polarizability, and there is thus no simple size-orbital-property relationship as for inorganic cations. Nevertheless, a large inorganic anion ($I^-$) is more chaotropic and polarizable than a small anion ($F^-$).[89,90] It should be stressed that the size used in these discussions does not include water since the ion-water complex of kosmotropic ions gives them a larger effective size in water.

The accumulation or adsorption of ions can lead to the introduction, cancellation, or reversal of the surface charge.[88d,92] A more general outcome is variations in the double layer repulsion mediated by a change in osmotic pressure due to the ion-specific properties of the counterion cloud. A way to quantify this is via the osmotic coefficient ($\varphi$) given by Equation (13),

$$\varphi = \frac{\Pi_{\text{experimental}}}{\Pi_{\text{ideal}}} = \frac{\Pi_{\text{ideal}} + \Pi_{\text{excess}}}{\Pi_{\text{ideal}}} \quad (13)$$

where $\Pi$ is the osmotic pressure. The experimental osmotic pressure is the sum of the ideal and the excess contributions. The ideal part is based on the concentration, while the excess part is ion-specific and related to the hydration and polarizability of the ions. The concentration-dependent osmotic coefficient of a few commonly used cation-chloride salts (Figure 18) shows significant differences in osmotic pressure. The kosmotropic ions $Li^+$, $Mg^{2+}$, and $Al^{3+}$, lead to higher osmotic pressure than the chaotropic ions $Cs^+$ and $Ba^{2+}$, or the ideal $Na^+$. The fact that the ion concentration close to a moderately charged surface is higher than 3 M or even 12 M when directly calculated from the Boltzmann equation for CNFs with a charge density of 1.5 mmol $g^{-1}$ shows that the ion-specific osmotic pressure is of considerable importance for the double layer repulsion and hence the colloidal behavior.[5]

The effect of chaotropic and polarizable monovalent ions is observed in the relationship between the swelling of CNF films and the polarizability of the counterions (Figure 19a). The same behavior is observed in the case of cationic CNFs and different anionic counterions (Figure 19b), although correlation effects are a potential for phosphate and citrate depending on their valency inside the film.[90] Noteworthy is that the swelling of cationic CNFs is one order of magnitude greater than that of anionic CNFs, which could be utilized in absorption applications.[25] It is unknown why this is the case, but suggested explanations are that cations are closer to ideal since their charge is not diminished by polarization. Another explanation could be the bulky properties of quaternary ammonium ions shown to induce short-range repulsion,[94] and

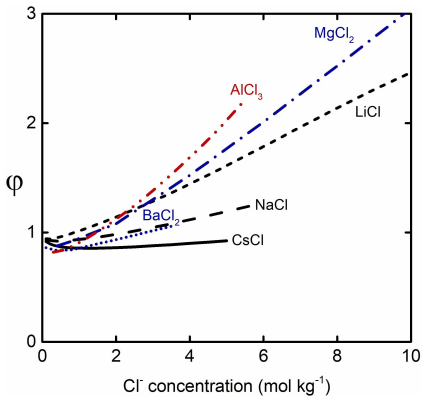


**Figure 18.** Osmotic coefficient of commonly used chloride salts as a function of chloride concentration.[93]

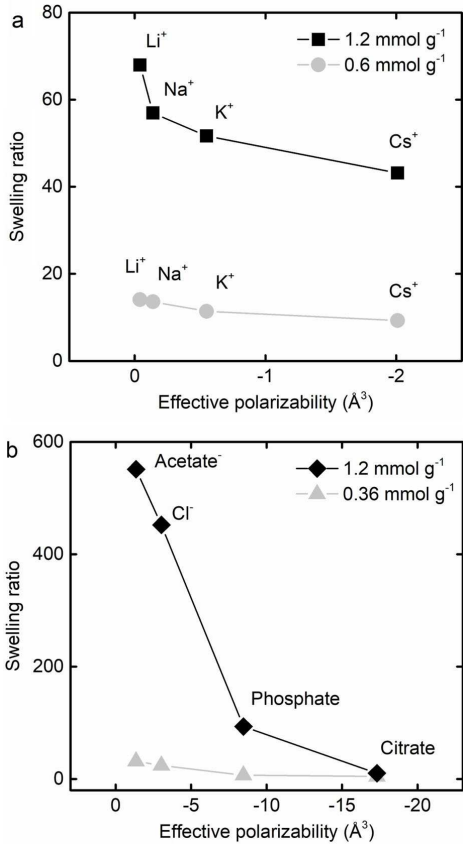


**Figure 19.** Swelling of CNF films in the presence of different counterions. a) Anionic CNF films with different charge densities [mmol $g^{-1}$]. b) Cationic CNF films with different charge densities. The data were kindly provided by Benselfelt et al.[90]


© 2023 The Authors. ChemSusChem published by Wiley-VCH GmbH

1864564x, 2023, 8, Downloaded from https://chemistry-europe.onlinelibrary.wiley.com/doi/10.1002/cssc.202201955 by Paul Scherrer Institut PSI, Wiley Online Library on [08/05/2023]. See the Terms and Conditions (https://onlinelibrary.wiley.com/terms-and-conditions) on Wiley Online Library for rules of use; OA articles are governed by the applicable Creative Commons License

this could prevent irreversible aggregation of cellulose upon drying (see Section 5.6). Cations and anions are also differently hydrated due to the asymmetry of water molecules and the geometrical limitations of arranging them close to the charge.[95]

The trend with ion-specific osmotic pressure is also observed in the aggregation of CNCs upon salt addition (Figure 20).[96] The critical salt concentration which induces aggregation of sulfated CNCs is consistent with the specific ion effect theories. For monovalent ions, a lower concentration of $Cs^+$ leads to aggregation due to the polarizability and chaotropic properties, and a higher amount of $Li^+$ can be added before aggregation starts due to its kosmotropic properties. Divalent and trivalent ions increase ion–ion correlation, which reduces colloidal stability and causes aggregation at lower salt concentrations. The critical aggregation concentration is thus proportional to the valency of the added cations. However, multivalent ions also encounter complexation with ligands and ion–ion correlation.

The third ion-specific effect is thus the well-known complexation of multivalent ions and ligands to form coordination bonds (Figure 17c). These complexes are typically observed for transition metal ions that can reach a noble gas-like configuration by sharing electrons with a ligand to fill the d-orbital. Inter-particle complexes are detrimental to colloidal stability, and intra-particle complexes screen the surface charge and reduce the colloidal stability. The strength of a complex is quantified by the stability constant, the first association constant between the ligand and the ion ($\log k_1$).[97]

Exposing nanocelluloses to multivalent ions induces complexation that causes gelation or increases the stiffness of an already-formed network. Indications that complexation has occurred can be obtained by comparing the swelling of CNF films[90,98] (Figure 21a) or the stiffness of hydrogels[65,99] (Figure 21b) to the stability constant of metal ions and the ligands on the particle surface. In both these cases, there is a strong correlation between the network strength and the stability

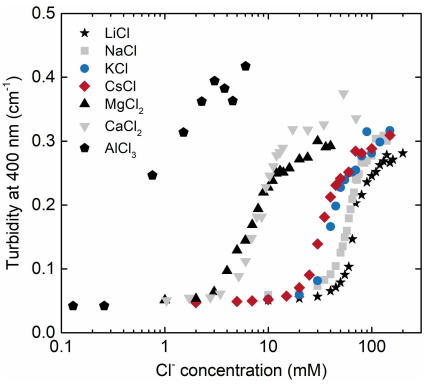


**Figure 20.** Aggregation of sulfated CNCs measured by turbidity as a function of electrolyte concentration of different salts. The data were kindly provided by Phan-Xuan et al.[96] and is replotted using the chloride concentration to compare charge concentration rather than cation concentration, which is more suitable for describing entropic mechanisms for cations of different valencies.

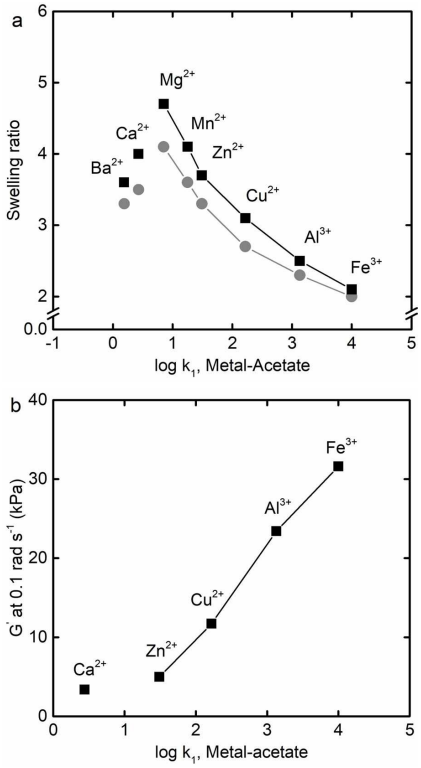


**Figure 21.** a) Swelling of TO-CNF films as a function of the stability constant of metal–acetate, which is a model for the carboxyl groups on the CNF surface. The charge densities of the CNFs were 1.2 mmol $g^{-1}$ (squares) and 0.64 mmol $g^{-1}$ (circles). The data kindly provided by Benselfelt et al.[90] b) Storage modulus of TO-CNF hydrogels (1.3 wt% and charge density 1.3 mmol $g^{-1}$) as a function of stability constant of metal–acetate. Data from Dong et al.[65]

constant for different metal ions, but the chaotropic and polarizable ions, $Ca^{2+}$ and $Ba^{2+}$, do not follow the expected trend. This deviation is then due to ion-specific properties such as ion-specific osmotic pressure, for example, $BaCl_2$ induces a lower osmotic pressure than $MgCl_2$ at the same concentration (Figure 18), or to the accumulation or adsorption of these ions onto the surfaces of the CNFs, as discussed previously. It has, however, been shown that the thermodynamics of the interaction between CNCs and ions are similar for ions in group II, indicating that the adsorption of ions to cellulose surfaces is perhaps not that important.[100]

An alternative way to explain complexation is Manning's condensation or counterion condensation, which is essential for theories of polyelectrolytes.[43] If two charged groups are closer than the Bjerrum length of 7 Å in water, a counterion will condense and neutralize one of the charged groups to minimize the free energy of the polymer or particle (see Section 3.5). Multivalent ions can thus condense at several charged groups, potentially at different colloids, and release monovalent ions, leading to the association and an overall increase in entropy.[101] In such processes, the kosmotropic or chaotropic nature of the ion is essential for the ion-specific entropy gain via the perturbation of water.[102]


© 2023 The Authors. ChemSusChem published by Wiley-VCH GmbH

1864564x, 2023, 8, Downloaded from https://chemistry-europe.onlinelibrary.wiley.com/doi/10.1002/cssc.202201955 by Paul Scherrer Institut PSI, Wiley Online Library on [08/05/2023]. See the Terms and Conditions (https://onlinelibrary.wiley.com/terms-and-conditions) on Wiley Online Library for rules of use; OA articles are governed by the applicable Creative Commons License

The accumulation, adsorption, or complexation of ions at interfaces brings the fourth mechanism. Ions are, in many cases, acids or bases, and their local concentration is thus associated with a local pH value (Figure 17d) due to a mechanism similar to the well-known Donnan equilibrium. An example affecting everyday experiments is the accumulation of chaotropic anions close to the glass electrode during pH measurements.[103] The accumulation of ions at the glass surface affects the local concentration of $H_3O^+$, and the measured pH value differs from that of the bulk solution, which is why the ideal salt KCl is used as the reference. pH measurements in other solutions than KCl involve minor to significant errors. It is thus vital to consider the ion-induced local environment when working with nanoparticle systems in which the colloidal stability is mediated by weakly acidic groups that can be neutralized, such as carboxyl or phosphate groups.

Determining the local pH inside solid materials is challenging. Infrared spectroscopy can measure relative changes in dried materials, such as the difference between associated (1730 $cm^{-1}$) and dissociated (1600 $cm^{-1}$) carboxyl groups.[90] An example is the different infrared absorbance of TO-CNF films treated with $Ca^{2+}$, $Cu^{2+}$, or $Fe^{3+}$ (Figure 22), which are increasingly acidic due to the complexation with water and subsequent hydrolysis (Figure 17d). One should, however, treat such experiments with care since the local conditions gradually change during drying and may also be affected by the state at which ions are introduced.

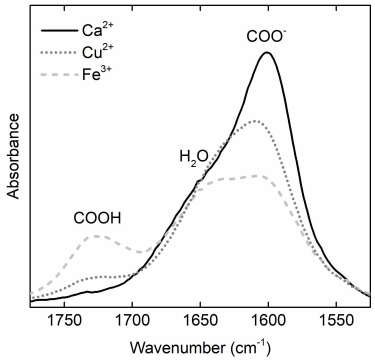


**Figure 22.** Carbonyl vibrations in a TO-CNF film with $Ca^{2+}$, $Cu^{2+}$, or $Fe^{3+}$ counterions. The data were kindly provided by Benselfelt et al.[90]

### 5.3. Relative importance of ion–ion correlation and specific ion effects

The remaining challenge is separating the contribution of ion–ion correlation and the different specific ion effects to understand their relative importance. An attempt was made by comparing TO-CNFs with nanoparticles lacking ligands and investigating the influence of metal-ligand complexes. The swelling data in Figure 23a was compared to data procured in the same way for exfoliated montmorillonite clay (MMT), which is negatively charged due to an isomorphic substitution of aluminum ions with ions of lower valency rather than anionic

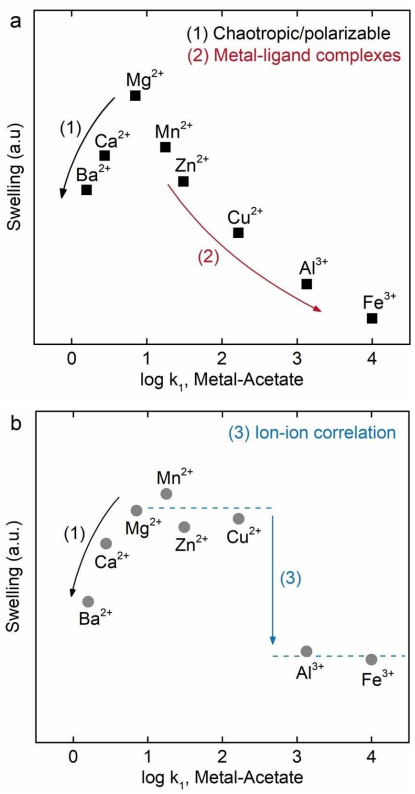


**Figure 23.** Relative swelling of films of TO-CNFs (a) and MMT clay (b) as a function of the stability constant of the complexation of the counterions and acetate. The data were kindly provided by Benselfelt et al.[90]

ligands.[90] This comparison (Figure 23) shows that the reduced swelling induced by the chaotropic and polarizable ions $Ca^{2+}$ and $Ba^{2+}$ (1) is not influenced by the specific ligand, and ion-specific interactions related to hydration and dispersion are thus to be expected for all nanoparticles. It is still difficult to separate these two mechanisms and tell which is most important.

The relationship between swelling and stability constant of complexes (2) was not observed for MMT because there are no ligands on the MMT surface. Instead, two discrete levels were observed, one for divalent and one for trivalent transition metals (Figure 23b). These levels were suggested to be the valency effect in ion–ion correlation (3) since a higher valency leads to a more polarized ion cloud, more correlation, and hence less repulsion in the double layer.[104]

The data in Figure 23 lead to the following conclusions:

- $Mg^{2+}$ is an ideal multivalent ion that is neither chaotropic nor polarizable and does not form strong complexes. $Mg^{2+}$ is thus the best reference for divalent ion–ion correlation.
- In addition to divalent ion–ion correlation, $Ca^{2+}$ and $Ba^{2+}$ induce stronger networks since they are chaotropic and polarizable.
- In addition to divalent or trivalent ion–ion correlation, transition metals induce stronger networks due to metal–ligand complexes and local acidic environments.


© 2023 The Authors. ChemSusChem published by Wiley-VCH GmbH

1864564x, 2023, 8, Downloaded from https://chemistry-europe.onlinelibrary.wiley.com/doi/10.1002/cssc.202201955 by Paul Scherrer Institut PSI, Wiley Online Library on [08/05/2023]. See the Terms and Conditions (https://onlinelibrary.wiley.com/terms-and-conditions) on Wiley Online Library for rules of use; OA articles are governed by the applicable Creative Commons License

Based on this information and the knowledge of the properties of different ions, a qualitative description can be derived to predict how different ions influence assemblies of charged nanocelluloses (Figure 24). This qualitative model assumes that cellulose is more chaotropic than kosmotropic at most charge densities and conditions since kosmotropic cellulose, such as carboxymethyl cellulose (CMC), would be soluble in water and not stay condensed as nanoparticles.

Still missing in the literature is how the properties of co-ions influence the colloidal behavior of nanocelluloses. Predictions can be made using specific ion effect theories, but further experiments are needed, such as any difference induced by $MgCl_2$, $MgBr_2$, $MgNO_3$, among others. The list is long and motivates future research efforts.

### 5.4. Nonadditivity at the nanoscale

A final complication is that the rule of additivity of interactions valid for micro to macroscopic systems is not necessarily accurate at the nanoscale.[2] Nonadditivity means that different interparticle interactions cannot be summed to a resulting interaction strength since they are interdependent. For example, the double layer composition affects the dielectric properties and, in turn, the van der Waals interactions. A remaining question is how this nonadditivity affects the assembly, that is, how different mechanisms co-depend during nanoparticle interactions. Other examples of nonadditivity are that metal-ligand complexes affect the local pH, which affects the titrating ligand the ion should form complexes with, or that chaotropic anions reduce the osmotic pressure and adsorb to surfaces to screen surface charges. Can different mechanisms be separated? Besides the struggle to quantify and understand ion–ion correlation and specific ion effects, nonadditivity is a significant future challenge for colloidal and physical chemistry.

### 5.5. Asymmetry-induced self-organization in chiral nematic phases

In many aspects, the mean-field approximations in the DLVO theory are unsuitable for nanoparticles. Another example is that nanoparticles with anisotropic properties self-organize into superstructures in a way continuum theories cannot predict. However, the most basic of such superstructures is mediated by the shape of the particle alone. Rod-shaped nanoparticles form nematic phases with parallel orientation to minimize the excluded volume of a random network (Figure 25a). During the transition to a nematic phase, a favorable increase of translational entropy is achieved at the cost of rotational entropy, which is already restricted in a random network of rods at higher concentrations. The Onsager theory describes this transition.[106]

For charged particles, the effect of the double layer has to be considered and the Onsager theory modified accordingly.[107] Since the critical volume fraction for forming nematic phases depends on the aspect ratio, the effective thickness of charged particles also includes the extension of double layers. The transition thus depends on the electrolyte concentration and the properties of the charged groups (Section 5.2).[108] For

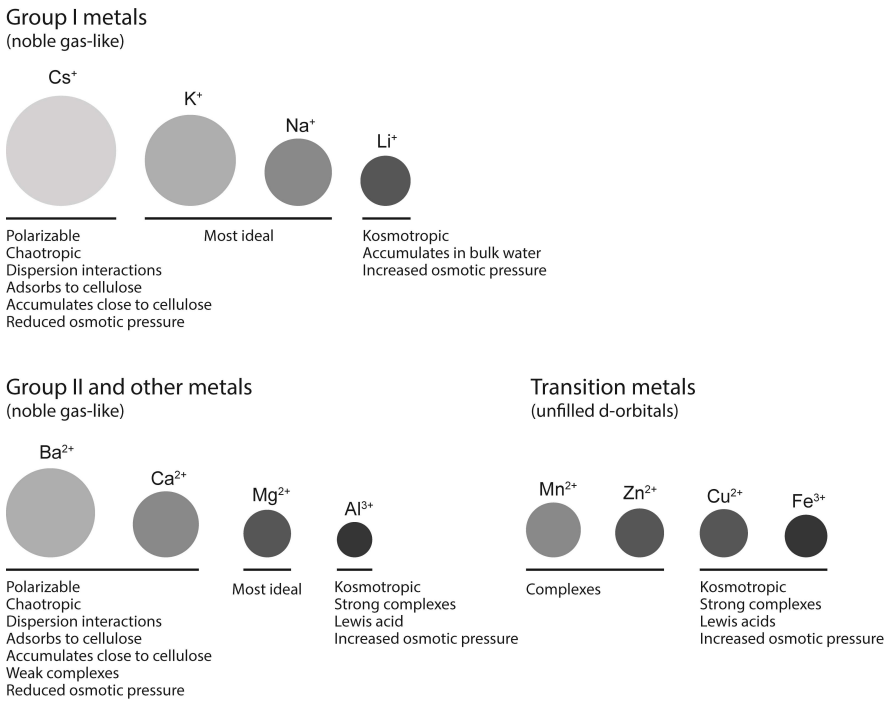


**Figure 24.** Qualitative classification of ions (chloride co-ions) and how they interact with nanocelluloses. The relative sizes in the schematic are based on the Shannon ionic radii.[105]


© 2023 The Authors. ChemSusChem published by Wiley-VCH GmbH

1864564x, 2023, 8, Downloaded from https://chemistry-europe.onlinelibrary.wiley.com/doi/10.1002/cssc.202201955 by Paul Scherrer Institut PSI, Wiley Online Library on [08/05/2023]. See the Terms and Conditions (https://onlinelibrary.wiley.com/terms-and-conditions) on Wiley Online Library for rules of use; OA articles are governed by the applicable Creative Commons License

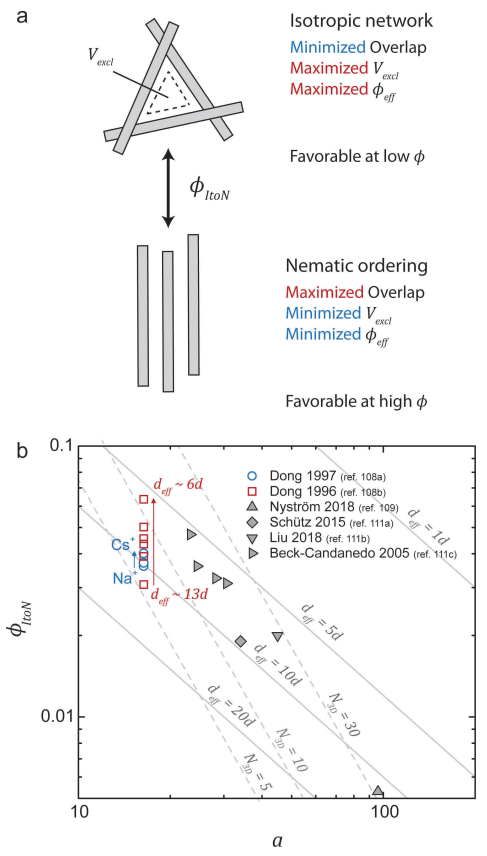


**Figure 25.** a) Schematic of the factors controlling the transition between isotropic networks and nematic ordering. b) Comparison between Equation (14) (solid grey lines) and a few examples of experimental data of the critical volume fraction for the onset of the chiral nematic ordering of CNCs with different aspect ratios.[108,109,111] The crowding factor from Equation (7) is also shown for comparison (dashed grey lines).

charged particles, the volume fraction of phase transition between the isotropic (*I*) and nematic (*N*) phase (ItoN) is given by Equation (14),[109]

$$\phi_{\mathrm{ItoN}} = 6a^{-1}\frac{d}{d_{\mathrm{eff}}} \tag{14}$$

compared to the uncharged case $\phi_{\mathrm{ItoN}} = 3.3\,a^{-1}$.[110] The influence of charge can qualitatively be described as a balance between three parameters (Figure 25a): i) excluded volume ($V_{\mathrm{excl}}$), that is, the inaccessible volume due to network restriction. ii) The repulsion due to overlapping double layers, i.e., the local osmotic pressure, dictating $d_{\mathrm{eff}}$. iii) The effective volume occupied by particles and their counterion clouds ($\phi_{\mathrm{eff}}$), relating to the total osmotic pressure when the excluded volume is considered. Nematic transitions minimize the overall entropy of the system, which is a balance between the osmotic pressure of counterions and the translational freedom of rods. For CNCs, it has been shown that $\phi_{\mathrm{ItoN}}$ scales with $L^2d$, which is proportional to the excluded volume. The experimental relationship was $\phi_{\mathrm{ItoN}} = 0.55/(L^2d)$ with length and diameter expressed in nanometers.[56]

Figure 25b compares the theory from Equation (14) with experiments, showing that the effective diameter due to double layer repulsion is 5 to 10 times the solid diameter. Compared to the crowding factor in Equation (7), the onset of the formation of the nematic phase occurs at $N_{3D}$ between 5 and 30 or when $N_{3D}$ is in the range of 0.3 to 0.7 times the aspect ratio, with the average being $N_{3D} \sim 0.5\,a$. This value shows that the nematic ordering starts well before the theoretical VAS transition at $N_{3D} \sim a$, as discussed in Section 4.2. It is indeed reasonable that the nematic phase transition must happen before the motion is restricted by the VAS. It is, however, well-known that low to moderately-charged CNFs have a neglectable order before the formation of the VAS due to entanglement imposed by their high aspect ratio and kinks that lead to deviations from ideal rods.

Following the relationship between the aspect ratio of the particles and $\phi_{\mathrm{VAS}}$ or $\phi_{\mathrm{ItoN}}$, there are two outcomes for nanocellulose dispersions that increase in concentration: below a critical aspect ratio, a nematic phase is formed, while above this critical aspect ratio, the dispersion transition into a VAS before nematic ordering becomes favorable. The length of the rod at which $\phi_{\mathrm{VAS}} > \phi_{\mathrm{ItoN}}$ and nematic ordering can occur has semi-empirically been shown for $L < 1.62\,d^{2.5}$.[56] For a cellulose crystal with diameters of 5 or 10 nm, this transition would be at a length of 90 and 500 nm, that is, critical aspect ratios of 18 and 50. Nyström et al.[109] showed nematic phases forming for aspect ratios up to 100 for CNCs with a diameter of 4 nm, which is higher than the semi-empirical estimate.

It is important to note that the aspect ratio is based on the solid dimensions in these and previous discussions about overlap concentration and VASs. The models can also be converted using an aspect ratio based on $d_{\mathrm{eff}}$, resulting in different equations. The work by Dong et al.[108b] describes how to calculate $d_{\mathrm{eff}}$.

Since the effective shape of the nanoparticle is determined by the extension and shape of the counterion cloud, asymmetric shapes or asymmetric coverage of charged groups influence their organization.[2] Cellulose crystals have a right-hand twist with a periodicity influenced by the surface charge density.[112] In the case of cellulose nanocrystals, asymmetry results in chiral nematic phases in which the nematic phase is further organized in a twist perpendicular to the nematic plane.[16,111a] This organization was initially observed for chiral molecules such as cholesterol, which is why this organization is sometimes called a cholesteric phase. The right-handed chirality of the cellulose crystal structure is a probable explanation for this behavior of CNC dispersions.[44] Consequently, the position of charged groups organizes the same way as the twist of the cellulose crystal, leading to a twisted counterion cloud that determines the interactions between particles.[2] The pitch of the nematic phase, that is, the length of a 360° turn and the resulting twist angle, is used to describe chiral nematic phases and is determined by, for example, small-angle X-ray scattering (SAXS).[111a]

CNFs, on the other hand, are not straight rods since they have kinks, which makes cholesteric phases very unlikely. They are also relatively long, leading to a kinetic arrest and a direct


© 2023 The Authors. ChemSusChem published by Wiley-VCH GmbH

1864564x, 2023, 8, Downloaded from https://chemistry-europe.onlinelibrary.wiley.com/doi/10.1002/cssc.202201955 by Paul Scherrer Institut PSI, Wiley Online Library on [08/05/2023]. See the Terms and Conditions (https://onlinelibrary.wiley.com/terms-and-conditions) on Wiley Online Library for rules of use; OA articles are governed by the applicable Creative Commons License

transition from dispersion to a VAS, per the previous discussion. Cholesteric phases have been formed for CNCs with an aspect ratio up to 100, but higher than this is very challenging.[109] The VAS prevents the relaxation into a nematic phase from occurring within a reasonable time, but the slow solvent casting of CNFs over several weeks or even months results in sheets with a nematic structure.[113]

Gray and co-workers made the first attempts to control the self-organization of CNCs by manipulating the counterion cloud. In the 1990s, they studied how ionic strength and specific counterions influenced the chiral nematic organization of sulfated CNCs.[11,108] The critical concentration for the phase transition was increased with increasing ionic strength (Dong et al.[108b] in Figure 25b) since the effective diameter of the rods is smaller at an elevated salt concentration, and tighter random packing is allowed before the excluded volume starts to be unfavorable. Adding salt to an already formed anisotropic phase reduced the volume fraction of the order phase for the same reason. Changing the counterions from an ideal to a more chaotropic, that is, $Na^+$ to $K^+$ to $Cs^+$, also pushed the onset to a higher volume fraction (Dong and Gray[108a] in Figure 25b). According to the previous discussion, the effective diameter of the particle is reduced due to the ion-specific osmotic pressure or the favorable adsorption of the chaotropic and polarizable ions and hence surface charge neutralization. Noteworthy is that the specific ion has little influence on the chiral pitch and that the particle shape and concentration, electrolyte concentration, or pH of the solution mainly determine the pitch.[108a,111a,c,114]

Any asymmetric property, such as dielectric response or magnetic susceptibility, may lead to ordered structures in condensed nanoparticle assemblies. In cellulose I crystals, all the glucan chains point in the same direction, generating a giant permanent dipole moment that is certainly something to consider in future studies and theories on nanocellulose self-assembly.[115]

### 5.6. Bulky counterions and charged groups

Exchanging small cationic counterions with bulker ions, such as tetrabutylammonium ions (TBA), lead to colloidal systems that are very different from those explained by continuum theories or ion–ion correlation and specific ion effects. It was first shown by Dong and Gray in 1997 that bulkier counterions pushed the onset of the nematic ordering of sulfated CNCs to higher concentrations.[108a] Recently, Benítez and Walther[116a] and the group of Isogai[116b] studied how this ion exchange influenced the mechanical properties of TO-CNF films. These and a fundamental theoretical study[94] show that bulker cations increase short-range electrostatic repulsion, which reduces the friction between nanoparticles. Reduced friction increases mobility, explaining why the concentration of CNCs can be increased before the entropy of the network is low enough for a parallel nematic ordering to be more favorable.[108a] This mechanism can also explain yielding at lower stresses and higher extension at the break of CNF films with bulky quaternary ammonium ions.[116] However, work is still needed to understand the behavior of these counterions and the behavior of CNFs with bulky charged groups, such as cationic or CM-CNFs.

For cationic CNFs, the bulky charged group influences their behavior in dispersion or networks. Besides the different chemical potentials of different charged groups, anions and cations are, as previously mentioned, different in how they interact with water.[95] Materials from cationic CNFs are known to swell a lot and even disintegrate in water.[25,90] The exact reason for this is still unknown, but it is probably related to the size, chemical potential, or hydration of the bulky cationic groups.

## 6. Interactions with Other Colloids

Tailoring assemblies of nanoparticles into composite materials is a promising tool for designing advanced functional materials. In designing new materials, we must understand colloidal behaviors in detail and how they can be used to our advantage. This section describes some of the most fundamental and interesting interactions between nanocellulose and other colloids.

### 6.1. Polyion complexes

The surface charge of CNFs can be used to assemble nanocellulose by forming complexes with oppositely charged colloids. Polyion association occurs when colloids of opposite charges meet in a solution or dispersion. The driving mechanism is not electrostatic interactions since the free energy is essentially the same whether counterions or an oppositely charged polyion compensate for the polyion charge. Instead, the increased entropy of releasing counterions and associated water makes the complexation thermodynamically favorable (Figure 26a).[117] According to specific ion effect theories, the counterion release also includes small enthalpic contributions from the interaction between counterions and water. Kosmotropic ions are easier to exchange since they more favorably reside in bulk water, whereas chaotropic and polarizable ions have a higher tendency to interact with the polyion and stay inside the complex as a dopant.[102] The conformational entropy of a polyion is already limited due to its polymeric nature and the repulsion of charged segments that extend their conformation. The entropic loss of the polyions is thus minimal compared to the entropy gained by the counterions, and in this respect, nanoparticles have even lower conformational entropy.

Forming polyion complexes using nanocellulose is not tricky; simply mix with a polyion of the opposite charge. However, using these complexes for a designated purpose is more challenging since the complexation is chaotic. For some applications, the chaotic aggregation into particulate complexes may be desired.[120] In the case of polyelectrolyte complexes (PECs), the association can easily be controlled by adding salt to the solution to limit the entropic gain, and the complexation


© 2023 The Authors. ChemSusChem published by Wiley-VCH GmbH

1864564x, 2023, 8, Downloaded from https://chemistry-europe.onlinelibrary.wiley.com/doi/10.1002/cssc.202201955 by Paul Scherrer Institut PSI, Wiley Online Library on [08/05/2023]. See the Terms and Conditions (https://onlinelibrary.wiley.com/terms-and-conditions) on Wiley Online Library for rules of use; OA articles are governed by the applicable Creative Commons License

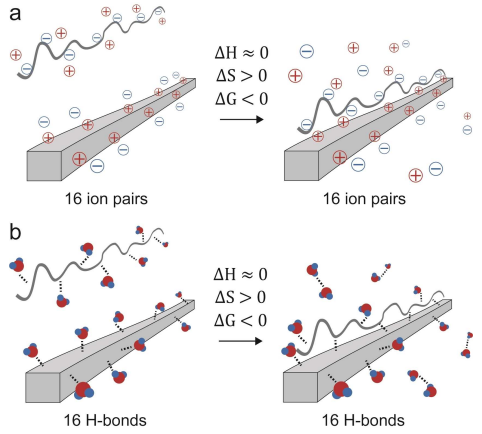


**Figure 26.** a) Schematic of the complexation between anionic polyelectrolytes and cationic CNFs driven by the increased entropy of releasing counterions (ion exchange).[102] b) Similar illustration for nonionic adsorption of a polymer, for example, xyloglucan, to nanocellulose driven by the increased entropy of released water.[118] Thermodynamic data about both mechanisms can be found in the review by Lombardo and Thielemans.[119] Partly readapted from Ref. [118c] with permission from Springer Nature.

can thus be prevented or the complex dissolved.[121] Controlling the entropic gain allows for a process where adding or removing excess salt can be utilized when forming and later consolidating materials based on PECs, known as saloplastic processing.[122] The problem is that this is not feasible for nanocelluloses, especially not CNFs, since salt addition leads to aggregation or gelation due to their rigidity. However, there are some examples where careful titration enabled the formation of complexes around individual cellulose nanoparticles, with subsequent processing into materials.[123] The sensitivity of such a system certainly limits its use for large-scale manufacturing. Interfacial complexation and layer-by-layer assembly are other examples of how to use polyion complexes with nanocelluloses, further discussed in Section 7.

### 6.2. Interactions with non-ionic molecules

Non-ionic interactions are more challenging to understand than interactions where charges are involved. Scientists frequently refer to hydrogen bonding when discussing the association between cellulose and hemicelluloses.[118a,b] The notion of hydrogen bonds driving a large-scale assembly in water is, however, incorrect for two reasons: first, hydrogen bonds are short-range and directional bonds that would not affect colloidal systems over large distances typically required for self-assembly, and second, hydrogen bonds show only slight variation in their interaction strength. It is thus difficult to explain why a hydrogen bond between, for example, cellulose chains would be preferred over hydrogen bonds between a cellulose chain and water.[118a,c] Hydrogen bonds indubitably form, as shown by deuterium exchange,[124] but that does not mean they are directly involved in the association. Hydrogen bonds might also form after the initial assembly as a secondary relaxation.

A review by Lombardo and Thielemans[119] showed that the adsorption of different polymers to nanocelluloses is mainly endothermic, meaning that hydrogen bonds do not drive adsorption. Instead, a distinct enthalpy entropy compensation was observed, typical for the sensitive balance of interacting with water or another molecule. For small molecules, the entropy of adsorption is unfavorable and similar to the adsorption of water, which means that an enthalpic contribution is needed, and the adsorption is exothermic.[118c] Aromatic groups are a typical structure of molecules that undergo exothermic adsorption to cellulose. Another example of their general importance is that 99% of all drugs contain at least one aromatic group.[125] In this respect, the structure of lignin and its interaction with cellulose is interesting for cell wall assembly. The seeming importance of aromatic groups for exothermic adsorption is still unknown but may be related to the polarity of aromatic groups and the significant structuring of water around them,[126] opening many options for enthalpy entropy compensation.

An ongoing debate, including the importance of hydrogen bonds, is the topic of the crystallization of cellulose. Several hydrogen bonds are involved in the crystal lattice of cellulose, but are they responsible for the initial association during crystallization? Lindman and co-workers are firmly against the notion of hydrogen bonds in this respect; instead, they highlight the amphiphilic nature of cellulose and propose that unfavorable interactions with water, hydrophobic effects, or solvation effects induce cellulose association.[127] A recent review on the subject outlines the diminishing role of hydrogen bonds in the crystallization of cellulose and many other aspects.[118c] Understanding cellulose association and what holds the crystals together is crucial when developing solvents for cellulose. It is also essential to explain the colloidal stability of nanocelluloses and their interactions with other colloids.[128]

The most studied non-ionic interactions with cellulose are found with hemicelluloses. Hemicelluloses interacting with cellulose in the cell wall can be extracted and dissolved in water.[129] From this state, they readily adsorb back onto cellulose. The most studied hemicellulose is probably xyloglucan which has a cellulose backbone with branches containing xylose, galactose, and fucose; hence the strong interaction with cellulose is not surprising.[130] Over the years, hydrogen bonding as the driving force has been increasingly questioned due to data pointing towards van der Waals interactions and an endothermic process.[131] It has been proposed that the increased entropy of releasing unfavorably bound water at cellulose and xyloglucan surfaces is the driving force (Figure 26b), which is also supported by molecular dynamic simulations.[118a,b] Such mechanisms have been discussed concerning the adsorption of other non-ionic polymers.[132] This mechanism is similar to the gained entropy of released counterions and associated water during polyelectrolyte association (see Section 6.1), pointing to a general associative behavior of polymers in water.


© 2023 The Authors. ChemSusChem published by Wiley-VCH GmbH

1864564x, 2023, 8, Downloaded from https://chemistry-europe.onlinelibrary.wiley.com/doi/10.1002/cssc.202201955 by Paul Scherrer Institut PSI, Wiley Online Library on [08/05/2023]. See the Terms and Conditions (https://onlinelibrary.wiley.com/terms-and-conditions) on Wiley Online Library for rules of use; OA articles are governed by the applicable Creative Commons License

Other hemicelluloses, such as xylans and glucomannans, also adsorb to nanocellulose surfaces,[133] but a detailed description of the literature is beyond the current scope. It is, however, noteworthy that the chemical structure of hemicelluloses, such as the degree of acetylation, depends on the plant source and extraction method. Even though the chemical structure affects interaction with cellulose,[118b,134] the adsorption is probably governed by a similar free energy balance for most hemicelluloses due to the chemical similarities of polysaccharides.

### 6.3. Interactions with surfactants

Surfactants interact with almost any surface due to their amphiphilic chemical structure that can be used to minimize surface energies. A deeper review of this research field is beyond the current scope, but the basic principles are discussed. The state of the research on interactions between surfactants and nanocelluloses and cellulose, in general, was recently summarized.[135]

Like polymers, surfactants can interact with cellulose through ionic or non-ionic interactions. Endothermic entropy-driven adsorption has been shown in the case of anionic surfactants and cationic cellulose.[136] The data were explained by releasing counterions and water bound to the surfactants, similar to polyion complexation and adsorption of hemicellulose onto cellulose. The entropy gain depends on the entropy of the exchanged ion, which means that a few connected charges are typically required to make the exchange favorable.[137] Consequently, isolated surfactants that only carry a single charge in the head group are unlikely to interact with cellulose by ionic means alone, which means that several mechanisms govern the interaction.

The complex thermodynamics of surfactant adsorption is shown in the fact that it usually follows pseudo-second-order kinetics with three concentration regimes (Figure 27a, b): 1) adsorption of individual surfactants to the surface and aggregation at the surface in 2) monolayers (hemi-micelles) or 3) bilayers (ad-micelles). Regimes 2 and 3 are similar to micelle formation in solution but at a concentration below the critical micelle concentration, called critical aggregation concentration (cac), critical surface aggregation concentration (csac), or hemimicelle concentration (hmc).[138] The interaction with charges on cellulose screens repulsion between head groups found in micelles and the assembly of hydrophobic tails is thus more favorable on an oppositely charged surface. The charge density of cellulose has been shown to affect the kinetics of the different regimes (Figure 27c), that is, low charge favors monolayers, whereas high charge favors bilayers.[138b] Different surface energies can intuitively explain this behavior, i.e., a more hydrophobic surface (low charge) favors monolayers, while a more hydrophilic surface (high charge) favors bilayers. Although the above models and studies are for macroscopic cellulose–water interfaces, the principles and the underlying thermodynamics apply to nanocelluloses in three dimensions.

In the case of non-ionic surfactants, the attraction is governed by van der Waals forces or solvophobic effects, similar to the situation for hemicelluloses. Hydrogen bonds are also frequently suggested in this research field, which is a doubtful contribution. Nonionic adsorption has similar kinetics to those observed for highly charged surfaces and oppositely charged surfactants, indicating a limited contribution from charge exchange in surfactant adsorption.[139]

In the case of the adsorption of surfactants with the same charge as the nanocellulose, there is a repulsive component to consider, which can be screened by adding salt or adding multivalent ions as an anchor to increase the adsorption.[138a,140] Although the adsorption of surfactants follows a specific mechanism, it can differ a lot depending on the properties of the surface and the surfactant, such as charge density, purity of the cellulose, and length and chemical structure of the hydrophobic tail.

Adsorption of surfactants to cellulose enables a simple surface modification technique that has been used to increase compatibility between reinforcing nanocelluloses and the matrix in nano-biocomposites.[141] Surfactant adsorption onto CNFs in the monolayer regime leads to more hydrophobic fibrils with a higher degree of compatibility with hydrophobic matrices.[141a,142] Surfactant adsorption has also been used to prepare Pickering emulsion or stabilized foams towards formulation or the preparation of dry nanocellulose foams, further discussed in Section 7.8.

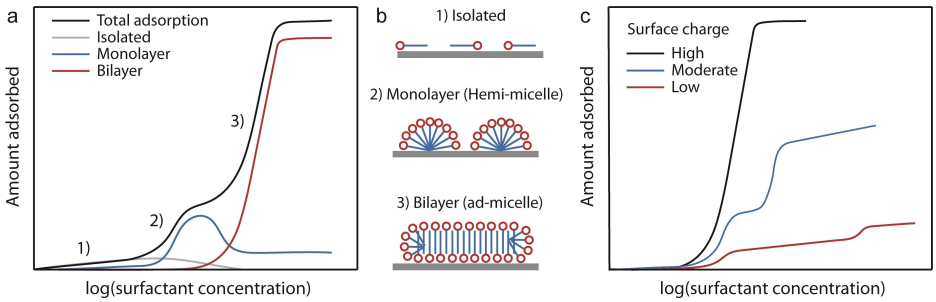


**Figure 27.** Conceptual drawings based on models and experimental data of surfactant adsorption isotherms to surfaces showing a) the different concentration regimes, b) the structure of the surfactant at the different regimes, and c) the influence of the charge density of the cellulose on the adsorption. The drawings were inspired by and based on the data by Alila et al.[138b]


© 2023 The Authors. ChemSusChem published by Wiley-VCH GmbH

1864564x, 2023, 8, Downloaded from https://chemistry-europe.onlinelibrary.wiley.com/doi/10.1002/cssc.202201955 by Paul Scherrer Institut PSI, Wiley Online Library on [08/05/2023]. See the Terms and Conditions (https://onlinelibrary.wiley.com/terms-and-conditions) on Wiley Online Library for rules of use; OA articles are governed by the applicable Creative Commons License

Mixing surfactant into CNF dispersion below the VAS threshold induces gel formation, but depending on the properties of the surfactant (cationic, anionic, or non-ionic), adding excess surfactant leads to disruption of the network by aggregation and sedimentation.[143] Adding cationic surfactants to CNCs leads to flocs that sediment instead of forming a gel network, a behavior related to the aspect-ratio-dependent overlap concentration (Section 4.1).[144]

### 6.4. Interactions with proteins

Proteins can be formed from 20 different amino acids with a large diversity in functional groups, which determine their ability to undergo various physical interactions, including ionic, hydrogen bonds, π–π stacking, or amphiphilic assembly.

The pH-dependent net charge of proteins is dictated by the protonation-deprotonation of titrating groups with the isoelectric point (pI) giving the point of zero net charge. Hence, at pH values below the pI the protein net charge is positive (protonated amines) and above the pI it is negative (deprotonated carboxylic groups).[145] Opposite charges on nanocellulose and proteins promote adsorption, and pH adjustments can thus be used to tune the interactions between nanocelluloses and proteins.[146] The adsorption of proteins onto nanocelluloses follows a typical Langmuir adsorption isotherm,[147] although it should be noted that the use of the Langmuir isotherm for polymer adsorption is not correct.[148] The thermodynamics of the adsorption was found to be endothermic and, as discussed in Section 6.2, driven by an increase of entropy from the release of bound water molecules and counterions.[119,147a]

Thermodynamics is more complicated for individual amino acids with many degrees o freedom. Lombardo et al. tested the adsorption of selected amino acids onto cellulose nanocrystals.[147a] They found that due to the low molecular weight of the amino acids, the overall entropy gain of the process was reduced and prevented the adsorption, that is, not enthalpically favorable enough to achieve enthalpy-entropy compensation. Guo and co-workers showed that adsorption occurs for peptides with a sequence as short as seven amino acid residues.[149] However, the studied peptide was a cellulose-binding domain (CBD) known to be adsorbed onto crystalline cellulose due to favorable enthalpy.

CBDs are often found in cellulose-degrading enzymes (cellulases) and enable specific binding even to densely packed crystalline cellulose, while the active site of the enzyme cleaves the glycosidic bonds. Apart from a well-defined secondary and tertiary structure, aromatic amino acids play an essential role in the interaction between enzymes and cellulose, as mentioned in Section 6.2.[150] CBDs are also used to add functionality to proteins/peptides, such as bifunctional antimicrobial peptides bound to nanocellulose.[151]

The main conclusion is that charge-driven interactions are possibly the most potent non-specific interactions between oppositely charged nanocellulose and proteins and have been exploited for protein immobilization (Table 2). Weishaupt and co-workers tested the adsorption capacities of TO-CNF for different proteins by mixing them in suspension and measuring the protein content in the supernatant after short incubation and centrifugation. The adsorption capacity for cytochrome c (pI = 10.5) at pH 7.7 and 5.8 remained the same, while myoglobin (pI = 7.0) and mp11 (pI = 7.0) were only adsorbed at the lower pH value (below their isoelectric point) when the protein was positively charged. Likewise, upon increasing the ionic strength, the screened opposite charges of the TO-CNF and the proteins reduced the adsorption efficiency. Furthermore, the protease papain (pI = 9.2) could be adsorbed onto TO-CNF and retained a reduced enzymatic activity.[147b] In further studies by the same authors, C-phycocyanin (pI = 6.1) was immobilized on TO-CNF at pH 5.2[152] and the antimicrobial peptide nisin (pI = 8.5) at pH 5.8.[153] Another example involves trypsin immobilization on TO-CNF (pI = 10.5) at neutral pH.[154] The adsorption of modified horseradish peroxidase close to the isoelectric point onto cellulose fibrils did not depend much on TEMPO-mediated oxidation of the cellulose substrate but rather on increased crystallinity (more hydrophobic effects due to less accessible hydroxyl groups) and increased hydrophobicity due to a modification with rosin.[155] This observation could indicate that hydrophobic effects play an essential role in the adsorption once ionic interactions are strongly reduced. The immobilization of enzymes on CNF can improve their temperature and pH stability and enable continuous biocatalysis and reusability of enzymes.[156]

The influence of proteins, in native and aggregated forms, on the chiral nematic liquid crystal phase (Section 5.5) has also been studied. De France et al. investigated the effects of lysozyme monomers and lysozyme amyloids, both short and rigid and long and semi-flexible, on the development of CNC chiral nematic phases.[158] While colloidal composites, including lysozyme amyloids, did not show a distinct effect on the chiral nematic pitch but rather limited the formation of a well-ordered chiral phase, the native lysozyme showed a clear blue shift of the resulting chiral nematic pitch with increasing protein concentration. In contrast to these bottom-up CNC–protein liquid crystals, Bast and co-workers successfully infiltrated pre-dried chiral nematic CNC films with bovine serum albumin (BSA), silk fibroin, and silk sericin.[159] In all cases, the presence of protein in the CNC films caused a redshift originating in an

**Table 2.** Overview of different proteins physically adsorbed/immobilized onto TO-CNFs. The buffer pH value at which the adsorption takes place must be below the isoelectric point (pI). Possible applications for the hybrid TO-CNF/protein particles are included.

| Protein | pI | Buffer pH | (Possible) application | Ref. |
|---|---|---|---|---|
| cytochrome c | 10.5 | 5.8 | – | [147b] |
| myoglobin | 7.0 | 5.8 | – | |
| microperoxidase (mp11) | 7.0 | 5.8 | biocatalysis | |
| papain | 9.2 | 5.8 | biocatalysis | |
| C-phycocyanin | 6.1 | 5.2 | metal sensing (after further modification) | [152] |
| nisin | 8.5 | 5.8 | antimicrobial materials | [153] |
| trypsin | 10.5 | 8.2 | biocatalysis | [154] |
| lysozyme | 10.7 | 7.4 | antimicrobial materials | [157] |


© 2023 The Authors. ChemSusChem published by Wiley-VCH GmbH

1864564x, 2023, 8, Downloaded from https://chemistry-europe.onlinelibrary.wiley.com/doi/10.1002/cssc.202201955 by Paul Scherrer Institut PSI, Wiley Online Library on [08/05/2023]. See the Terms and Conditions (https://onlinelibrary.wiley.com/terms-and-conditions) on Wiley Online Library for rules of use; OA articles are governed by the applicable Creative Commons License

increased chiral nematic pitch. The redshift suggests that positively charged lysozyme effectively screens the negative charges of the CNCs and decreases the pitch, while negatively charged proteins increase the repulsion and take up space between the CNCs, resulting in an increased pitch. However, differences resulting from the bottom-up versus top-down assembly mechanism cannot be excluded.[159]

### 6.5. Interactions with carbon nanoparticles

Integrating renewable materials such as nanocellulose with carbon nanoparticles towards electroactive cellulose-based materials is highly desirable, for example, in battery applications. During the first attempts at this, it was observed that nanocellulose was a highly efficient dispersing agent for unmodified carbon nanotubes (CNTs), which was not easily explained.[160] The first proposal was that a strong interaction is present due to the hydrophobic properties of CNTs and the amphiphilic properties of cellulose and that the charge of the nanocellulose stabilizes the CNT–CNF complex.[160a] Another hypothesis was specific binding via CH–π interactions.[160b,161] It was later shown that the interactions strongly depended on the charge density of CNFs so that the dispersive action was more efficient at higher charge density of the CNFs.[162] Furthermore, the same study showed a close relationship between the ionic strength of the solution and the interaction between CNF and graphene model surfaces, in the sense that the strength of the interaction decreased with increasing electrolyte concentration (Figure 28). These observations indicate that there is an electrostatic component involved in the interaction.

The current best hypothesis to explain this phenomenon is that if electron-electron correlation (dispersion forces) and ion–ion correlation exist, why should ion–electron correlation not exist? The spontaneous fluctuation of ions in the counterion cloud of the nanocellulose induces electron density fluctuations in the highly polarizable $sp^2$ carbon lattice, and the correlation of these fluctuations induces attraction. It has been shown that a higher surface charge increases ion–ion correlations, and ion-electron correlation would theoretically hence show a similar trend, which was also observed.[162] However, this hypothesis cannot fully explain the relatively large influence of ionic strength.

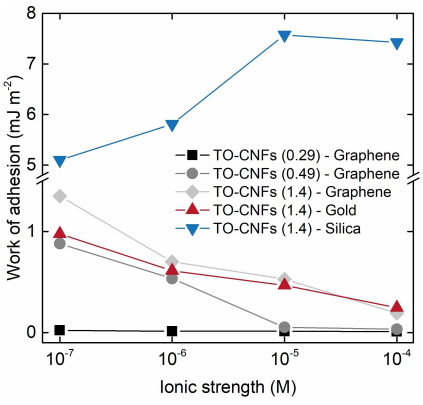


**Figure 28.** Adhesion between a CNF-coated silica microsphere and different flat surfaces as a function of the ionic strength of the solution (NaCl). The data were acquired by colloidal probe AFM, and kindly provided by Hajian et al.[162] In the legend, the values in parenthesis refer to the charge densities of the CNFs in mmol g$^{-1}$.

An alternative is to consider the balance between osmotic pressure and excluded volume. In a mixture of nanocellulose and CNTs, the lowest osmotic pressure would be achieved with a homogeneous distribution of CNTs between nanocellulose particles. If this state is reached by forcing CNTs to separate with mechanical force during the dispersing step, a phase separation back to CNT-rich and nanocellulose-rich phases with much higher osmotic pressure would be unfavorable in terms of entropy. This mechanism can be pictured as if the dielectric properties of CNTs screen the double layer repulsion between nanocelluloses. A nanocellulose with a higher charge density can accommodate more screening before aggregation and would be able to, and maybe even favorably, incorporate more CNTs and hence show better dispersive action. Increasing the ionic strength would favor phase separation, reducing the dispersive action. However, this is not directly comparable to the force observed by colloidal probe measurements.[162] This mechanism is often observed in mixtures of ionic and nonionic polymers where the ionic polymer is homogenously distributed to minimize the osmotic pressure.[163]

Besides the proposed mechanisms, fibril networks could also be a considerable mechanical barrier in the semi-dilute regime, preventing CNTs from finding each other after sonication due to the network properties discussed in Section 4. In conclusion, research is still needed to understand the interaction between nanocellulose and conducting nanoparticles.

The alternative explanation is similar to the recently discovered colloidal stabilization phenomena known as nanoparticle halos, which involves the segregation of charged nanoparticles to regions near large uncharged microparticles to act as stabilizing agents while minimizing the osmotic pressure in the nanoparticle phase.[164] An interaction between CNTs and CNFs, such as ion-electron correlation, would favor such an organization further.

## 7. Bottom-Up Assembly by Controlling Nanocellulose Interactions

A crucial part of materials development is structural control. Structural control at the nanoscale is needed to utilize the mechanical properties of the nano-component but can also give unique properties. For nanocellulose, nanostructural control is, for example, the parallel orientation of crystal domains in which the stiffness of the cellulose crystal is best utilized since the fibrils point in the same direction. Another structure is forming nanometer-thin layered films with other components that add optical, electronic, or other functions. This section elaborates on how understanding and controlling the colloidal


© 2023 The Authors. ChemSusChem published by Wiley-VCH GmbH

1864564x, 2023, 8, Downloaded from https://chemistry-europe.onlinelibrary.wiley.com/doi/10.1002/cssc.202201955 by Paul Scherrer Institut PSI, Wiley Online Library on [08/05/2023]. See the Terms and Conditions (https://onlinelibrary.wiley.com/terms-and-conditions) on Wiley Online Library for rules of use; OA articles are governed by the applicable Creative Commons License

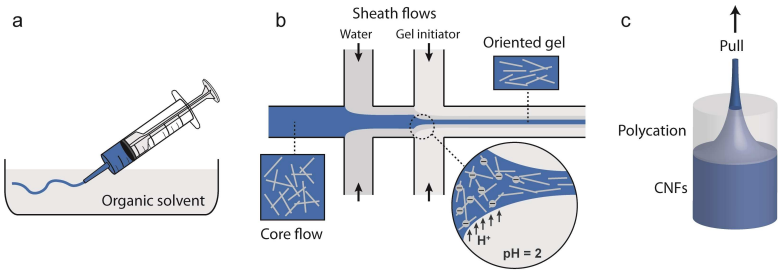


**Figure 29.** Illustration showing methods for preparing filaments: a) shear-induced alignment and precipitation,[167] b) flow-focusing and acid-induced gelation,[38b,91] and c) interfacial complexation with polyelectrolytes.[171a]

properties of nanocellulose is used in the bottom-up assembly of materials. The subject has been recently summarized in detail,[165] and this section thus focuses on assemblies that directly relate to the colloidal stability-instability concepts previously discussed.

### 7.1. Hydrodynamic alignment

One way to achieve parallel orientation of crystal domains is the hydrodynamic alignment of nanocelluloses[166] and subsequent gelation with acid or organic solvents to produce stiff and strong filaments. In 2011 Iwamoto et al.[167] first demonstrated this using shear-induced alignment by syringe extrusion into an acetone bath (Figure 29a), in which gelation occurs since the colloidal stability is severely limited due to the low dielectric constant of acetone (see Equation (6)). A higher flow rate resulted in more significant shear in the TO-CNF dispersion and a higher degree of orientation along the axis of the gel thread and hence a stiffer fiber upon drying.

Since 2011, several other techniques have been developed, and the property space of the prepared fiber has been studied.[168] However, the highest shear is found close to the wall, and shear-induced alignment thus has limitations in orientational homogeneity and degree of orientation. An elongational flow method was developed by Håkansson et al. to alleviate the problem with only local orientation of the fibrils for a more homogeneous alignment.[169] In this approach, one or two sheath flows accelerate a core flow containing CNFs (Figure 29b). The last sheath flow is a gel initiator, usually an acid, that rapidly locks the oriented structure by the colloidal instability upon charge neutralization. This approach has led to the manufacturing the strongest artificial bio-based material known today.[170]

Another way of forming filaments from nanocellulose is to utilize the complexation with polyelectrolytes and the interfacial complexation method.[171] In this method, a nanocellulose dispersion is carefully covered with an oppositely charged polyelectrolyte solution or placed next to a drop of the same. A complex phase is then formed at the interface between the suspensions. A tweezer is used to grab the interfacial complex and pull it upwards so that a filament is formed continuously, where the interface quickly forms new complexes as the filament is pulled out (Figure 29c).[171a] However, due to the limited alignment and chaotic complexation, such filaments are weaker than those prepared by accelerating flow or shear. The advantage is that other properties can be more easily tailored, such as the functionality and morphology of the surface.

Other hydrodynamic-influenced alignment methods for nanocellulose were recently summarized,[172] including casting or drying,[173] spinning,[174] and templating.[81,175]

### 7.2. Alignment by magnetic and electric fields

In addition to shear or accelerated flows, magnetic and electric fields can provide the required energy to align nanocelluloses (Figure 30). The orientation of CNCs from tunicate cellulose perpendicular to magnetic fields was first shown in 1992 by Sugiyama et al.[176] The suggested explanation was that orientation is due to the magnetic susceptibility of the different covalent bonds in cellulose and their relative orientation in the crystal, leading to a negative diamagnetic anisotropy. It was later demonstrated how this could align CNCs during deposition on flat surfaces using casting or the layer-by-layer (LbL) technique.[177] The disadvantage is that the process is relatively slow and requires high magnetic field strengths.

Few successful attempts have achieved a high degree of alignment of CNFs in magnetic fields. The generated force and the alignment rate are probably not enough to disentangle CNF networks. Instead, electrical fields have been shown to align high aspect ratio nanocelluloses.[178]

The first example of alignment of CNCs in an electric field was shown in 2006, using an organic solvent to avoid issues with the conductivity of water.[179] Similarly, CNFs have been aligned after transfer to silicone oil.[180] This type of alignment is most favorable in the case of metallic nanoparticles or nano-

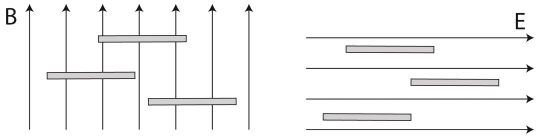


**Figure 30.** Schematic of how magnetic (left) and electric fields (right) align nanocelluloses.


© 2023 The Authors. ChemSusChem published by Wiley-VCH GmbH

18645564x, 2023, 8, Downloaded from https://chemistry-europe.onlinelibrary.wiley.com/doi/10.1002/cssc.202201955 by Paul Scherrer Institut PSI, Wiley Online Library on [08/05/2023]. See the Terms and Conditions (https://onlinelibrary.wiley.com/terms-and-conditions) on Wiley Online Library for rules of use; OA articles are governed by the applicable Creative Commons License

particles with permanent dipole moments.[181] Since the alignment by electrical fields and the permanent dipole moment is related, the dipole moment of CNCs has been determined to be 4400 ± 400 D using this experiment, which is giant compared to 100–20 D in the case of frequently used CdSe or CdS nanorods.[115,181,182] The reason is suggested to be the parallel arrangements of glucan chains in the cellulose I crystal lattice (all chains pointing in the same direction) and the accumulative dipole moments of the glucosyl monomers. Cellulose I is a metastable crystal structure, and after regeneration, cellulose II is formed, in which the glucan chains are antiparallel. Although it has not been shown, if the hypothesis is true, the giant permanent dipole moment should thus only be found in native cellulose.[183] It is considered a unique property that probably influences the colloidal properties of nanocelluloses to a higher degree than expected. The giant dipole moment may influence phenomena such as ions-specific interactions, stabilization of nanocarbons, and chiral nematic organization.

Alignment by magnetic or electrical fields has been used to align nanocelluloses in reinforced composites or to create filaments with alignment after the initial gelling.[178,184] Efforts have been made to combine hydrodynamic alignment and alignment by electric fields to stabilize and improve the order.[185] Furthermore, in electrically aligned nanocellulose materials, the dipole of the particles points in the same direction, improving the piezoelectric properties of nanocellulose films used for sensors or nanogenerators.[186]

### 7.3. Layer-by-layer assembly

A way of making polyion complexation (see Section 6.1) into a process with a higher degree of control is to adapt the layer-by-layer (LbL) assembly technique, in which cationic and anionic nanometer-thin layers are assembled sequentially (Figure 31). Kirkland[187a] and Iler[187b] first reported the LbL technique in the 1960s for assemblies of colloidal particles, but its revolution came in the 1990s when Decher and Hong[187c] involved polyelectrolytes, which were easier to assemble and provided more versatility. The first publication of LbL involving nanocellulose was shown for CNCs in 2005 by the group led by Kotov.[188] The first example where CNFs were used resulted from a collaboration between Wågberg et al. and Decher in 2008, producing smooth films that showed well-defined interference colors.[9b] Since then, there have been many examples of LbL assembly of nanocellulose to design materials for applications, such as barrier films, fire retardant coatings, and more.[189]

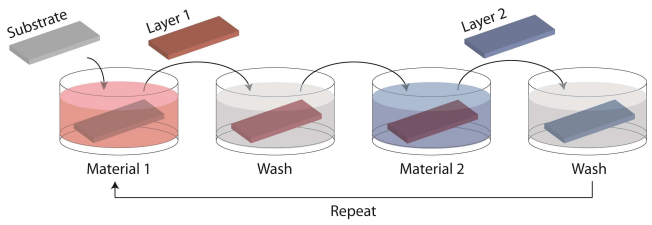


**Figure 31.** Schematic showing the typical procedure of LbL assembly by dipping.

However, the classical LbL process, involving rinsing between each step, is time-consuming and only advantageous when nanoscale control is required to achieve the sought properties. An example is when preparing model surfaces to study the interaction between nanocellulose and other components using high-resolution measurement techniques, such as quartz crystal microbalance, surface plasmon resonance spectroscopy, or reflectometry.[118b,174,190]

The interactions between hemicelluloses and cellulose (see Section 6.2) have also been used for the controlled assembly of multilayered thin films of CNCs and xyloglucan using the LbL technique.[191] Potentially any colloid that interacts with nanocellulose can be used in multilayer assemblies. There are also examples where LbL assembly based on polyion and the non-ionic association have been combined to create microcapsules with ion-responsive permeability, potentially used in drug delivery and other applications.[192] Imagination and application-driven demands are the only limitations when working with LbL since variations in assembly sequences are, in principle, unlimited.

### 7.4. Ion-specific assembly

Since the counterion cloud has a significant impact on the properties of nanoparticles, exchanging the counterions can be implemented to control the assembly of nanocellulose, as discussed in Section 5. Exchanging the sodium counterions to multivalent ions produce CNF hydrogels with remarkable mechanical properties.[65] Exposure to multivalent ions has also been used to develop water-resilient CNF films with wet mechanical properties surpassing those of many plastics.[90,98,193] In these examples, different cations enable the tailoring of mechanical properties primarily in the wet state, where the high aspect ratio of CNFs leads to a high strength at low solids content, which is difficult to achieve in polymeric systems. When comparing the relative moduli of these materials as a function of the stability constants of complexes (Figure 32), a clear trend appears related to the properties of the metal ions, discussed in Section 5.

Soaking dry nanocellulose films in a solution of multivalent ions leads to highly water-resilient materials.[90,98,193] The material reaches a strength of 40–50 MPa at 2–10% strain, a modulus of 1–3 GPa, and has improved gas barrier properties when soaked in deionized water. These properties are comparable to high-performance plastics, such as high-density polyethylene (HDPE),[194] demonstrating that nanocellulose films are promising for packaging applications even under wet or moist conditions.

An interesting property of wet CNF networks is the highly nonlinear relationship between the solidity of the network and its stiffness.[98] In a dry paper, the stiffness is directly proportional to the density of the network, but in a wet CNF network, the in-plane stiffness is proportional to the solidity to the power


© 2023 The Authors. ChemSusChem published by Wiley-VCH GmbH

1864564x, 2023, 8, Downloaded from https://chemistry-europe.onlinelibrary.wiley.com/doi/10.1002/cssc.202201955 by Paul Scherrer Institut PSI, Wiley Online Library on [08/05/2023]. See the Terms and Conditions (https://onlinelibrary.wiley.com/terms-and-conditions) on Wiley Online Library for rules of use; OA articles are governed by the applicable Creative Commons License

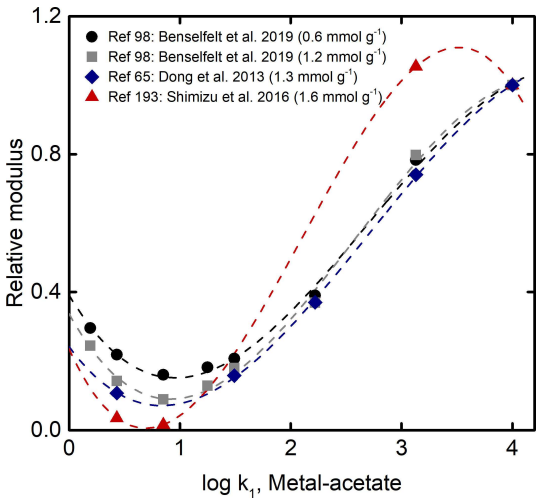


**Figure 32.** Relative modulus of metal ion-treated TO-CNF materials as a function of the stability constant of metal–acetate.[98] The charge density of the CNFs is marked in parenthesis in the legend.[65,98,193] The data were kindly provided by Benselfelt et al.[98] and in mentioned references.

of 4. These results show that the mechanical property space of CNF hydrogels is vast and can be tailored by solidity. However, without crosslinking with, for example, metal ions, the water resilience of CNF materials is a compromise between charge density and yield. A lower charge density leads to more wet-stable CNF-based materials, but producing low-charge-density CNFs requires a higher amount of energy and results in a lower yield of colloidally stable nanoparticles. Thus, an optimal relationship between charge density and wet strength should exist.

### 7.5. Utilizing the chiral-nematic organization

The passive ordering of nanocelluloses into nematic phases can be utilized in materials design. CNF films prepared by vacuum filtration or solvent casting have different mechanical properties due to the ordering in the latter case.[113] The same has been observed for CNCs, but the alignment mainly affects the stiffness of these films.[195] The chiral-nematic ordering of CNCs has been used to manufacture renewable and biodegradable glitter.[196]

The nematic ordering of CNCs has also been used as a sacrificial template to create different materials, such as resins or inorganic materials, with a chiral nematic nanostructure. Much of this work has been conducted and summarized by MacLachlan and co-workers.[197] These materials show photonic behaviors that can be used for optical applications. Controlling the colloidal properties of the CNCs in the presence of other materials is challenging but, as demonstrated, necessary for developing CNC-templated cholesteric composites.

### 7.6. Assembly using proteins

The association of nanocelluloses and proteins can be used to form gels. Wu and co-workers observed the complexation of TO-CNF upon adding positively charged lysozyme (Figure 33a), which resulted in the screening of the negative charge of TO-CNF, leading to increased turbidity and promoting the formation of microgels. An increased viscosity and network formation ($G' > G''$) upon the addition of lysozyme was measured (Figure 33b). The complexation was reversible by charge inversion (going above the pI of lysozyme to have a negative net charge) (Figure 33c).[157] Electrostatically enabled complexation was also recently used to assemble hydrogels and

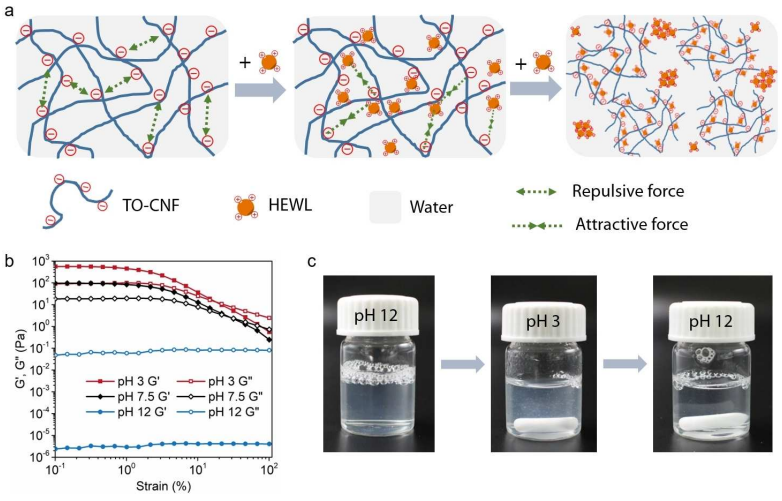


**Figure 33.** a) Schematic of the charge screening and complexation of negatively charged TO-CNF upon addition of positively charged hen egg-white lysozyme (HEWL) at pH 7.4. b) pH-dependent viscoelastic moduli showing a fluid-like behavior for a CNF: HEWL, 10:7 ratio at pH 12, at which TO-CNF and HEWL are both negatively charged. c) Images of a CNF: HEWL, 10:7 ratio sample undergoing a pH change from pH 12 to pH 3 (increased turbidity through charge screening/complexation) and back to pH 12 demonstrating the reversibility of the process. Data, schematics, and figures were kindly provided or adapted from Wu et al.[157] Copyright: Elsevier 2021.


© 2023 The Authors. ChemSusChem published by Wiley-VCH GmbH

18645564x, 2023, 8, Downloaded from https://chemistry-europe.onlinelibrary.wiley.com/doi/10.1002/cssc.202201955 by Paul Scherrer Institut PSI, Wiley Online Library on [08/05/2023]. See the Terms and Conditions (https://onlinelibrary.wiley.com/terms-and-conditions) on Wiley Online Library for rules of use; OA articles are governed by the applicable Creative Commons License

aerogels consisting of binary cellulose-protein combinations of CNCs, TO-CNFs, and full-length and shortened lysozyme amyloid fibrils.[198]

Understanding the interactions between nanocelluloses and proteins is crucial for developing new hybrid particles and biocomposites. Demonstrated applications for these materials include biocatalysis with immobilized enzymes,[147b,154,156] metal sensing,[152] bio-sensing[199] and antimicrobial materials.[151,153,158] Although colloidal interactions between CNF and fibrillar proteins remain largely unexplored, combinations of nanocellulose and silk fibroin, gelatin, and collagen have resulted in new functional materials for biomedical applications, usually with improved mechanical properties and biocompatibility.[200] Nanocellulose mixed with amyloid fibrils has been explored for wound dressing applications[158,201] and water filtration.[202]

### 7.8. Assembly at interfaces in emulsions

Nanocelluloses adsorb to air–water (A/W) and oil–water (O/W) interfaces.[203] Due to their strong negative charge and the resulting apparent hydrophilicity, nanocelluloses were generally considered non-surface-active[203a] until changes in surface pressure were measured by Bertsch et al. for CNCs[203b] and CNFs[204] adsorbing to the air-water interface and CNCs[205] to the oil–water interface. A possible explanation for the surface activity could be that different planes in the crystalline structure of cellulose expose hydrophilic hydroxyl groups and hydrophobic CH groups, respectively, giving CNCs slightly amphiphilic properties favoring interfacial adsorption.[206]

The adsorption kinetics of CNCs were slow, showing a lag phase of diffusion of the nanocellulose to the interface. A stable interfacial pressure was only reached after several hours, attributed to the electrostatic adsorption barrier, that is, the repulsion between already adsorbed CNCs at the interface and bulk CNCs.[203b,205,207] It was also shown that the adsorption kinetics were accelerated by adding NaCl, reducing the Debye length and the osmotic pressure difference in the double layer repulsion (Section 1.2).[203b,204,205] In the case of CNCs, NaCl addition above 20 mM led to viscoelastic interfacial layers ($G_i' > G''_i$), while the layers showed a viscous behavior ($G_i' < G''_i$) at lower ionic strength, as confirmed by interfacial shear rheology. In this case, charge screening led to the formation of CNC networks even at low interface coverage of around 20%.[203b]

Another way to control double layer repulsion is by the charge density (Section 1.2). TO-CNFs with lower charge density are adsorbed much faster at the A/W interface than highly oxidized TO-CNFs.[204] Dilatational rheology experiments found viscoelastic layers of CNFs at the A/W interface, independent of their charge density. The viscoelastic layer was explained by the higher aspect ratio leading to entanglement and the higher interface coverage of 40%.[204] The interfacial structure has been examined by immobilizing the interface on a mica disk in a Langmuir-Schaefer deposition followed by AFM imaging, confirming higher particle densities at the interface than in the bulk.[203b,207] This procedure is relatively simple but invasive, possibly causing structural changes during the deposition and the drying of the samples.

Non-destructive structural analysis of interfaces has been achieved with small-angle neutron scattering (SANS)[7] and neutron reflectometry[203b,204] experiments. Cherhal et al. exploited contrast variation in SANS experiments to measure the thickness of CNC layers at the O/W interface for sulfated CNCs (7 nm) and desulfated CNCs (18 nm), suggesting that the charged CNCs formed monolayers with alignment along the interface. In contrast, uncharged CNCs formed rougher, more unorganized interfaces.[206b] Furthermore, it was shown that the CNCs were fully submerged in the water phase, later supported by neutron reflectometry measurements of CNCs and CNFs at flat A/W interfaces.[203b,204] The results from neutron reflectometry also allowed the estimation of the interface coverage mentioned above. Grazing incidence small-angle neutron and X-ray scattering (GISANS and GISAXS) experiments of nanocellulose stabilized interfaces have so far not been reported. Such non-invasive measurements could give valuable additional insights into the lateral arrangement of the particles (i.e., alignment, 2D liquid crystal formation) and interfacial roughness, and give a direct comparison of bulk and interfacial structure.[208]

The structure of the interface, especially the protrusion of the nanocellulose particles into the respective phase, plays a crucial role in the interfacial stabilization and is described as the contact angle ($\theta$) in the so-called Pickering effect (Equations (15) and (16)).[203a,209]

$$\Delta E = -\pi r^2 \gamma (1 - |\cos\theta|)^2 \quad (15)$$

$$\Delta E = -Ld\gamma (1 - |\cos\theta|)^2 \quad (16)$$

The equations differ in terms of the contact area $\pi r^2$ (sphere) and $Ld$ (product of length and width of the rod), where $\gamma$ is the interfacial tension of the O/W or A/W interface. The contact angle $\theta$ is determined by the wetting behavior of the particle, which depends on the surface chemistry of the particle. The decrease in interfacial energy is maximized at $\theta = 90°$, contact angles below 90° ($\theta < 90°$) are seen for preferential wetting by the water phase, and contact angles above 90° ($\theta > 90°$) for wetting by the hydrophobic phase. Based on Equation (16), the calculated desorption energy for particles is 103–104 $k_BT$, while surfactants are easily desorbed with desorption energies of a few $k_BT$.[203a,207]

While CNCs can form Pickering emulsions,[206a,210] stable particle-stabilized foams from CNCs have not been observed.[207] Despite successfully adsorbing and forming viscoelastic layers at air-water interfaces, linked with a decrease in surface tension, the fact that CNCs have an extremely low contact angle (almost submerged in the water phase) leads to a reduction of the desorption energy of the particles from the interface according to Equation (16) and to the inability to stabilize foams.[203b,204] To reach higher desorption energies, the surface chemistry of the nanocellulose particles has to be modified to obtain a more preferential contact angle.


© 2023 The Authors. ChemSusChem published by Wiley-VCH GmbH

1864564x, 2023, 8, Downloaded from https://chemistry-europe.onlinelibrary.wiley.com/doi/10.1002/cssc.202201955 by Paul Scherrer Institut PSI, Wiley Online Library on [08/05/2023]. See the Terms and Conditions (https://onlinelibrary.wiley.com/terms-and-conditions) on Wiley Online Library for rules of use; OA articles are governed by the applicable Creative Commons License

Chemical (covalent) modification of nanocellulose creating more hydrophobic surface chemistry, for example, by methylation of CNCs, led to adsorption at the air-water interface within seconds,[211] and ultra-stable foams have been reported for ethylcellulose nanoparticles.[212] Alternatively, nanocelluloses can be hydrophobized by adsorbing a cationic surfactant onto their surface, as described by Cervin et al. in the production of low-density dried nanocellulose foams.[213] Nanocellulose-surfactant interactions are described in more detail in Section 6.3. Cervin et al. also showed that the viscoelastic properties of the nanocellulose network at the A/W interface are of utmost importance and are determined by the aspect ratio and charge density of the CNFs.[213b] Several recent review papers summarized the literature on nanocellulose-stabilized interfaces, emulsions, and foams and their applications.[203a,207,214]

### 7.9. Utilizing the mesh size of nanocellulose networks

Nordenström et al.[72] did not only measure the mesh size by tracer nanoparticles but also the stabilizing action of CNF networks on microparticles of 1–5 μm in diameter. In a dilute CNF dispersion with a concentration of 0.2 wt%, that is, above the rigidity threshold of 3 contacts per fibril, the sedimentation velocity of the microparticles was reduced to 1% of the initial velocity in water (Figure 34a). The similar behavior of 2 and 5 μm particles showed that sedimentation in these networks was dictated by network dynamics rather than the gravitational pull on the microparticles. By further arresting the network using HCl to form a gel, the sedimentation of the microparticles was already prevented at a CNF concentration of 0.05 wt% (Figure 34b). This low concentration shows that tiny amounts of CNFs can be used to prevent sedimentation over long periods, which could be extremely valuable in some industrial processes, such as in coating dispersions in papermaking and the production of nonwoven products containing very long fibers. As another example, Bai et al.,[215] showed that adding CNFs to Pickering emulsions stabilized by CNCs provided additional stability. Although the authors called it depletion stabilization, the mechanism is probably more similar to the stabilization of silica particles.

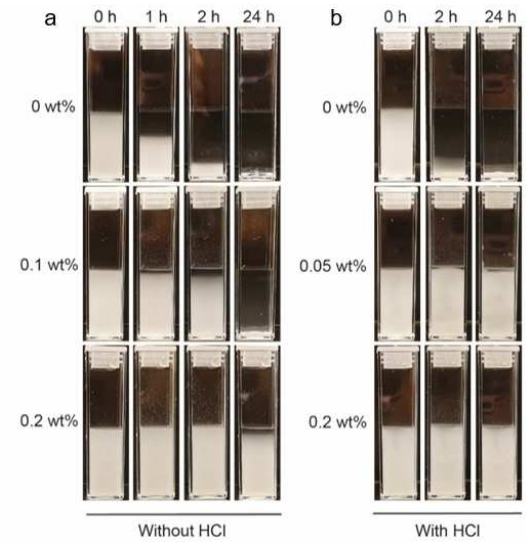


**Figure 34.** Photographs of the sedimentation of silica microparticles in a) nanocellulose glasses and b) nanocellulose gels. Reprinted from Nordenström et al.[72] with permission from Elsevier.

A few authors have investigated sedimentation or microbubble buoyancy in nanocellulose networks.[216] These studies showed that the yield stress is almost directly proportional to the nanocellulose concentration [wt%]. However, the microscopic yield stress was an order of magnitude higher than the net yield stress of the bulk due to the local densification of the network around moving objects. The long-range stress transfer of nanocellulose networks amplifies this mechanism. The effective stressed area is thus much larger than the particle dimensions, leading to increased stability than predicted from bulk yield by rheology. Note that for repulsive networks over longer times, the network can relax and allow bubbles to escape or particles to sediment since the yield depends on the relaxation time of the nanocellulose network.

## 8. Drying and Redispersing Nanocellulose

CNFs are commonly handled as aqueous dispersions of low concentration due to their hydrophilic character and tendency to aggregate at higher solids content. These concentrations are problematic for some potential applications in which the presence of water is highly disadvantageous, for example, the production of many polymer composites or in charge storage applications. Therefore there is a need for dry CNFs that are easily redispersed. Drying or concentrating CNF is also desirable due to the environmental impact and high costs of transporting such dilute dispersions and the reduced risk of bacterial growth, which enables an extended shelf-life. The main obstacle for drying CNFs is the formation of irreversible aggregation, known as hornification in the pulp and paper industry, resulting in larger nanoparticles upon redispersion, diminishing the outstanding properties associated with nanofibrils. In comparison, the redispersion of CNCs is considerably more straightforward, and redispersible CNC powders are commercially available.[217]

In a CNF dispersion, the nanoparticles have several interactions: double-layer, van der Waals, specific ion effects, and ion–ion correlation, as described in Sections 1 and 5. The repulsive interactions should exceed the attractive interactions to achieve colloidal stability, leading to a substantial distance between the CNFs. If water is evaporated during drying, the interfibrillar distance decreases, and capillary forces are exerted on adjacent CNFs. Consequently, the CNFs are pulled closer together, allowing an enhanced influence of relatively short-ranged attractive interactions, such as van der Waals interactions. Thus, the CNFs form aggregates that are generally not disassociated upon dilution. Traditionally, the irreversible change of properties induced by the drying of cellulosic materials has often been explained by hydrogen bonds. Although hydrogen bonds may form as the interfibrillar


© 2023 The Authors. ChemSusChem published by Wiley-VCH GmbH

1864564x, 2023, 8, Downloaded from https://chemistry-europe.onlinelibrary.wiley.com/doi/10.1002/cssc.202201955 by Paul Scherrer Institut PSI, Wiley Online Library on [08/05/2023]. See the Terms and Conditions (https://onlinelibrary.wiley.com/terms-and-conditions) on Wiley Online Library for rules of use; OA articles are governed by the applicable Creative Commons License

distance decreases during drying, they are not likely to endure by themselves after water is reintroduced.[118c]

Comparing different published studies on nanocellulose redispersibility is not straightforward due to the different drying techniques, redispersion- and evaluation methods used. The impact of different drying techniques will be described later in this section. The redispersion protocols often involve mechanical stirring, sometimes combined with magnetic stirring or ultrasonication, but it can also be as gentle as simply shaking the sample after dilution.[218] Some of the most commonly reported evaluation strategies are measuring the effect of redispersion on the mechanical properties of nanopapers,[219] morphology,[219b,220] sedimentation,[219a,220b–d,221] rheological properties[219b,220a,c,d,221,222] or particle size.[218] Some of these methods measure the redispersibility on a nano-/microscale, while others measure its macroscale effects. It has been shown that even if the CNFs are aggregated to some extent, it does not necessarily have a noticeable impact on macroscale properties, such as the tensile properties of CNF sheets.[223] Consequently, it is essential to consider what redispersibility is aimed for in the different contributions.

### 8.1. Drying methods

The morphology of dry nanocellulose and the redispersing ability are highly dependent on the drying method. The most straightforward technique for drying nanocellulose is solvent evaporation accelerated by heat, but other commonly reported drying methods include freeze-drying, spray drying, and supercritical drying. Peng et al.,[224] compared these techniques in terms of the effect of particle size and morphology. They found that aggregates formed regardless of the drying method, but the mechanisms responsible for their creation differed.

During oven drying, the interfibrillar distances decrease due to solvent evaporation. There is a balance between repulsive double-layer forces and attractive van der Waals and capillary forces, and when the CNFs are nearby, they aggregate due to the van der Waals interactions. Similarly, in spray drying, water is evaporated when droplets of the dispersion are placed in contact with hot air, and the result is aggregated CNF particles of different shapes and sizes, depending on operating conditions.[224] For TEMPO-oxidized CNFs, produced using the TEMPO/NaBr/NaClO method at pH 10,[17] there is an additional mechanism causing aggregation. In the oxidation process, small but significant amounts of aldehydes and ketones are formed, and when heat is applied during drying, interfibrillar hemiacetal/hemiketal bonds may be created. These bonds decrease dispersibility and are responsible for the yellow color characteristic of this type of dried CNFs.[222b]

The capillary forces that pull CNFs together during water evaporation can be reduced or avoided using supercritical drying or freeze-drying. In supercritical drying, this is achieved by avoiding the formation of a liquid/gas interface by replacing the water with a supercritical fluid, commonly carbon dioxide, before drying. Under the appropriate operating conditions, the structure in the sample is assumed to be unchanged. The disadvantages are associated with the relatively large amounts of solvents needed since an intermediate solvent exchange step is required due to the poor miscibility of most supercritical fluids in water.

In freeze-drying, the sample is dehydrated by first freezing the water, followed by sublimation of the ice at low pressure. In the freezing stage, ice crystals grow in the direction of the temperature gradient and exclude the CNFs, pushing them closer to each other. As a result, the CNF concentration increases in the spaces between the ice crystals, and a lateral aggregation behavior can often be observed.[224,225] To reduce lateral aggregation and facilitate redispersion, the formation of large ice crystals must be diminished. Since ice crystal growth decreases with an increased freezing rate, liquid nitrogen is commonly used in the freezing stage. However, even with this strategy, achieving completely individualized CNFs after redispersion is not easy.

### 8.2. Surface modifications for increased redispersibility

Introducing charged groups to the CNF surfaces allows for the preparation of colloidally stable dispersions and also increases the redispersibility upon drying. The positive effect of charges on redispersibility is related to the osmotic effect, which increases the driving force for swelling, and a steric effect caused by the bulky charged groups.[222a] Generally, the ability to regain the original properties after redispersion increases with surface charge density.[220b,222a] As an example, freeze-dried TEMPO-oxidized CNFs with a charge of 1.2 mmol $g^{-1}$ has been shown to redisperse into individualized fibrils upon dilution, while the same treatment of 0.7 mmol $g^{-1}$ CNFs results in extensive aggregation.[223b] Eyholzer et al.[220b] reported that redispersible powders of carboxymethylated CNFs (surface charge density approximately 0.9 mmol $g^{-1}$) could be produced by solvent exchange followed by oven drying. The redispersibility was evaluated by sedimentation tests and SEM. Furthermore, the redispersibility is influenced by the size of the charged group since larger charged groups ( for example, cationic CNFs in Section 5.6) enhance the steric repulsion between the CNFs.[226] While introducing high amounts of charged groups enables the preparation of redispersible CNFs, there are drawbacks, for example, slow and costly de-watering, which is not always feasible.[222a]

For CNFs prepared using the TEMPO/NaBr/NaClO protocol,[17] interfibrillar hemiacetals/hemiketals formed between aldehydes/ketones and hydroxyl groups is an additional driving force for irreversible aggregation during drying. The aldehyde and ketone content can be reduced by $NaBH_4$ reduction to minimize this effect. Alternatively, already-formed interfibrillar bonds can be broken by treatment in hot water (80 °C) in alkaline conditions.[227] Oxidation of aldehydes using $NaClO_2$ slightly improves redispersibility, but irreversible aggregation still occurs due to the remaining ketones.[222b]


© 2023 The Authors. ChemSusChem published by Wiley-VCH GmbH

1864564x, 2023, 8, Downloaded from https://chemistry-europe.onlinelibrary.wiley.com/doi/10.1002/cssc.202201955 by Paul Scherrer Institut PSI, Wiley Online Library on [08/05/2023]. See the Terms and Conditions (https://onlinelibrary.wiley.com/terms-and-conditions) on Wiley Online Library for rules of use; OA articles are governed by the applicable Creative Commons License

1864564x, 2023, 8, Downloaded from https://chemistry-europe.onlinelibrary.wiley.com/doi/10.1002/cssc.202201955 by Paul Scherrer Institut PSI, Wiley Online Library on [08/05/2023]. See the Terms and Conditions (https://onlinelibrary.wiley.com/terms-and-conditions) on Wiley Online Library for rules of use; OA articles are governed by the applicable Creative Commons License

### 8.3. Redispersing agents

A common method for improving nanoparticle redispersibility is adding redispersing agents, such as polymers or small molecules. An advantage of this strategy is that separation of the redispersing agents from the CNF is possible by dialysis[220a] or filtration,[220c] and no irreversible surface modification is required. Polymeric redispersing agents can reduce the friction between the fibrils by steric and/or electrostatic interactions or by forming a hydrated layer close to the CNF surface. They can also affect the surrounding water's fluid properties, thereby reducing the risk of collisions and aggregation between CNFs.[228]

One of the most frequently reported redispersion agents for cellulose nanofibrils is carboxymethylated cellulose (CMC).[219b,221,222,223b,229] The reported amounts of CMC required to achieve redispersion vary immensely (between 1 wt% and 100 wt%, based on the amount of CNF), due to different drying methods, redispersing techniques, types of CNF, as well as the definition and evaluation of redispersibility. The amount of CMC irreversibly adsorbed onto CNF is generally modest,[228,230] but efforts have been made to increase the adsorbed amount to enhance the effect on redispersibility. More efficient adsorption can be accomplished by increasing the temperature to above 120 °C and adding a preferably divalent electrolyte.[230] In a study by Butchosa and Zhou,[219b] 2.3 wt% CMC was adsorbed to CNF at high temperatures, and this treatment improved the stability of redispersed samples, as evaluated by sedimentation tests.

Herrick[229] compared the viscosities of redispersed nanocellulose dispersions with those of the original dispersions and the impact of different redispersing agents. He found that low molecular weight compounds, especially sucrose, had a more positive effect on redispersibility than polymeric compounds. Missoum et al.[220a] also used ions as redispersion agents, namely NaCl. A water-dispersible powder was obtained by adding 10 mM NaCl to enzymatically pretreated CNF before freeze-drying, as evaluated by rheology and SEM. The authors explain the effect of NaCl due to its ability to block hydrogen bonds by ion–dipole interactions with the hydroxyl groups of the CNFs. Other additives that have been shown to have a positive effect on nanocellulose redispersibility include polyethylene glycol (PEG),[218,223b,231] glycerol,[219a,232] cetyltrimethylammonium bromide (CTAB),[233] polyvinyl alcohol (PVA),[220d] maltodextrin[220c] and lignin.[223b]

## 9. Future Perspectives

For biological materials such as nanocellulose, there are naturally occurring variations in properties. For example, the yearly growth cycle of trees will lead to different densities in the wood, known as early- and latewood. Year-to-year variations in weather will also affect the structure of the wood tissue. These structural variations mean that the utilization of nanocellulose will always be based on naturally occurring variations in quality. Control over quality and properties is a minimum requirement for efficient bottom-up engineering. An essential future perspective is thus quality control, which requires well-established standards and methods. In the future, as nanocellulose becomes more industrially available, academia should develop and agree on such a quality control system. Today's available methods are somewhat time-consuming, and there is a strong need for fast and reliable benchmarking techniques. The classification of nanocellulose is also related, raising questions like: where is the dividing line between CNCs and CNFs? At what lateral stacking of cellulose crystals do CNFs transition into microfibrils (MFCs)? How do we best describe entangled systems? How do we define the kink-induced flexibility of CNFs? A critical future perspective is thus control over the quality, definitions, nomenclature, and the establishment of the impact of molecular properties of the cellulose constituting the different nanocelluloses. It was early established that the mechanical properties of nanopapers from CNF are highly dependent on the molecular mass of the glucan chains in the nanocelluloses, but astonishingly few publications have been devoted to this important aspect.

The theoretical description of small nanoparticles is also essential in future efforts. This need applies to nanocelluloses and nanoparticles in general and is currently one of the most pressing challenges in colloidal and physical chemistry. Kotov and co-workers[2] nicely summarized these issues. For cellulose, this challenge involves the anisotropic properties, such as the twist of the cellulose crystal and how it leads to cholesteric liquid crystal phases. The reason for and effects of the twist of the cellulose crystal is still an open discussion, and a proper colloidal chemical description of CNFs and CNCs is still needed and should be further prioritized.

The preparation of nanocellulose is a struggle against colloidal instability and solving the challenges in this process requires understanding why cellulose associates so strongly. One example is the irreversible aggregation upon drying, known as hornification, which creates difficulties in efficiently transporting nanocelluloses since it has to be done in a dispersed state comprising more than 90% water. Shipping water is not energy efficient and thus very expensive. There are many hypotheses on the mechanism of hornification, but nothing has been established, even though it has been discussed for hundreds of years. More efforts should be put into understanding hornification and how it can be prevented, which will greatly benefit the pulp and paper industry.

As a final note, it is reasonable to be slightly concerned about the lacking large-scale manufacturing and utilization of nanocellulose. Although there are many demonstrations of excellent materials and applications, there is not yet a killer application that will take nanocellulose production and utilization to a large industrial scale. Nanocellulose at an industrial scale is desirable to benefit from all resources spent on research and is needed to motivate further research. Nanocellulose research may soon be leaving the initial academic "bubble," and industrial production and academic research must go hand in hand to motivate long-term investments and developments. There are many inspiring start-ups, but we are still waiting for the boom. It must also be stressed that the production costs for


© 2023 The Authors. ChemSusChem published by Wiley-VCH GmbH

nanocelluloses, maybe with a special focus on CNFs, must be decreased. Hence, there is a need for new process developments for the full-scale use of CNFs.

Where then can we find the killer application for nanocellulose? The reason we have not found it yet is related to some of the challenges discussed in this comprehensive overview, for example, the high viscosity at a low concentration which makes nanocellulose challenging to produce at scale, or the strong interaction with water that makes drying of nanocellulose materials energy-demanding. On the other hand, these properties might also hint where to find the killer application, such as viscosity modifiers in food, paints, construction materials, or inks where the trends moving towards the use of more benign solvents, including water, may be an additional factor playing to the advantage of the use of nanocellulose. Maybe as a stabilizer for other more functional colloidal particles such as conducting or optical nanomaterials. The ability of nanocelluloses to form rigid stabilizing networks at low concentrations in water is indeed one of the most remarkable properties of nanocelluloses. Stabilizing cells and multicellular structures are perhaps why cellulose evolved in the primordial oceans, and we should use this property to our advantage.

## Acknowledgments

*The authors would like to thank Prof. Emily D. Cranston for sharing and discussing the definition of CNFs and CNCs. The authors acknowledge the funding from the Knut and Alice Wallenberg foundation via the Wallenberg Wood Science Center (WWSC) and an individual fellowship for Tobias Benselfelt (KAW 2019.0564). The authors gratefully acknowledge the support from the Digital Cellulose Centre, an excellence center partly funded by the Swedish Innovation Agency VINNOVA (Grant number 2016-05193).*

## Conflict of Interest

The authors declare no conflict of interest.

## Data Availability Statement

The data that support the findings of this study are available from the corresponding author upon reasonable request.

**Keywords:** aspect ratio · assembly · colloidal interactions · nanocellulose · networks

[1] a) E. J. W. Verwey, J. T. G. Overbeek, K. Van Nes, *Theory of the stability of lyophobic colloids: the interaction of sol particles having an electric double layer*, Elsevier Publishing Company, **1948**; b) B. Derjaguin, L. Landau, *Acta Physicochim: USSR* **1941**, *14*, 633–662.
[2] C. A. Silvera Batista, R. G. Larson, N. A. Kotov, *Science* **2015**, *350*.
[3] a) H. C. Hamaker, *Physica* **1937**, *4*, 1058–1072; b) E. M. Lifshitz, *J. Exp. Theor. Phys. USSR* **1954**, *29*, 94–110; c) J. N. Israelachvili, in *Intermolecular and Surface Forces (Third Edition)*, Academic Press, San Diego, **2011**, pp. 253–289.
[4] a) M. Gouy, *J. Phys. Theor. Appl.* **1910**, *9*, 457–468; b) D. L. Chapman, *Lond. Edinb. Dublin philos. Mag.* **1913**, *25*, 475–481; c) E. Hückel, P. Debye, *Phys. Z.* **1923**, *24*, 1.
[5] D. F. Evans, H. Wennerström, *The Colloidal Domain: Where Physics, Chemistry, Biology, and Technology Meet*, Wiley-Vch, **1999**.
[6] B. G. Rånby, *Acta Chem. Scand.* **1949**, *3*, 649–650.
[7] A. F. Turbak, F. W. Snyder, K. R. Sandberg, in *J. Appl. Polym. Sci.: Appl. Polym. Symp.; (United States), Vol. 37*, ITT Rayonier Inc., Shelton, WA, **1983**.
[8] L. Wågberg, L. Winter, L. Ödberg, T. Lindström, *Colloids Surf.* **1987**, *27*, 163–173.
[9] a) T. Saito, Y. Nishiyama, J.-L. Putaux, M. Vignon, A. Isogai, *Biomacromolecules* **2006**, *7*, 1687–1691; b) L. Wågberg, G. Decher, M. Norgren, T. Lindström, M. Ankerfors, K. Axnäs, *Langmuir* **2008**, *24*, 784–795.
[10] J. N. Israelachvili, in *Intermolecular and surface forces*, Academic press, **2011**.
[11] X. M. Dong, J.-F. Revol, D. G. Gray, *Cellulose* **1998**, *5*, 19–32.
[12] I. Siró, D. Plackett, *Cellulose* **2010**, *17*, 459–494.
[13] R. Shinoda, T. Saito, Y. Okita, A. Isogai, *Biomacromolecules* **2012**, *13*, 842–849.
[14] a) H. Tang, N. Butchosa, Q. Zhou, *Adv. Mater.* **2015**, *27*, 2070–2076; b) K. Yao, S. Huang, H. Tang, Y. Xu, G. Buntkowsky, L. A. Berglund, Q. Zhou, *ACS Appl. Mater. Interfaces* **2017**, *9*, 20169–20178.
[15] R. H. Marchessault, F. F. Morehead, N. M. Walter, *Nature* **1959**, *184*, 632–633.
[16] J. F. Revol, H. Bradford, J. Giasson, R. H. Marchessault, D. G. Gray, *Int. J. Biol. Macromol.* **1992**, *14*, 170–172.
[17] T. Saito, S. Kimura, Y. Nishiyama, A. Isogai, *Biomacromolecules* **2007**, *8*, 2485–2491.
[18] T. Benselfelt, J. Engström, L. Wågberg, *Green Chem.* **2018**, *20*, 2558–2570.
[19] A. Sjöstedt, J. Wohlert, P. T. Larsson, L. Wågberg, *Cellulose* **2015**, *22*, 2943–2953.
[20] A. B. Fall, S. B. Lindström, O. Sundman, L. Ödberg, L. Wågberg, *Langmuir* **2011**, *27*, 11332–11338.
[21] S. Janardhnan, M. M. Sain, *Bioresources* **2006**, *1*(2), 176–188
[22] a) A. J. Svagan, M. A. S. Azizi Samir, L. A. Berglund, *Biomacromolecules* **2007**, *8*, 2556–2563; b) M. Henriksson, G. Henriksson, L. A. Berglund, T. Lindström, *Eur. Polym. J.* **2007**, *43*, 3434–3441.
[23] M. Hasani, E. D. Cranston, G. Westman, D. G. Gray, *Soft Matter* **2008**, *4*, 2238–2244.
[24] C. Aulin, E. Johansson, L. Wågberg, T. Lindström, *Biomacromolecules* **2010**, *11*, 872–882.
[25] A. Pei, N. Butchosa, L. A. Berglund, Q. Zhou, *Soft Matter* **2013**, *9*, 2047–2055.
[26] A. Naderi, T. Lindström, G. Flodberg, J. Sundström, K. Junel, A. Runebjörk, C. F. Weise, J. Erlandsson, *Nord. Pulp Pap. Res. J.* **2016**, *31*, 20–29.
[27] M. Božič, P. Liu, A. P. Mathew, V. Kokol, *Cellulose* **2014**, *21*, 2713–2726.
[28] M. Ghanadpour, F. Carosio, P. T. Larsson, L. Wågberg, *Biomacromolecules* **2015**, *16*, 3399–3410.
[29] U.-J. Kim, S. Kuga, M. Wada, T. Okano, T. Kondo, *Biomacromolecules* **2000**, *1*, 488–492.
[30] J. Zhang, N. Jiang, Z. Dang, T. J. Elder, A. J. Ragauskas, *Cellulose* **2007**, *15*, 489.
[31] J. A. Sirviö, T. Hasa, J. Ahola, H. Liimatainen, J. Niinimäki, O. Hormi, *Carbohydr. Polym.* **2015**, *133*, 524–532.
[32] V. López Durán, J. Hellwig, P. T. Larsson, L. Wågberg, P. A. Larsson, *ACS Appl. Nano Mater.* **2018**, *1*, 1959–1967.
[33] S. Galland, F. Berthold, K. Prakobna, L. A. Berglund, *Biomacromolecules* **2015**, *16*, 2427–2435.
[34] X. Yang, M. S. Reid, P. Olsén, L. A. Berglund, *ACS Nano* **2020**, *14*, 724–735.
[35] X. Yang, L. A. Berglund, *Adv. Mater.* **2021**, *33*, 2001118.
[36] A. B. Fall, A. Burman, L. Wågberg, *Nord. Pulp Pap. Res. J.* **2014**, *29*, 176–184.
[37] a) K. J. De France, T. Hoare, E. D. Cranston, *Chem. Mater.* **2017**, *29*, 4609–4631; b) F. Rol, M. N. Belgacem, A. Gandini, J. Bras, *Prog. Polym. Sci.* **2019**, *88*, 241–264; c) S. J. Cho, K. H. Choi, J. T. Yoo, J. H. Kim, Y. H. Lee, S. J. Chun, S. B. Park, D. H. Choi, Q. Wu, S. Y. Lee, *Adv. Funct. Mater.* **2015**, *25*, 6029–6040; d) X. Du, Z. Zhang, W. Liu, Y. Deng, *Nano Energy* **2017**, *35*, 299–320.


© 2023 The Authors. ChemSusChem published by Wiley-VCH GmbH

1864564x, 2023, 8, Downloaded from https://chemistry-europe.onlinelibrary.wiley.com/doi/10.1002/cssc.202201955 by Paul Scherrer Institut PSI, Wiley Online Library on [08/05/2023]. See the Terms and Conditions (https://onlinelibrary.wiley.com/terms-and-conditions) on Wiley Online Library for rules of use; OA articles are governed by the applicable Creative Commons License

[38] a) M. Nordenström, A. Fall, G. Nyström, L. Wågberg, *Langmuir* **2017**, *33*, 9772–9780; b) L. Geng, N. Mittal, C. Zhan, F. Ansari, P. R. Sharma, X. Peng, B. S. Hsiao, L. D. Söderberg, *Macromolecules* **2018**, *51*, 1498–1506.
[39] E. J. Foster, R. J. Moon, U. P. Agarwal, M. J. Bortner, J. Bras, S. Camarero-Espinosa, K. J. Chan, M. J. Clift, E. D. Cranston, S. J. Eichhorn, *Chem. Soc. Rev.* **2018**, *47*, 2609–2679.
[40] A. Isogai, T. Hänninen, S. Fujisawa, T. Saito, *Prog. Polym. Sci.* **2018**, *86*, 122–148.
[41] a) D. Bratko, B. Jönsson, H. Wennerström, *Chem. Phys. Lett.* **1986**, *128*, 449–454; b) L. Guldbrand, B. Jönsson, H. Wennerström, P. Linse, *J. Chem. Phys.* **1984**, *80*, 2221–2228.
[42] a) J. Araki, *Soft Matter* **2013**, *9*, 4125–4141; b) H. Oguzlu, C. Danumah, Y. Boluk, *Curr. Op. Coll. Interf. Sci.* **2017**, *29*, 46–56; c) H. Fukuzumi, R. Tanaka, T. Saito, A. Isogai, *Cellulose* **2014**, *21*, 1553–1559.
[43] G. S. Manning, *J. Chem. Phys.* **1969**, *51*, 924–933.
[44] I. Usov, G. Nyström, J. Adamcik, S. Handschin, C. Schütz, A. Fall, L. Bergström, R. Mezzenga, *Nat. Commun.* **2015**, *6*, 7564.
[45] Y. Boluk, C. Danumah, *J. Nanopart. Res.* **2013**, *16*, 2174.
[46] I. Usov, R. Mezzenga, *Macromolecules* **2015**, *48*, 1269–1280.
[47] J. G. de la Torre, V. A. Bloomfield, *Q. Rev. Biophys.* **1981**, *14*, 81–139.
[48] T. Benselfelt, T. Pettersson, L. Wågberg, *Langmuir* **2017**, *33*, 968–979.
[49] D. H. Napper, *J. Colloid Interface Sci.* **1977**, *58*, 390–407.
[50] J. Leguy, A. Diallo, J.-L. Putaux, Y. Nishiyama, L. Heux, B. Jean, *Langmuir* **2018**, *34*, 11066–11075.
[51] T. Kaldéus, M. Nordenström, A. Carlmark, L. Wågberg, E. Malmström, *Carbohydr. Polym.* **2018**, *181*, 871–878.
[52] S. Fujisawa, T. Saito, S. Kimura, T. Iwata, A. Isogai, *Biomacromolecules* **2013**, *14*, 1541–1546.
[53] a) K. Missoum, M. N. Belgacem, J. Bras, *Materials* **2013**, *6*, 1745–1766; b) Z. Hu, R. M. Berry, R. Pelton, E. D. Cranston, *ACS Sustainable Chem. Eng.* **2017**, *5*, 5018–5026; c) M. T. Islam, M. M. Alam, M. Zoccola, *Int. J. Innov. Res. Sci. Eng. Technol.* **2013**, *2*, 5444–5451; d) T. Kaldéus, A. Träger, L. A. Berglund, E. Malmström, G. Lo Re, *ACS Nano* **2019**, *13*, 6409–6420; e) S. J. Eichhorn, A. Dufresne, M. Aranguren, N. Marcovich, J. Capadona, S. J. Rowan, C. Weder, W. Thielemans, M. Roman, S. Renneckar, *J. Mater. Sci.* **2010**, *45*, 1–33.
[54] O. van den Berg, J. R. Capadona, C. Weder, *Biomacromolecules* **2007**, *8*, 1353–1357.
[55] a) A. Svensson, P. T. Larsson, G. Salazar-Alvarez, L. Wågberg, *Carbohydr. Polym.* **2013**, *92*, 775–783; b) H. Sehaqui, Q. Zhou, O. Ikkala, L. A. Berglund, *Biomacromolecules* **2011**, *12*, 3638–3644.
[56] Y. Xu, A. Atrens, J. R. Stokes, *Adv. Colloid Interface Sci.* **2020**, *275*, 102076.
[57] Q. Ying, B. Chu, *Macromolecules* **1987**, *20*, 362–366.
[58] R. Kerekes, C. Schell, *J. Pulp Pap. Sci.* **1992**, *18*, J32-J38.
[59] A. Celzard, V. Fierro, R. Kerekes, *Cellulose* **2009**, *16*, 983–987.
[60] I. Shibata, A. Isogai, *Cellulose* **2003**, *10*, 151–158.
[61] H. Tanaka, J. Meunier, D. Bonn, *Phys. Rev. E* **2004**, *69*, 031404.
[62] a) B. Ruzicka, L. Zulian, E. Zaccarelli, R. Angelini, M. Sztucki, A. Moussaïd, G. Ruocco, *Phys. Rev. Lett.* **2010**, *104*, 085701; b) E. Zaccarelli, *J. Phys. Condens. Matter* **2007**, *19*, 323101.
[63] J. Appel, B. Fölker, J. Sprakel, *Soft Matter* **2016**, *12*, 2515–2522.
[64] A. B. Fall, S. B. Lindström, J. Sprakel, L. Wågberg, *Soft Matter* **2013**, *9*, 1852–1863.
[65] H. Dong, J. F. Snyder, K. S. Williams, J. W. Andzelm, *Biomacromolecules* **2013**, *14*, 3338–3345.
[66] M. J. Solomon, P. T. Spicer, *Soft Matter* **2010**, *6*, 1391–1400.
[67] a) A. Lu, U. Hemraz, Z. Khalili, Y. Boluk, *Cellulose* **2014**, *21*, 1239–1250; b) Y. Xu, A. D. Atrens, J. R. Stokes, *Soft Matter* **2018**, *14*, 1953–1963; c) M.-C. Li, Q. Wu, K. Song, S. Lee, Y. Qing, Y. Wu, *ACS Sustainable Chem. Eng.* **2015**, *3*, 821–832.
[68] N. Mittal, F. Ansari, K. Gowda, V. C. Brouzet, P. Chen, P. T. Larsson, S. V. Roth, F. Lundell, L. Wågberg, N. A. Kotov, L. D. Söderberg, *ACS Nano* **2018**, *12*(7), 6378–6388.
[69] M. Arcari, R. Axelrod, J. Adamcik, S. Handschin, A. Sánchez-Ferrer, R. Mezzenga, G. Nyström, *Nanoscale* **2020**, *12*, 11638–11646.
[70] P.-G. De Gennes, P.-G. Gennes, *Scaling concepts in polymer physics*, Cornell university press, **1979**.
[71] K. Kroy, E. Frey, *Phys. Rev. E* **1997**, *55*, 3092–3101.
[72] M. Nordenström, T. Benselfelt, R. Hollertz, S. Wennmalm, P. A. Larsson, A. Mehandzhiyski, N. Rolland, I. Zozoulenko, D. Söderberg, L. Wågberg, *Carbohydr. Polym.* **2022**, *297*, 120046.
[73] D. Langevin, F. Rondelez, *Polymer* **1978**, *19*, 875–882.
[74] a) E. Prince, E. Kumacheva, *Nat. Rev. Mater.* **2019**, *4*, 99–115; b) F. C. MacKintosh, J. Käs, P. A. Janmey, *Phys. Rev. Lett.* **1995**, *75*, 4425–4428.
[75] E. Lasseuguette, D. Roux, Y. Nishiyama, *Cellulose* **2008**, *15*, 425–433.
[76] T. Rosén, N. Mittal, S. V. Roth, P. Zhang, F. Lundell, L. D. Söderberg, *Soft Matter* **2020**, *16*, 5439–5449.
[77] D. Gethin, A. Rees, L. Powell, G. Chinga-Carassco, T. Claypole, D. Deganello, K. Hill, D. Thomas, K. Syverud, *Adv. Print. Sci. Technol.* **2014**, *41*, 91.
[78] K. Markstedt, A. Mantas, I. Tournier, H. c. Martínez Ávila, D. Hagg, P. Gatenholm, *Biomacromolecules* **2015**, *16*, 1489–1496.
[79] a) M. A. Hubbe, P. Tayeb, M. Joyce, P. Tyagi, M. Kehoe, K. Dimic-Misic, L. Pal, *BioResources* **2017**, *12*, 9556–9661; b) N. Takaaki, "The Promise of Nanocellulose", can be found under https://www.nippon.com/en/behind/l00151/the-promise-of-cellulose-nanofibers.html, **2016**, (Accessed 6 January 2023).
[80] J. Rostami, T. Benselfelt, L. Maddalena, C. Avci, F. A. Sellman, G. C. Ciftci, P. A. Larsson, F. Carosio, F. Akhtar, W. Tian, *Adv. Mater.* **2022**, *34*(38), 2204800.
[81] T. Benselfelt, L. Wågberg, *Biomacromolecules* **2019**, *20*, 2406–2412.
[82] E. J. F. Dickinson, R. G. Compton, *J. Phys. Chem. C* **2009**, *113*, 17585–17589.
[83] F. Oosawa, in *Polyelectrolytes*, Marcel Dekker, **1971**, pp. 50–126.
[84] Y. Min, M. Akbulut, K. Kristiansen, Y. Golan, J. Israelachvili, *Nat. Mater.* **2008**, *7*, 527–538.
[85] R. Kjellander, S. Marcělja, *Chem. Phys. Lett.* **1984**, *112*, 49–53.
[86] D. G. Truhlar, *J. Chem. Educ.* **2019**, *96*, 1671–1675.
[87] F. Hofmeister, *Archiv für experimentelle Pathologie und Pharmakologie* **1888**, *25*, 1–30.
[88] a) W. Kunz, *Curr. Op. Coll. Interf. Sci.* **2010**, *15*, 34–39; b) U. Sivan, *Curr. Op. Coll. Interf. Sci.* **2016**, *22*, 1–7; c) A. P. Dos Santos, Y. Levin, *Phys. Rev. Lett.* **2011**, *106*, 167801; d) A. Sthoer, J. Hladílková, M. Lund, E. Tyrode, *Phys. Chem. Chem. Phys.* **2019**, *21*, 11329–11344.
[89] B. W. Ninham, P. L. Nostro, *Molecular Forces and Self Assembly: In Colloid, Nano Sciences and Biology*, Cambridge University Press, **2010**.
[90] T. Benselfelt, M. Nordenström, M. M. Hamedi, L. Wågberg, *Nanoscale* **2019**, *11*, 3514–3520.
[91] N. Mittal, T. Benselfelt, F. Ansari, K. Gordeyeva, S. V. Roth, L. Wågberg, L. D. Söderberg, *Angew. Chem. Int. Ed.* **2019**, *58*, 18562–18569; *Angew. Chem.* **2019**, *131*, 18735–18742.
[92] M. A. Brown, Z. Abbas, A. Kleibert, R. G. Green, A. Goel, S. May, T. M. Squires, *Phys. Rev. X* **2016**, *6*, 011007.
[93] a) R. A. Robinson, R. H. Stokes, *Trans. Faraday Soc.* **1949**, *45*, 612–624; b) M. E. Guendouzi, A. Dinane, A. Mounir, *J. Chem. Thermodyn.* **2001**, *33*, 1059–1072.
[94] G. I. Guerrero-García, P. González-Mozuelos, M. Olvera de la Cruz, *ACS Nano* **2013**, *7*, 9714–9723.
[95] D. L. Mobley, A. E. Barber, C. J. Fennell, K. A. Dill, *J. Phys. Chem. B* **2008**, *112*, 2405–2414.
[96] T. Phan-Xuan, A. Thuresson, M. Skepö, A. Labrador, R. Bordes, A. Matic, *Cellulose* **2016**, *23*, 3653–3663.
[97] a) J. E. House, in *Inorganic Chemistry (Second Edition)*, Academic Press, **2013**, pp. 643–664; b) J. E. House, in *Inorganic Chemistry (Second Edition)*, Academic Press, **2013**, pp. 591–616; c) R. J. P. Williams, *J. Chem. Soc. (Resumed)* **1952**, 3770–3778; d) H. Irving, R. J. P. Williams, *J. Chem. Soc. (Resumed)* **1953**, 3192–3210.
[98] T. Benselfelt, M. Nordenström, S. B. Lindström, L. Wågberg, *Adv. Mater. Interfaces* **2019**, *6*, 1900333.
[99] K. S. Williams, J. W. Andzelm, H. Dong, J. F. Snyder, *Cellulose* **2014**, *21*, 1091–1101.
[100] S. Lombardo, A. Gençer, C. Schütz, J. Van Rie, S. Eyley, W. Thielemans, *Biomacromolecules* **2019**, *20*, 3181–3190.
[101] J. Ray, G. S. Manning, *Langmuir* **1994**, *10*, 2450–2461.
[102] J. Fu, J. B. Schlenoff, *J. Am. Chem. Soc.* **2016**, *138*, 980–990.
[103] M. Boström, V. S. J. Craig, R. Albion, D. R. M. Williams, B. W. Ninham, *J. Phys. Chem. B* **2003**, *107*, 2875–2878.
[104] B. Jönsson, H. Wennerström, *J. Adhes.* **2004**, *80*, 339–364.
[105] R. Shannon, *Acta Crystallogr. Sect. A* **1976**, *32*, 751–767.
[106] L. Onsager, *Ann. N. Y. Acad. Sci.* **1949**, *51*, 627–659.
[107] a) A. Stroobants, H. Lekkerkerker, T. Odijk, *Macromolecules* **1986**, *19*, 2232–2238; b) R. Mezzenga, J.-M. Jung, J. Adamcik, *Langmuir* **2010**, *26*, 10401–10405.
[108] a) X. M. Dong, D. G. Gray, *Langmuir* **1997**, *13*, 2404–2409; b) X. M. Dong, T. Kimura, J.-F. Revol, D. G. Gray, *Langmuir* **1996**, *12*, 2076–2082.
[109] G. Nyström, M. Arcari, J. Adamcik, I. Usov, R. Mezzenga, *ACS Nano* **2018**, *12*, 5141–5148.
[110] J. P. F. Lagerwall, C. Schütz, M. Salajkova, J. Noh, J. Hyun Park, G. Scalia, L. Bergström, *NPG Asia Mater.* **2014**, *6*, e80-e80.


© 2023 The Authors. ChemSusChem published by Wiley-VCH GmbH

1864564x, 2023, 8, Downloaded from https://chemistry-europe.onlinelibrary.wiley.com/doi/10.1002/cssc.202201955 by Paul Scherrer Institut PSI, Wiley Online Library on [08/05/2023]. See the Terms and Conditions (https://onlinelibrary.wiley.com/terms-and-conditions) on Wiley Online Library for rules of use; OA articles are governed by the applicable Creative Commons License

[111] a) C. Schütz, M. Agthe, A. B. Fall, K. Gordeyeva, V. Guccini, M. Salajková, T. S. Plivelic, J. P. F. Lagerwall, G. Salazar-Alvarez, L. Bergström, *Langmuir* **2015**, *31*, 6507–6513; b) Y. Liu, M. Agthe, M. Salajková, K. Gordeyeva, V. Guccini, A. Fall, G. Salazar-Alvarez, C. Schütz, L. Bergström, *Nanoscale* **2018**, *10*, 18113–18118; c) S. Beck-Candanedo, M. Roman, D. G. Gray, *Biomacromolecules* **2005**, *6*, 1048–1054.
[112] M. Arcari, E. Zuccarella, R. Axelrod, J. Adamcik, A. Sánchez-Ferrer, R. Mezzenga, G. Nyström, *Biomacromolecules* **2019**, *20*, 1288–1296.
[113] M. Zhao, F. Ansari, M. Takeuchi, M. Shimizu, T. Saito, L. A. Berglund, A. Isogai, *Nanoscale Horiz.* **2018**, *3*, 28–34.
[114] C. Li, J. Evans, N. Wang, T. Guo, S. He, *Sci. Rep.* **2019**, *9*, 11290.
[115] B. Frka-Petesic, B. Jean, L. Heux, *EPL Europhys. Lett.* **2014**, *107*, 28006.
[116] a) A. J. Benítez, A. Walther, *Biomacromolecules* **2017**, *18*, 1642–1653; b) M. Shimizu, T. Saito, H. Fukuzumi, A. Isogai, *Biomacromolecules* **2014**, *15*, 4320–4325.
[117] A. S. Michaels, *Ind. Eng. Chem.* **1965**, *57*, 32–40.
[118] a) S. Kishani, T. Benselfelt, L. Wågberg, J. Wohlert, *J. Colloid Interface Sci.* **2021**, *588*, 485–493; b) T. Benselfelt, E. D. Cranston, S. Ondaral, E. Johansson, H. Brumer, M. W. Rutland, L. Wågberg, *Biomacromolecules* **2016**, *17*, 2801–2811; c) M. Wohlert, T. Benselfelt, L. Wågberg, I. Furó, L. A. Berglund, J. Wohlert, *Cellulose* **2021**, *29*, 1–23.
[119] S. Lombardo, W. Thielemans, *Cellulose* **2019**, *26*, 249–279.
[120] a) H. Wang, M. Roman, *Biomacromolecules* **2011**, *12*, 1585–1593; b) K. Chi, J. M. Catchmark, *Food Hydrocolloids* **2018**, *80*, 195–205.
[121] a) J. Van der Gucht, E. Spruijt, M. Lemmers, M. A. C. Stuart, *J. Colloid Interface Sci.* **2011**, *361*, 407–422; b) J. Kötz, T. Beitz, *Trends Polym. Sci.* **1997**, *3*, 86–90.
[122] P. Schaaf, J. B. Schlenoff, *Adv. Mater.* **2015**, *27*, 2420–2432.
[123] M. S. Toivonen, S. Kurki-Suonio, F. H. Schacher, S. Hietala, O. J. Rojas, O. Ikkala, *Biomacromolecules* **2015**, *16*, 1062–1071.
[124] O. Sepall, S. G. Mason, *Can. J. Chem.* **1961**, *39*, 1944–1955.
[125] S. D. Roughley, A. M. Jordan, *J. Med. Chem.* **2011**, *54*, 3451–3479.
[126] T. M. Raschke, M. Levitt, *Proc. Nat. Acad. Sci.* **2005**, *102*, 6777–6782.
[127] B. Medronho, A. Romano, M. G. Miguel, L. Stigsson, B. Lindman, *Cellulose* **2012**, *19*, 581–587.
[128] B. Medronho, B. Lindman, *Adv. Colloid Interface Sci.* **2015**, *222*, 502–508.
[129] S. Kishani, F. Vilaplana, W. Xu, C. Xu, L. Wågberg, *Biomacromolecules* **2018**, *19*, 1245–1255.
[130] a) T. Hayashi, *Annu. Rev. Plant Physiol. Plant Mol. Biol.* **1989**, *40*, 139–168; b) E. Chanliaud, J. De Silva, B. Strongitharm, G. Jeronimidis, M. J. Gidley, *Plant J.* **2004**, *38*, 27–37.
[131] a) M. Lopez, H. Bizot, G. Chambat, M.-F. Marais, A. Zykwinska, M.-C. Ralet, H. Driguez, A. Buléon, *Biomacromolecules* **2010**, *11*, 1417–1428; b) Q. Zhang, H. Brumer, H. Ågren, Y. Tu, *Carbohydr. Res.* **2011**, *346*, 2595–2602; c) Z. Zhao, V. Crespi, J. Kubicki, D. Cosgrove, L. Zhong, *Cellulose* **2014**, *21*, 1025–1039; d) J. Hanus, K. Mazeau, *Biopolymers* **2006**, *82*, 59–73.
[132] M. S. Reid, M. Villalobos, E. D. Cranston, *Curr. Op. Coll. Interf. Sci.* **2017**, *29*, 76–82.
[133] P. Eronen, M. Österberg, S. Heikkinen, M. Tenkanen, J. Laine, *Carbohydr. Polym.* **2011**, *86*, 1281–1290.
[134] a) N. J. Grantham, J. Wurman-Rodrich, O. M. Terrett, J. J. Lyczakowski, K. Stott, D. Iuga, T. J. Simmons, M. Durand-Tardif, S. P. Brown, R. Dupree, M. Busse-Wicher, P. Dupree, *Nat. Plants* **2017**, *3*, 859–865; b) Z. Jaafar, K. Mazeau, A. Boissière, S. Le Gall, A. Villares, J. Vigouroux, N. Beury, C. Moreau, M. Lahaye, B. Cathala, *Carbohydr. Polym.* **2019**, *226*, 115315.
[135] B. L. Tardy, S. Yokota, M. Ago, W. Xiang, T. Kondo, R. Bordes, O. J. Rojas, *Curr. Op. Coll. Interf. Sci.* **2017**, *29*, 57–67.
[136] Y. Zhang, W. Shi, H. Zhou, X. Fu, X. Chen, *Water Environ. Res.* **2010**, *82*, 567–573.
[137] D. Horn, *Polymeric amines and ammonium salts*, (E. Goethals), Pergamon press, New York, **1980**.
[138] a) S. Paria, C. Manohar, K. C. Khilar, *Colloids Surf. Physicochem. Eng. Aspects* **2005**, *252*, 221–229; b) S. Alila, S. Boufi, M. N. Belgacem, D. Beneventi, *Langmuir* **2005**, *21*, 8106–8113; c) J. M. Cases, F. Villieras, *Langmuir* **1992**, *8*, 1251–1264.
[139] L. H. Torn, L. K. Koopal, A. de Keizer, J. Lyklema, *Langmuir* **2005**, *21*, 7768–7775.
[140] S. Paria, C. Manohar, K. C. Khilar, *Ind. Eng. Chem. Res.* **2005**, *44*, 3091–3098.
[141] a) M. Nagalakshmaiah, N. El Kissi, A. Dufresne, *ACS Appl. Mater. Interfaces* **2016**, *8*, 8755–8764; b) K. Chi, J. M. Catchmark, *Cellulose* **2017**, *24*, 4845–4860; c) Z. Emami, Q. Meng, G. Pircheraghi, I. Manas-Zloczower, *Cellulose* **2015**, *22*, 3161–3176.
[142] K. Xhanari, K. Syverud, G. Chinga-Carrasco, K. Paso, P. Stenius, *Cellulose* **2011**, *18*, 257–270.
[143] N. Quennouz, S. M. Hashmi, H. S. Choi, J. W. Kim, C. O. Osuji, *Soft Matter* **2016**, *12*, 157–164.
[144] N. Dhar, D. Au, R. C. Berry, K. C. Tam, *Colloids Surf. Physicochem. Eng. Aspects* **2012**, *415*, 310–319.
[145] E. Buxbaum, in *Fundamentals of Protein Structure and Function*, Springer, Cham, **2015**.
[146] H. Orelma, I. Filpponen, L. S. Johansson, J. Laine, O. J. Rojas, *Biomacromolecules* **2011**, *12*, 4311–4318.
[147] a) S. Lombardo, S. Eyley, C. Schütz, H. Van Gorp, S. Rosenfeldt, G. Van Den Mooter, W. Thielemans, *Langmuir* **2017**, *33*, 5473–5481; b) R. Weishaupt, G. Siqueira, M. Schubert, P. Tingaut, K. Maniura-Weber, T. Zimmermann, L. Thöny-Meyer, G. Faccio, J. Ihssen, *Biomacromolecules* **2015**, *16*, 3640–3650.
[148] G. Fleer, M. C. Stuart, J. M. Scheutjens, T. Cosgrove, B. Vincent, *Polymers at interfaces*, Springer Science & Business Media, **1993**.
[149] J. Guo, J. M. Catchmark, M. N. A. Mohamed, A. J. Benesi, M. Tien, T. H. Kao, H. D. Watts, J. D. Kubicki, *Biomacromolecules* **2013**, *14*, 1795–1805.
[150] M. Linder, T. T. Teeri, *J. Biotechnol.* **1997**, *57*, 15–28.
[151] R. Weishaupt, J. N. Zünd, L. Heuberger, F. Zuber, G. Faccio, F. Robotti, A. Ferrari, G. Fortunato, Q. Ren, K. Maniura-Weber, A. G. Guex, *Adv. Healthcare Mater.* **2020**, *9*.
[152] R. Weishaupt, G. Siqueira, M. Schubert, M. M. Kämpf, T. Zimmermann, K. Maniura-Weber, G. Faccio, *Adv. Funct. Mater.* **2017**, *27*.
[153] R. Weishaupt, L. Heuberger, G. Siqueira, B. Gutt, T. Zimmermann, K. Maniura-Weber, S. Salentinig, G. Faccio, *ACS Appl. Mater. Interfaces* **2018**, *10*, 20170–20181.
[154] T. Nikolic, M. Korica, J. Milanovic, A. Kramar, Z. Petronijevic, M. Kostic, *Cellulose* **2017**, *24*, 1863–1875.
[155] S. Di Risio, N. Yan, *J. Colloid Interface Sci.* **2009**, *338*, 410–419.
[156] S. Arola, T. Tammelin, H. Setälä, A. Tullila, M. B. Linder, *Biomacromolecules* **2012**, *13*, 594–603.
[157] T. Wu, N. Kummer, K. J. D. France, S. Campioni, Z. Zeng, G. Siqueira, J. Dong, G. Nyström, *Carbohydr. Polym.* **2021**, *251*, 117021–117021.
[158] K. J. De France, N. Kummer, Q. Ren, S. Campioni, G. Nyström, *Biomacromolecules* **2020**, *21*, 5139–5147.
[159] L. K. Bast, K. W. Klockars, L. G. Greca, O. J. Rojas, B. L. Tardy, N. Bruns, *Biomacromolecules* **2021**, *22*, 2067–2080.
[160] a) C. Olivier, C. Moreau, P. Bertoncini, H. Bizot, O. Chauvet, B. Cathala, *Langmuir* **2012**, *28*, 12463–12471; b) H. Koga, T. Saito, T. Kitaoka, M. Nogi, K. Suganuma, A. Isogai, *Biomacromolecules* **2013**, *14*, 1160–1165.
[161] S. Yokota, T. Ueno, T. Kitaoka, H. Wariishi, *Carbohydr. Res.* **2007**, *342*, 2593–2598.
[162] A. Hajian, S. B. Lindström, T. Pettersson, M. M. Hamedi, L. Wågberg, *Nano Lett.* **2017**, *17*, 1439–1447.
[163] L. Piculell, B. Lindman, *Adv. Colloid Interface Sci.* **1992**, *41*, 149–178.
[164] V. Tohver, J. E. Smay, A. Braem, P. V. Braun, J. A. Lewis, *Proc. Nat. Acad. Sci.* **2001**, *98*, 8950–8954.
[165] a) E. Niinivaara, E. D. Cranston, *Carbohydr. Polym.* **2020**, *247*, 116664; b) K. De France, Z. Zeng, T. Wu, G. Nyström, *Adv. Mater.* **2021**, *33*, 2000657.
[166] T. Ebeling, M. Paillet, R. Borsali, O. Diat, A. Dufresne, J. Y. Cavaillé, H. Chanzy, *Langmuir* **1999**, *15*, 6123–6126.
[167] S. Iwamoto, A. Isogai, T. Iwata, *Biomacromolecules* **2011**, *12*, 831–836.
[168] M. J. Lundahl, V. Klar, L. Wang, M. Ago, O. J. Rojas, *Ind. Eng. Chem. Res.* **2017**, *56*, 8–19.
[169] K. M. O. Håkansson, A. B. Fall, F. Lundell, S. Yu, C. Krywka, S. V. Roth, G. Santoro, M. Kvick, L. Prahl Wittberg, L. Wågberg, L. D. Söderberg, *Nat. Commun.* **2014**, *5*.
[170] N. Mittal, F. Ansari, K. Gowda, V. C. Brouzet, P. Chen, P. T. Larsson, S. V. Roth, F. Lundell, L. Wågberg, N. A. Kotov, L. D. Söderberg, *ACS Nano* **2018**, *12*, 6378–6388.
[171] a) M. S. Toivonen, S. Kurki-Suonio, W. Wagermaier, V. Hynninen, S. Hietala, O. Ikkala, *Biomacromolecules* **2017**, *18*, 1293–1301; b) K. Zhang, H. Liimatainen, *Small* **2018**, *14*, 1801937.
[172] K. Li, C. M. Clarkson, L. Wang, Y. Liu, M. Lamm, Z. Pang, Y. Zhou, J. Qian, M. Tajvidi, D. J. Gardner, H. Tekinalp, L. Hu, T. Li, A. J. Ragauskas, J. P. Youngblood, S. Ozcan, *ACS Nano* **2021**, *15*, 3646–3673.
[173] a) Y. Liu, D. Stoeckel, K. Gordeyeva, M. Agthe, C. Schütz, A. B. Fall, L. Bergström, *ACS Macro Lett.* **2018**, *7*, 172–177; b) C. Q. Pritchard, F. Navarro, M. Roman, M. J. Bortner, *J. Colloid Interface Sci.* **2021**, *603*, 450–458.
[174] C. Edgar, D. Gray, *Cellulose* **2003**, *10*, 299–306.
[175] N. Lavoine, L. Bergström, *J. Mater. Chem. A* **2017**, *5*, 16105–16117.


© 2023 The Authors. ChemSusChem published by Wiley-VCH GmbH

1864564x, 2023, 8, Downloaded from https://chemistry-europe.onlinelibrary.wiley.com/doi/10.1002/cssc.202201955 by Paul Scherrer Institut PSI, Wiley Online Library on [08/05/2023]. See the Terms and Conditions (https://onlinelibrary.wiley.com/terms-and-conditions) on Wiley Online Library for rules of use; OA articles are governed by the applicable Creative Commons License

[176] J. Sugiyama, H. Chanzy, G. Maret, *Macromolecules* **1992**, *25*, 4232–4234.
[177] a) E. Cranston, D. Gray, *Sci. Technol. Adv. Mater.* **2006**, *7*, 319; b) Y. Habibi, T. Heim, R. Douillard, *J. Polym. Sci. Part B* **2008**, *46*, 1430–1436.
[178] H. C. Kim, J. W. Kim, L. Zhai, J. Kim, *Cellulose* **2019**, *26*, 5821–5829.
[179] D. Bordel, J.-L. Putaux, L. Heux, *Langmuir* **2006**, *22*, 4899–4901.
[180] A. Kadimi, K. Benhamou, Z. Ounaies, A. Magnin, A. Dufresne, H. Kaddami, M. Raihane, *ACS Appl. Mater. Interfaces* **2014**, *6*, 9418–9425.
[181] K. M. Ryan, A. Mastroianni, K. A. Stancil, H. Liu, A. P. Alivisatos, *Nano Lett.* **2006**, *6*, 1479–1482.
[182] L.-s. Li, A. P. Alivisatos, *Phys. Rev. Lett.* **2003**, *90*, 097402.
[183] G. Delepierre, S. Eyley, W. Thielemans, C. Weder, E. D. Cranston, J. O. Zoppe, *Nanoscale* **2020**, *12*, 17480–17493.
[184] a) T. Pullawan, A. N. Wilkinson, S. J. Eichhorn, *Biomacromolecules* **2012**, *13*, 2528–2536; b) S. Xu, D. Liu, Q. Zhang, Q. Fu, *Compos. Sci. Technol.* **2018**, *156*, 117–126.
[185] H. Takana, M. Guo, *Nanotechnology* **2020**, *31*, 205602.
[186] L. Csoka, I. C. Hoeger, O. J. Rojas, I. Peszlen, J. J. Pawlak, P. N. Peralta, *ACS Macro Lett.* **2012**, *1*, 867–870.
[187] a) J. J. Kirkland, *Anal. Chem.* **1965**, *37*, 1458–1461; b) R. K. Iler, *J. Colloid Interface Sci.* **1966**, *21*, 569–594; c) G. Decher, J. D. Hong, *Makromol. Chem. Macromol. Symp.* **1991**, *46*, 321–327.
[188] P. Podsiadlo, S.-Y. Choi, B. Shim, J. Lee, M. Cuddihy, N. A. Kotov, *Biomacromolecules* **2005**, *6*, 2914–2918.
[189] a) M. Ghanadpour, F. Carosio, L. Wågberg, *Appl. Mater. Today* **2017**, *9*, 229–239; b) C. Aulin, E. Karabulut, A. Tran, L. Wågberg, T. Lindström, *ACS Appl. Mater. Interfaces* **2013**, *5*, 7352–7359; c) C. Martin, B. Jean, *Nord. Pulp Pap. Res. J.* **2014**, *29*, 19–30.
[190] a) C. Aulin, S. Ahola, P. Josefsson, T. Nishino, Y. Hirose, M. Österberg, L. Wågberg, *Langmuir* **2009**, *25*, 7675–7685; b) S. Ahola, J. Salmi, L. S. Johansson, J. Laine, M. Österberg, *Biomacromolecules* **2008**, *9*, 1273–1282.
[191] a) B. Jean, L. Heux, F. Dubreuil, G. Chambat, F. Cousin, *Langmuir* **2009**, *25*, 3920–3923; b) C. Cerclier, F. Cousin, H. Bizot, C. Moreau, B. Cathala, *Langmuir* **2010**, *26*, 17248–17255.
[192] T. Paulraj, A. V. Riazanova, A. J. Svagan, *Acta Biomater.* **2018**, *69*, 196–205.
[193] M. Shimizu, T. Saito, A. Isogai, *J. Membr. Sci.* **2016**, *500*, 1–7.
[194] K. Sakakibara, Y. Moriki, H. Yano, Y. Tsujii, *ACS Appl. Mater. Interfaces* **2017**, *9*, 44079–44087.
[195] A. B. Reising, R. J. Moon, J. P. Youngblood, *J. Sci. Technol. Forest Prod. Processes* **2012**, *2*, 32–41.
[196] B. E. Droguet, H.-L. Liang, B. Frka-Petesic, R. M. Parker, M. F. L. De Volder, J. J. Baumberg, S. Vignolini, *Nat. Mater.* **2022**, *21*, 352–358.
[197] M. Giese, L. K. Blusch, M. K. Khan, M. J. MacLachlan, *Angew. Chem. Int. Ed.* **2015**, *54*, 2888–2910; *Angew. Chem.* **2015**, *127*, 2930–2953.
[198] L. Severini, K. J. De France, D. Sivaraman, N. Kummer, G. Nyström, *ACS Omega* **2022**, *7*, 578–586.
[199] a) H. Orelma, I. Filpponen, L. S. Johansson, M. Österberg, O. J. Rojas, J. Laine, *Biointerphases* **2012**, *7*, 1–12; b) Y. Zhang, R. G. Carbonell, O. J. Rojas, *Biomacromolecules* **2013**, *14*, 4161–4168; c) Y. Zhang, O. J. Rojas, *Biomacromolecules* **2017**, *18*, 526–534.
[200] a) E. Kontturi, P. Laaksonen, M. B. Linder, Nonappa, A. H. Gröschel, O. J. Rojas, O. Ikkala, *Adv. Mater.* **2018**, *30*; b) T. Abitbol, A. Rivkin, Y. Cao, Y. Nevo, E. Abraham, T. Ben-Shalom, S. Lapidot, O. Shoseyov, *Curr. Opin. Biotechnol.* **2016**, *39*, 76–88; c) H. Kargarzadeh, J. Huang, N. Lin, I. Ahmad, M. Mariano, A. Dufresne, S. Thomas, A. Gałęski, *Prog. Polym. Sci.* **2018**, *87*, 197–227; d) N. Mittal, R. Jansson, M. Widhe, T. Benselfelt, K. M. O. Håkansson, F. Lundell, M. Hedhammar, L. D. Söderberg, *ACS Nano* **2017**, *11*, 5148–5159.
[201] a) N. H. C. S. Silva, P. Figueira, E. Fabre, R. J. B. Pinto, M. E. Pereira, A. J. D. Silvestre, I. M. Marrucho, C. Vilela, C. S. R. Freire, *Carbohydr. Polym.* **2020**, *238*, 116210–116210; b) N. H. C. S. Silva, P. Garrido-Pascual, C. Moreirinha, A. Almeida, T. Palomares, A. Alonso-Varona, C. Vilela, C. S. R. Freire, *Int. J. Biol. Macromol.* **2020**, *165*, 1198–1210.
[202] Y. Huang, P. Yang, F. Yang, C. Chang, *J. Membr. Sci.* **2021**, *635*, 119537–119537.
[203] a) I. Capron, O. J. Rojas, R. Bordes, *Curr. Opin. Colloid Interface Sci.* **2017**, *29*, 83–95; b) P. Bertsch, M. Diener, J. Adamcik, N. Scheuble, T. Geue, R. Mezzenga, P. Fischer, *Langmuir* **2018**, *34*, 15195–15202.
[204] P. Bertsch, M. Arcari, T. Geue, R. Mezzenga, G. Nyström, P. Fischer, *Biomacromolecules* **2019**, *20*, 4574–4580.
[205] J. Bergfreund, Q. Sun, P. Fischer, P. Bertsch, *Nanoscale Adv.* **2019**, *1*, 4308–4312.
[206] a) I. Kalashnikova, H. Bizot, B. Cathala, I. Capron, *Biomacromolecules* **2012**, *13*, 267–275; b) F. Cherhal, F. Cousin, I. Capron, *Biomacromolecules* **2016**, *17*, 496–502; c) M. Uhlig, A. Fall, S. Wellert, M. Lehmann, S. Prévost, L. Wågberg, R. von Klitzing, G. Nyström, *Langmuir* **2016**, *32*, 442–450.
[207] P. Bertsch, P. Fischer, *Adv. Colloid Interface Sci.* **2020**, *276*, 102089–102089.
[208] a) G. Renaud, R. Lazzari, F. Leroy, *Surf. Sci. Rep.* **2009**, *64*, 255–380; b) P. Müller-Buschbaum, *Polym. J.* **2013**, *45*, 34–42.
[209] S. U. Pickering, *J. Chem. Soc. Trans.* **1907**, *91*, 2001–2021.
[210] a) I. Kalashnikova, H. Bizot, B. Cathala, I. Capron, *Langmuir* **2011**, *27*, 7471–7479; b) I. Kalashnikova, H. Bizot, P. Bertoncini, B. Cathala, I. Capron, *Soft Matter* **2013**, *9*, 952–959.
[211] N. Scheuble, T. Geue, E. J. Windhab, P. Fischer, *Biomacromolecules* **2014**, *15*, 3139–3145.
[212] H. Jin, W. Zhou, J. Cao, S. D. Stoyanov, T. B. J. Blijdenstein, P. W. N. De Groot, L. N. Arnaudov, E. G. Pelan, *Soft Matter* **2012**, *8*, 2194–2205.
[213] a) N. T. Cervin, L. Andersson, J. B. S. Ng, P. Olin, L. Bergström, L. Wågberg, *Biomacromolecules* **2013**, *14*, 503–511; b) N. T. Cervin, E. Johansson, J. W. Benjamins, L. Wågberg, *Biomacromolecules* **2015**, *16*, 822–831.
[214] a) S. Saffarionpour, *Food Bioproc. Technnol.* **2020**, *13*, 1292–1328; b) Q. Li, Y. Wu, R. Fang, C. Lei, Y. Li, B. Li, Y. Pei, X. Luo, ShilinLiu, *Trends Food Sci. Technol.* **2021**, *110*, 573–583; c) S. Parajuli, E. E. Ureña-Benavides, *Adv. Colloid Interface Sci.* **2022**, *299*, 102530–102530; d) M. Zhu, S. Huan, S. Liu, Z. Li, M. He, G. Yang, S. Liu, D. J. McClements, O. J. Rojas, L. Bai, *Curr. Opin. Colloid Interface Sci.* **2021**, *56*, 101512–101512.
[215] L. Bai, S. Huan, W. Xiang, O. J. Rojas, *Green Chem.* **2018**, *20*, 1571–1582.
[216] a) H. Emady, M. Caggioni, P. Spicer, *J. Rheol.* **2013**, *57*, 1761–1772; b) J. Song, M. Caggioni, T. M. Squires, J. F. Gilchrist, S. W. Prescott, P. T. Spicer, *Rheol. Acta* **2019**, *58*, 217–229.
[217] E. J. Foster, R. J. Moon, U. P. Agarwal, M. J. Bortner, J. Bras, S. Camarero-Espinosa, K. J. Chan, M. J. D. Clift, E. D. Cranston, S. J. Eichhorn, D. M. Fox, W. Y. Hamad, L. Heux, B. Jean, M. Korey, W. Nieh, K. J. Ong, M. S. Reid, S. Renneckar, R. Roberts, J. A. Shatkin, J. Simonsen, K. Stinson-Bagby, N. Wanasekara, J. Youngblood, *Chem. Soc. Rev.* **2018**, *47*, 2609–2679.
[218] M. S. Reid, H. S. Marway, C. Moran-Hidalgo, M. Villalobos, E. D. Cranston, *Cellulose* **2017**, *24*, 4743–4757.
[219] a) C. Moser, G. Henriksson, M. Lindström, *Nord. Pulp Pap. Res. J.* **2018**, *33*, 647–650; b) N. Butchosa, Q. Zhou, *Cellulose* **2014**, *21*, 4349–4358.
[220] a) K. Missoum, J. Bras, M. N. Belgacem, *Biomacromolecules* **2012**, *13*, 4118–4125; b) C. Eyholzer, N. Bordeanu, F. Lopez-Suevos, D. Rentsch, T. Zimmermann, K. Oksman, *Cellulose* **2010**, *17*, 19–30; c) J. Velásquez-Cock, P. Gañán, C. Gómez, H. P. Posada, C. Castro, A. Dufresne, R. Zuluaga, *Food Hydrocolloids* **2018**, *79*, 30–39; d) J. Velásquez-Cock, B. E. Gómez, H. P. Posada, A. Serpa, G. C. Gómez, H. C. Castro, P. Gañán, R. Zuluaga, *Carbohydr. Polym.* **2018**, *179*, 118–125.
[221] M. P. Lowys, J. Desbrières, M. Rinaudo, *Food Hydrocolloids* **2001**, *15*, 25–32.
[222] a) A. Naderi, T. Lindström, J. Sundström, G. Flodberg, *Nord. Pulp Pap. Res. J.* **2015**, *30*, 568; b) S. Takaichi, T. Saito, R. Tanaka, A. Isogai, *Cellulose* **2014**, *21*, 4093–4103.
[223] a) P. A. Larsson, A. V. Riazanova, G. Cinar Ciftci, R. Rojas, H. H. Øvrebø, L. Wågberg, L. A. Berglund, *Cellulose* **2019**, *26*, 1565–1575; b) M. Nordenström, T. Kaldéus, J. Erlandsson, T. Pettersson, E. Malmström, L. Wågberg, *ACS Sustainable Chem. Eng.* **2021**, *9*, 11003–11010.
[224] Y. Peng, D. J. Gardner, Y. Han, *Cellulose* **2012**, *19*, 91–102.
[225] J. Han, C. Zhou, Y. Wu, F. Liu, Q. Wu, *Biomacromolecules* **2013**, *14*, 1529–1540.
[226] A. Naderi, P. T. Larsson, J. S. Stevanic, T. Lindström, J. Erlandsson, *Cellulose* **2017**, *24*, 1307–1317.
[227] J. Erlandsson, T. Pettersson, T. Ingverud, H. Granberg, P. A. Larsson, M. Malkoch, L. Wågberg, *J. Mater. Chem. A* **2018**, *6*, 19371–19380.
[228] H. Liimatainen, S. Haavisto, A. Haapala, J. Niinimäki, *BioResources* **2009**, *4*, 20.
[229] F. W. Herrick (Rayonier Inc), US4481076 A, **1984**.
[230] J. Laine, T. Lindström, *Nord. Pulp Pap. Res. J.* **2000**, *15*, 520–526.
[231] D. Cheng, Y. Wen, L. Wang, X. An, X. Zhu, Y. Ni, *Carbohydr. Polym.* **2015**, *123*, 157–163.
[232] F. W. Herrick (Rayonier Inc), US4481076 A, **1983**.
[233] E. Fairman, PhD thesis, Honors College **2014**.

Manuscript received: October 20, 2022
Revised manuscript received: January 16, 2023
Accepted manuscript online: January 17, 2023
Version of record online: February 28, 2023


© 2023 The Authors. ChemSusChem published by Wiley-VCH GmbH

1864564x, 2023, 8, Downloaded from https://chemistry-europe.onlinelibrary.wiley.com/doi/10.1002/cssc.202201955 by Paul Scherrer Institut PSI, Wiley Online Library on [08/05/2023]. See the Terms and Conditions (https://onlinelibrary.wiley.com/terms-and-conditions) on Wiley Online Library for rules of use; OA articles are governed by the applicable Creative Commons License